By

Nengovhela Rotshidzwa Thuso

Student number: 13131621

EFFECT OF GEOTECHNICAL PROPERTIES OF TAILINGS ON THE STABILITY OF TAILINGS DAM FACILITIES

A dissertation submitted in accordance with the requirements for the degree of

MASTER OF ENGINEERING

at the

UNIVERSITY OF SOUTH AFRICA

School of Engineering

College of Science, Engineering, and Technology

Supervisor: Dr N.M. Chiloane

Co-Supervisor: Dr V.C. Madanda

Co-Supervisor: Prof B.D. Ikotun

June 2026

Declaration

Name: Rotshidzwa Thuso

Surname: Nengovhela

Degree: Master of Engineering

Topic: Effect of geotechnical properties of tailings on the stability of tailings dam facilities

I declare that the above dissertation is my own work and that all the sources that I have used or quoted have been indicated and acknowledged by means of complete references. I declare that my work has not been previously submitted to anyone, and any portion of work submitted in my study has been referenced accordingly. I further declare that I have not previously submitted this work, or part of it, for examination at Unisa for another qualification or at any other higher education institution.

Signature

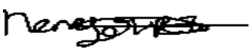

Date

09 June 2026

Acknowledgement

I would like to thank my mother, Mafhungo E, for the moral support she gave me and the words of encouragement that carried me throughout the journey towards acquiring the Master of Engineering.

I have a great appreciation for Mudzielwana G.C., who has been my mentor in the geotechnical aspects of my study; his input and guidance have added significant value to this study. The continuous encouragement he has made has strengthened and fuelled me to push through and aim to produce quality work

I would like to thank my pastor, Bishop Muhali M.G who has assisted with the provision of finances to purchase the laptop, which was a vital study material that enabled me to write my dissertation. I would also like to thank him for the words of encouragement and prayers. I would also like to thank the Prophetess Mathebula T.J. for her prayers and words of encouragement, which helped me not give up during hard times.

The sincere acknowledgment to my friends who have been the pillar of strength and the daily motivation they give me, which pushed me, boosted my hope, and comforted me in difficult times. Their input kept me going.

I appreciate my cousin Mafhungo T and my sister Zhombere K for the financial support they gave me for my studies to progress

I acknowledge the Department of Mining, Mineral, and Geomatic Engineering (UNISA) for the educational and financial support, which enabled me to progress with my studies.

Finally, yet importantly, I acknowledge my supervisor, Dr. Chiloane N.M., for believing in me; this has given me the courage to keep putting effort into my work and the eagerness to deliver the best. Her motivation has increased my growth of interest in furthering my studies to the PhD level.

Abstract

The stability of tailings storage facilities is a great concern in the mining environment. Tailings storage failure releases toxic chemicals into the environment, causing habitat loss, ecosystem disruption, and pollution. The geotechnical properties of tailings, such as shear strength parameters (cohesion and friction angle), pore water pressure, permeability, moisture content, etc, are reported to have a massive influence on the stability of tailings storage facilities (TSF). The main objective of this study is to determine the correlation between the geotechnical properties of tailings and the stability of TSFs by examining how each geotechnical property affects TSF stability. The study was conducted through an experimental analysis of various geotechnical properties, including shear strength, moisture content, pore water pressure, and permeability. Limit equilibrium analysis was employed to quantify the results from experimental analysis of geotechnical properties. RockScience Slide 2 software was used to determine the FoS of tailings materials using the limit-equilibrium methods of analysis (Bishop simplified, Janbu, and Spencer).

The study found that shear strength is the most significant geotechnical parameter influencing the stability of TSF. The study found that shear strength parameters (cohesion, friction angle, and effective stress) are directly proportional to shear strength. An increase in shear strength increases the FoS of the TSF slope and vice versa. This is because shear strength acts as a resisting force against the driving forces (shear stress), which influences the factor of the TSF slope. Moreover, shear strength is significantly affected by various water parameters, including pore water pressure, moisture content, and permeability. The study shows that a higher content of water parameters, such as pore water pressure, moisture content, and tailings' permeability, significantly reduces tailings' stability and, by extension, the stability of the TSF.

This study emphasises that effective management of water parameters is crucial for maintaining the shear strength of tailings material. Water parameters such as moisture content, unit weight of tailings, pore water pressure, and permeability should always be minimised and kept below their maximum allowable limits. Increases in these parameters directly reduce shear strength and, consequently, compromise TSF stability. Future studies should explore remote methods for monitoring the geotechnical properties of tailings. This could involve installing smart sensors around

TSF to continuously assess these properties. Additionally, new technological solutions are needed to monitor and manage water levels in TSF during rainy seasons, as well as to efficiently reduce water levels when slurry is continuously deposited into the TSF.

Table of Contents

List of Figures

List of Tables

Abbreviations

ASTM-	American Society for Testing and Materials
Av-	Average
CBR-	California Bearing Ratio
DVOL-	Dissipative volume
FoS	Factor of safety
g-	Gravitational acceleration
GM-	Gravel sand
GW-	Well-graded gravel
IP-	Induced polarization
LL-	Liquid Limit
LS-	Linear shrinkage
PI-	Plasticity Index
PL-	Plasticity Limit
SL-	Shrinkage Limit

TDF-	Tailing dam failure
TSF-	Tailing storage facilities
PWP-	Pore water pressure
VOL-	Volume
SM-	Silt sand
SP-	Uniform sand/ Poorly graded sand
SW-	well-graded sand
USCS-	Unified Soil Classification System

SYMBOLS

σ :	Normal stress
σ_1:	Principal/primary normal stress
σ_3:	Confining pressure/ stress on the side of the earth material (soil/block of rock)
σ' :	Effective stress
τ:	shear stress/ shear strength
c:	cohesion
γ:	unit weight of tailings
γw:	unit weight of water
ϕ:	Internal frictional angle/ angle of internal friction
τ_f:	shear strength
E:	elastic modulus
ε_v:	(norma/lateral/vertical strain)
ε_{axial}:	Axial strain
Pv:	Poisson's ratio
u:	Pore water pressure Displacement (in calculation equation)
ρ:	density of tailings
ρw:	density of water ($1g/m^3$)
g:	9.8 m/s2
h:	height of water column
&:	and

CHAPTER 1 INTRODUCTION

1.1 Background of the study

Tailings are residual materials from the beneficiation process, which remain after valuable materials are recovered (Owens et al., 2019). They are transported as a slurry through pipes and deposited into constructed ponds called tailings dams (Owen et al., 2019). There has been a sudden rise in cases of Tailings Dam Failures (TDFs) in South Africa (SA) and worldwide (Villavicencio et al., 2014). A study by Stark et al. (2022) shows major reported cases of TDF worldwide that have led to fatalities and severe environmental damage. This includes the Jagerfotein dam collapse in South Africa, which resulted in one fatality (MacRobert, 2022); the Vale dam collapse in Brazil in 2019; the Fundao tailing dam in Brazil; and other notable incidents.

Dareeju et al. (2021) have reported that the rate of tailings dam failure is higher compared to the rate of failure of a normal water dam. The increasing rate of tailings dam failure is attributed to a poor understanding of the properties of tailings and the foundation material (Dareeju et al., 2021). The geotechnical properties of soil have a significant influence on the stability of various engineering structures (Roy and Bhalla, 2017). Poor geotechnical properties of tailings, such as moisture content, shear strength, bearing capacity, density, and specific gravity, lead to instability of tailing dams' slopes, causing tailings dam failure (Hu et al., 2017). Omuwomi (2018) also attests that the poor geotechnical properties of the underlying soil are the major cause of failure in engineering structures (Omuwomi, 2018). For example, the causes of failure of the tailings dams at Mount Polley, Canada, and Samarco in 2014 were undrained shearing of the tailing materials, which reduced their shear strength (Brown and Gillani, 2016).

This research aims to investigate the influence of tailings' geotechnical properties on the stability of tailings dams. The primary objective is to identify critical geotechnical characteristics that contribute to instability and potential failure. This knowledge will be instrumental in developing preventive measures to enhance the overall stability of tailings dams, thereby mitigating the risk of failure. Tailings dam failure incurs significant economic and environmental consequences. This study aims to understand the correlation between Tailings storage facility (TSF) failures and the geotechnical parameters of tailings to reduce the number of TSF failures. A more stable TSF will have a positive economic impact on the mines, as there will be no need for the associated costs of post-failure clean-up and remediation.

To achieve this objective, a comprehensive experimental and geotechnical analysis technique was undertaken. Field sampling of tailings material was conducted, followed by a series of laboratory experiments designed to quantify the relevant geotechnical properties. These properties included moisture content, shear strength, specific gravity, bulk density, and bearing capacity. All sampling and testing procedures adhered to established protocols outlined in the American Association of Highway and Transport officials (AASHTO) and the American Society for Testing and Materials (ASTM) standards to ensure data quality and consistency. To complement the laboratory analyses, a geotechnical analysis technique was employed to assess the slope stability of tailings dam structures. This combined approach provided a robust understanding of the interplay between geotechnical properties and tailings dam stability. Limit Equilibrium methods, such as Bishop, Spencer, and Janbu simplified, were used to present the findings. The limit equilibrium method assumes the factor of safety (FoS) to determine the critical slip surface failure. This study investigates the effects of geotechnical factors in tailings on the TSF, with a particular focus on the use of cohesionless tailings. While numerous studies have assessed TSF stability, there is a lack of documented research specifically addressing the influence of cohesionless tailings on TSF stability.

1.2. Geographical location of the study area

The study area is situated in the northern part of South Africa, specifically in the province of Limpopo. It is situated in the town of Palaborwa, in the Mopani District, on the northeastern border of the Kruger National Park. The map of the study area is illustrated in Figure 1.1.

Figure 1.1: Map of the study area where tailings samples were collected.

The geology of the Palaborwa area comprises an igneous complex, a Paleoproterozoic, pipe-like, alkaline intrusion that formed 2 billion years ago (Decree et al., 2020). The intrusion intruded into the older Archaean granite and gneiss basement formation of the Kapvall craton. The complex consists mainly of host rocks such as Carbonitite, Pyroxenite, and Foskorite. It is the oldest carbonatite complex known in South Africa (Decree et al., 2020; Wu et al., 2011). Palaborwa is famous for its economically valuable minerals, including copper, feldspar, pyroxenite, vermiculite, and apatite. Feldspatic pyroxenite was formed through the interaction of pyroxenite with the surrounding gneiss. Vermiculite was formed as a result of surface weathering of phlogopite in pyroxenite, and apatite was derived from carbonatitic magma through an igneous process from the mantle (Munro and Harris, 2020). The Apoatrite magma also includes the constituents of light rare earth elements (LRRE) (Munro and Harris, 2020).

Two faults have been identified in the Kaapval craton of Palaborwa. These are: the N-Strending mica fault zone and the younger E-W inflecting central fault that consists of the copper mineralisation as fault emplacement/filling (Bassons et al., 2017)

1.3. Aim and objectives of the research

This research aims to investigate the influence of tailings' geotechnical properties on the stability of tailings dams, encompassing both slope and dam foundation stability.

The primary objective is to establish a correlation between the geotechnical properties and the overall stability of these structures. This will be achieved through the following specific objectives:

- To determine the key geotechnical factors of tailings contributing to the failure of tailings dams.
- To evaluate the impact of various geotechnical properties of tailings material on the stability of tailings dam facilities.
- To assess the stability of tailings dam slopes using limit equilibrium geotechnical analysis by quantifying the FoS under varying geotechnical conditions.

1.4. Statement of the research problem

Tailings dam failures pose a significant hazard to mining operations. The exponential growth of mining activities has unfortunately coincided with an increase in reported TSF incidents (Villavicencio et al., 2014). The primary cause of TDFs is often attributed to the unfavourable geotechnical properties of tailings, which directly influence the stability of the dam structure (Dareeju et al., 2021; Lyu et al., 2019). These failures can have devastating consequences, incurring substantial economic and social costs for both the mining company and the surrounding communities (Silva et al., 2024; Kossoff et al., 2014; Lyu et al., 2019).

Tailings consist of fine materials whose stability is easily influenced by moisture content, when compared to coarse-grained soil (Roy, 2017). Studying this earth material will aid in understanding their engineering behavior, thereby enabling effective handling by increasing their stability and reducing the chances of TDFs. A careful geotechnical analysis of tailings' physical properties will reduce the likelihood of dam collapse, thereby protecting the community, livestock, and the natural environment surrounding the mine area (Alshawmar, 2021; Hatjie et al., 2017). The quantitative relationship between the geotechnical parameters of cohesionless tailings and the stability of TSF is not well documented. Therefore, this study employs the limit equilibrium method to address this gap.

1.5. Significance/ justification of the study

Slurry materials are continuously deposited into tailing dams, and because slurry contains a higher volume of water, it reduces the stability of the entire soil mass. This often results in the collapse of many tailings dams (Hu et al., 2017). The proper management of tailing dams is a growing concern in the mining industry, as there has been a sudden increase in tailing dam failures (Hu et al., 2017). Therefore, there is an urgent need to study the geotechnical properties of these tailing materials to advance knowledge of the proper handling of slurry and tailings for the safe design and operation of the tailing dam.

Geotechnical properties of soil have a huge influence on the stability of various engineering structures (Roy and Bhalla, 2017). A tailing dam is one of the engineering structures whose stability is largely influenced by the geotechnical properties of the tailings (Dareeju et al., 2021). There is insufficient information on the geotechnical properties affecting the stability of tailing storage facilities, and limited guidance on how to apply geotechnical engineering to ensure more stable tailing dam storage (Piciullo, 2022). The number of reported cases worldwide is increasing, driven by rising demand for mining resources (Toderas et al., 2023). Further research on how geotechnical properties affect the stability of tailing storage facilities is necessary to ensure the construction of more stable tailing dams (Lyu et al., 2019; Kossoff et al., 2014).

Researchers commonly study various factors that affect the stability of tailing dams, including hydrological, mining, and geological factors. On the other hand, there is minimal focus on assessing the geotechnical properties of residual material as a critical/ major factor causing failure (Kossof et al., 2014). Meanwhile, the safety and stability of tailing dam facilities are a greater concern in mining industries in many countries, including South Africa (Toderas et al., 2023). Geotechnical evaluations are primarily conducted to assess the suitability of soil for road and infrastructure construction in a desired location, with limited geotechnical investigation typically performed before the construction of a tailing dam. This study focuses on the geotechnical analysis of tailings material to understand its mechanical behaviour for the proper handling of these materials. A proper analysis of the soil residual materials mechanism can have a greater positive impact on the stability of tailing dam facilities

Tailing dam failure leads to severe environmental impacts (water and land pollution), increased human fatalities, and loss of biodiversity in the surrounding environment (Hatje et al., 2017). Tailing dam failure requires massive damage control by the mine, resulting in unexpected cleanup costs that are excessive for the mine (Chamber and Higman, 2011). Stability analysis of the tailing's mechanism will play a vital role in addressing the problems associated with tailings dam failures and collapses. The study area was selected at the request of the mine, as its life of mine is extending. Consequently, a stability assessment of the TSF is necessary to determine whether the mine can continue depositing tailings in the existing TSF or should construct a new TSF.

1.6. Structure of the dissertation

This dissertation is organised into five chapters, each addressing a key component of the research process and contributing to a coherent evaluation of the geotechnical stability of the tailings storage facility (TSF).

Chapter 1 introduces the research problem, outlines the objectives and scope of the study, and provides the contextual background necessary for understanding the geotechnical and operational challenges associated with tailings deposition.

Chapter 2 presents a review of relevant literature, covering previous work on tailings behaviour, geotechnical characterisation, and stability assessment methods. This chapter establishes the theoretical foundation for the study.

Chapter 3 outlines the methodology used in collecting empirical data. It details the sampling procedures, laboratory testing methods, analytical techniques, and modelling approaches used to evaluate the geotechnical properties of the tailings.

Chapter 4 examines the influence of key geotechnical factors on the stability of the TSF. Laboratory results, field observations, and analytical interpretations are presented and discussed to assess how parameters such as compaction, density, moisture content, and shear strength affect the facility's overall performance.

Chapter 5 focuses on the limit equilibrium analysis of the study. It describes the development of the stability models, boundary conditions, material parameter selection, and simulation outputs. The chapter evaluates how the TSF's slope FoS responses contribute to understanding the TSF's stability under various loading and environmental scenarios.

Chapter 6 presents the study's conclusions and offers practical recommendations. It synthesises the key findings, evaluates their implications for TSF design and management, and suggests areas for future research to strengthen geotechnical understanding and operational safety.

Chapter 2 Literature Review

2.1. Introduction

This section reviews some of the exceptional studies done by notable researchers on the stability analysis of tailing dams. This section examines the findings of other studies on soil geotechnical properties. This includes: (i) identifying and defining those geotechnical properties of soil that mainly influence slope stability; (ii) unpacking how the stated geotechnical properties of soil influence slope stability and foundation stability.

These tailing dams are also known as tailing storage facilities (TSF). Slurry materials are continuously deposited into tailing dams. Since slurry contains a higher volume of water, it reduces the stability of the entire soil mass, which often leads to many tailing dams collapsing (Hu et al., 2017). There has been a sudden rise in Tailing Dam Failures worldwide and in SA (Villavicencio et al., 2014). The increasing rate of tailing dam failures reflects a poor understanding of the properties of tailings and the foundation material (Dareeju et al., 2021). TSF failure cases are common, causing environmental pollution and contamination of aquatic bodies, destruction of the ecological habitats of flora and fauna, and harm to the communities surrounding the dam (Adamo et al., 2020).

A study by Stark et al. (2022) reveals a significant number of reported tailing dam failures worldwide, resulting in fatalities and severe environmental damage. This includes the Jagerfotein dam collapse in South Africa, which resulted in one fatality (MacRobert, 2022; Marais, 2024). A Vale dam collapsed in Brazil in 2019 (Jamasmie, 2019). The Fundao tailing dam in Brazil that took 17 lives in 2015 (Palu and Julien, 2019; Stark, 2022). The Brumadino dam in Brazil that killed 270-320 people (Lumbroso, 2020; Zhu et al., 2024). Mount Polley dam in Canada, the Samarco dam in 2014 (Brown and Gillani, 2016), and other cases of TSF failure. Tailings dam failures pose a significant hazard to mining operations. The primary cause of tailing dam failure is often attributed to the unfavourable geotechnical properties of the tailings, which directly influence the dam's stability (Dareeju et al., 2021; Lyu et al., 2019). These failures can have severe consequences, incurring substantial economic and social costs for both the mining company and surrounding communities (Kossoff et al., 2014; Lyu et al., 2019).

A comprehensive literature review was conducted to examine geotechnical factors influencing the stability of TSFs. The search was conducted across multiple reputable databases, including ScienceDirect, ResearchGate, Nature, Google Scholar, and Scopus. Geotechnical elements, particularly the mechanical properties of tailings, are recognized as essential for maintaining slope stability in these structures (Roy and Bhalla, 2017). Nonetheless, there is insufficient information on the geotechnical properties affecting the stability of TSFs, and little guidance on how to apply geotechnical engineering to ensure more stable tailing dam storage (Piciullo, 2022). However, the number of reported TDF cases worldwide is increasing, driven by rising demand for mining resources (Toderas et al., 2023; Stark et al., 2022). Further research on how geotechnical properties affect the stability of tailing storage facilities is necessary to ensure the construction of a more stable tailing dam (Lyu et al., 2019; Kossoff et al., 2014).

Shear strength, bearing capacity, dry density, Moisture content, and particle size distribution are some physical properties of soil affecting slope stability (Rahman et al., 2019). Studies by Owen et al. (2019) and Toderas et al. (2023) suggest that tailings dam failure is significantly influenced by the geotechnical characteristics of the tailing materials stored within. This section also reviews the geotechnical properties of tailings as a root cause of tailing dam failure, as well as the hydrological factors affecting tailing dam stability. This is intended to provide a comprehensive understanding of soil geotechnical properties.

2.2. An overview of geotechnical parameters of tailings affecting tailing dam stability

Physical parameters influencing the design selection, stability, and drainage of the impoundment are relative density, particle size distribution, shear strengths, and stress parameters (Islam, 2021). Poor geotechnical properties of tailings, such as moisture content, shear strength, bearing capacity, density, pore water pressure, and permeability, lead to instability of tailing dams' slopes, causing tailing dam failure (Hu et al., 2017). Wang (2021) also attests that these poor geotechnical properties of the underlying soil are the major cause of failure of engineering structures. Particle size distribution, composition, and mineralogy of tailings, as well as consolidation and compaction, void ratio, and porosity, are among the physical properties that play a vital role in selecting an appropriate tailing dam design.

2.2.1. Particle size distribution

Particle size distribution (PSD) refers to the analysis of particle size ranges, such as clay, silt, and sand, within a soil sample. Particle-size gradation of soil is a classification that categorises particles into coarse-grained, fine-grained, or gravel-size fractions (Koohmishi and Azarhoosh, 2020; Musbahh, 2014). It is essential in stability analysis because it determines geotechnical properties such as permeability, shear strength, and density (Bhanbhro, 2014; Witt et al., 2004). Soil particle size can be either well-graded or poorly graded, depending on the arrangement/structural alignment of grains in a soil mass (Sivakugan, 2000). Soil is considered well-graded if it has a good range and distribution of coarse-grained soil mixed with fine-grained particles (Sivakugan, 2000). It is therefore important to conduct a PSD analysis during the construction of an engineering structure, such as a TSF, to enhance the stability of the foundation. Soil texture (coarse- and fine-grained soil) influences soil shear strength in different ways (Chen et al., 2023; Wen et al., 2018). A study conducted in the Ganakbari area of Dhaka has found that montmorillonite clay has lower strength than kaolinite and illite. Kaolinite has higher strength than the aforementioned clay minerals (Haque et al 2013). However, when sand is mixed with montmorillonite, it gains greater strength than plain kaolinite (Haque et al., 2013). Well-graded soil has greater shear strength, which makes it stable.

Park et al (2017) discussed the relationship between soil texture (fine and coarse grains) and soil stability. Their article aimed to investigate the impact of fine-rich content soil on physical properties, including density, void ratio, moisture content, and quick undrained shear strength. Static standard penetration test (SPT) and cone penetration test (CPT) were conducted to determine shear strength and density, respectively. The findings revealed that an increase in soil coarse content leads to a corresponding increase in rapid undrained shear strength. This indicates that increasing the coarse-grain size of saturated soil increases its shear strength, allowing it to resist shear stress (Wen et al., 2018).

Saturated fine-grained tailings have low cohesion, which therefore leads to poor shear strength (Zhang et al 2022a). This is because the water content in saturated tailings reduces friction between tailings particles, causing them not to adhere to each other and therefore to lose their stickiness (cohesion) (Yang et al., 2016). When subjected to stress, they contract and their pore water pressure increases, rather than consolidating as unsaturated tailings do (Dimitrova and Yanful, 2012). On the contrary, saturated coarse-grained soil has higher inter-particle friction; as a result, it is stronger and more stable (Lees, 2024). Clay soils are fine-grained materials, and their cohesion increases when they are dry, making them stiffer and stronger (Du et al., 2023). However, when a large amount of water is continuously added, it loses its capacity to stick together; instead, it shears, slides, and weakens (Du et al., 2023). Fines are made up of silt and clay sizes ranging from grain size less than 0 to 0.05 mm, followed by course particles ranging from 0.05 to 2mm according to the U.S Department of Agriculture (USDA) classification (Musbahh, 2014). A high content of fines in foundation soil reduces bearing capacity and, therefore, reduces soil stability (Rad et al., 2024). The weak interconnection between fine-grained soils makes them deform easily under external loads (Zhang et al., 2022b).

It is essential to evenly control the deposition of both coarse- and fine-grained tailings to enhance tailing stability (Li et al., 2019). The mechanical strength of tailings varies with different grain sizes (Tians et al., 2022). It is worth noting that water content significantly influences the particle size distribution and gradation of tailing particles (Nie et al., 2023). However, particle size, shape, and texture control the movement of water through soil, thereby affecting its stability (Zamara, 2024). A study by Nie et al. (2023) has demonstrated that particle gradation changes when a high volume of water passes through tailings. Therefore, changing the strength and density of tailings, particularly during heavy rain seasons, is necessary.

2.2.2 Void ratio, porosity, and permeability

Void ratio is defined as the ratio between the volume of pore spaces in a soil and the volume of particles in a soil (Meng et al., 2025). According to Xu et al. (2019), the void ratio of the entire soil mass is significantly influenced by particle-size distribution (PSD) and particle shape. An article by Xu et al. (2019) indicates that finer particles are the primary factors affecting the void ratio. Tailings usually consist of finer particles since they are the by-product of the beneficiation process; hence, the void ratio has a significant impact on the tailings and stability of the tailing dam. Additionally, irregular particles have a higher void ratio due to reduced particle contact, leading to more voids/pores between particles/grains (Xu et al., 2019). Void ratio, on the other hand, has a direct influence on the permeability, shear strength (internal friction angle and shear stress), and compressive properties of soil (Shinohara et al, 2000). Thus, the void ratio is a function of particle size and particle shape, which together determine shear strength and soil permeability (Abu et al., 2025).

Particle shape affects the shear resistance of granular soil (Abu et al., 2025; Zamara, 2024). This is because particle shape affects the interconnection/interlocking between grains, which, in turn, influences the sliding mechanism between grains (Roy and Bhalla, 2017). The interconnection between grains also influences hydraulic conductivity (permeability) and, therefore, the stability of soil material (Roy and Bhalla, 2017; Zamara, 2024). Highly angular particles resist displacement between particles compared to less angular particles; therefore, they exhibit lower deformation (Ali et al., 2023; Mahinroosta and Oshtaghi, 2021). This results in soil with high angular particles exhibiting high shear strength and being more stable than soil with fewer angular particles.

Meanwhile, porosity is the percentage of voids in a given mass of material (soil/rock) and represents the percentage of open spaces (pores/voids) in that mass (Cameron and Buchan, 2008). Pore spaces can be filled by either air or water, whereby the water exerts pressure on the tailing's material (Hoissain et al 2021). Tailing dam failure is caused mainly by pore pressure (US EPA, 1994). According to Reid (2013), the normal forces exerted by water within pore spaces in a porous material are known as pore pressure. This is because the force exerted by pore water on the tailings affects the amount of water transmitted through the porous tailings (Zardari, 2011). An increase in the tailing's pore pressure reduces the tailing's effective stress by rearranging the tailings particles, thereby reducing the shear strength of the tailing (Morton, 2021; Zardari, 2011). Pore water pressure affects the undrained shear strength and stability of soil (Wu et al., 2021; Zhou et al., 2016). This occurs when pore water affects the soil's friction angle and cohesion (Zhou et al., 2016). An increase in pore water pressure reduces the frictional angle and particle cohesion, lowering shear strength and stability (Zhou et al., 2016). A study by Padovani and Bretas (2023) posits that overloading during TSF construction (especially during the addition of raises/levels) leads to pore pressure buildup. The pore pressure will therefore lead to a failure of the undrained shear strength of foundation materials (soil/tailings) and a reduction in TSF stability.

The ability of a material to transmit fluid is known as permeability (Mondol et al., 2008), according to Cal and Barik (2020). Permeability is similar to hydraulic conductivity, which is the ability of a fluid to pass through soil pores. (Cal and Barik, 2020). It is a parameter commonly used to analyse geotechnical problems, such as shear failure, and is also used for seepage monitoring and control (Boadu, 2000).

The Swiss in the early 1990s developed the soil permeability guideline (SN 670 010b), presented in Table 2.1, for every soil texture, from silt to gravel-sized particles. This guideline was amended by Starck et al. in 2017 and was issued by the Association of Swiss Road and Traffic Engineers. The permeability guideline provides characteristic coefficients and correlations for various soil properties, including permeability (hydraulic conductivity).

Table 2.1: Depicting the Swiss guideline for permeability of soil (Starck et al., 2017)

soil coefficient of permeability guidelines		
soil description	**k (m/s)**	**degree of permeability**
gravel	10^{-3}	highly pervious
sandy gravel, clean sand, silty sand	10^{-3}-10^{-5}	medium
sand, dirty sand, silty sand	10^{-5}-10^{-7}	low
silt, silty clay	10^{-7}-10^{-9}	very low to impermeable
clay	<10^{-3}	practically impermeable

Fluid transmission is readily achieved in a soil mass with interconnected voids (Cal and Barik, 2020). Permeability is primarily determined by particle and pore size distributions, porosity, compaction and consolidation properties, and soil geometry (Ati and Kareem, 2014; Bhanbhro, 2014). Fine-grained soils have low permeability and low strength, which consequently reduces their stability (Hu et al., 2017). Water passing into or through soil pores affects soil strength and stability; consequently, permeability affects geotechnical settlement and soil slope stability (Zamara, 2024). According to Darcy's law, the rate of water flow through the soil depends on the hydraulic gradient (the pressure difference between two points) (Zamara, 2024).

Meanwhile, the clay-rich soil swells when additional moisture saturates the soil material, resulting in reduced pore sizes and narrowing of pore channels (Flit and Flit, 2002). The small pore channels, in turn, affect soil porosity, permeability, and bulk density, thereby influencing its stability (Flit and Flit, 2002). On the other hand, a sandy soil mass has large pore spaces but fewer pores (porosity) than clay soil. As a result, their porosity is low and quickly drains water (Cameron and Buchan, 2005). On the contrary, clay soil has many pores and small pore spaces, which give it high porosity and allow it to store water (Cameron and Buchan, 2005). This attests to the capacity of tailings (fine-grained material) to store large amounts of water, which reduces their internal friction angle and, consequently, their shear strength, thereby decreasing the stability of TSF.

Figure 2.1 depicts how porosity and permeability largely depend on the void ratio, particle size, and particle shape (which determine the interconnection of pore spaces). The diagram illustrates that when pore spaces are interconnected in a soil mass, water can be easily transmitted through the pores, allowing more water to be stored in the porous medium**.** A porous, permeable soil allows high water transmission through well-connected pore spaces (Wolschick et al., 2021). Top-layer tailings that are porous and permeable will allow rainfall water to seep into the tailings dam. As a result, water content will increase and reduce the shear strength of tailings, thereby reducing TSF stability (Duong et al., 2013). It is also evident in the diagram below that the soil mass can be porous but impermeable (i.e., with no interconnection between pore spaces). This type of soil structure has poor drainage, allowing accumulated water to remain in the soil for a long duration, increasing pore water pressure and thereby reducing stability (Lees, 2020).

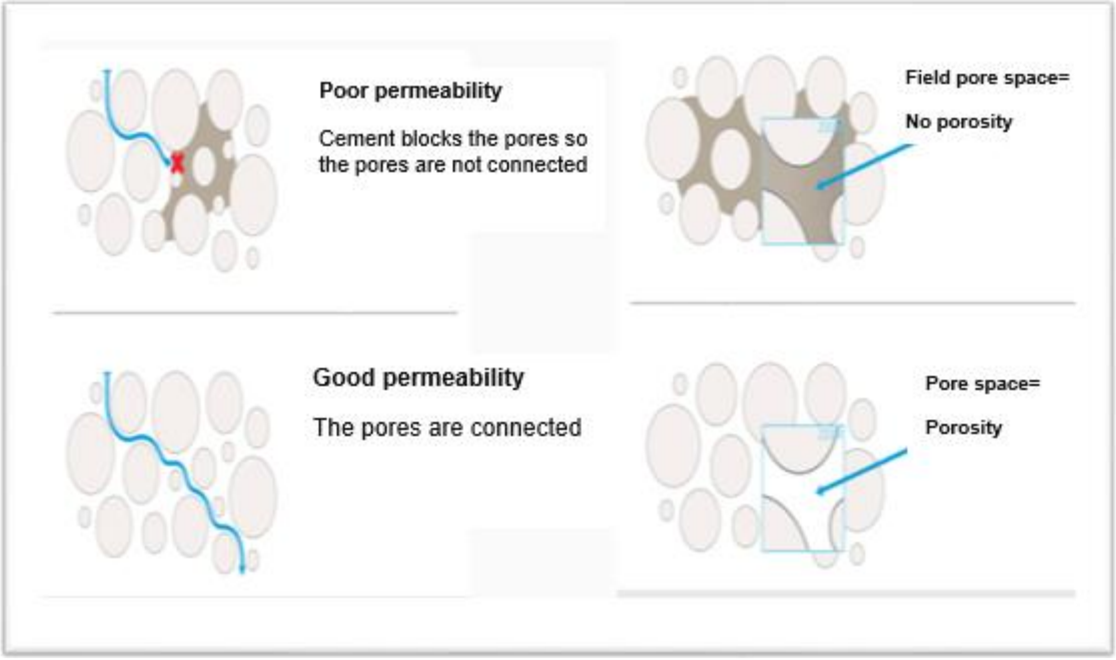

Figure 2.1: The relationship between porosity and permeability (Resource Victoria, 2021)

Under static loading, pore-water pressure increases, reducing the shear strength, bearing capacity, and stability of the foundation soil. Tailings mostly have uneven particle size, which increases their permeability, and consequently are usually saturated with reduced stability (Hu et al., 2017; Pan et al., 2021)

2.2.3. Consolidation and compressibility characteristic

Consolidation is a natural process of compaction of soil grains, expelling water from the soil over a long period due to external pressure from the overlying load (Evans et al., 2021). The consolidation process depends mainly on the texture of the materials (fine/coarse), the gradation of the material (particle arrangement), and the particle distribution (US EPA, 1994). Consolidation also depends on permeability, as permeability controls the rate at which water is expelled from the soil during the consolidation process (Jayalekshmi and Elamathi, 2017). The stability of the tailing dam is influenced by the consolidation and compression characteristics of materials (Zardari, 2011). Additionally, consolidation also controls the deformation mechanism of tailings by destroying the pore structures between particles and rearranging the particle structure (Tian et al., 2022). Meanwhile, Hu et al. (2017) add that fine tailings exhibit high compressibility characteristics and are unstable. A study by Wiklund (2018) affirms that an increase in the content of fine particle tailings increases compressibility. The study also shows that consolidation increases particle settlement when fine particles migrate to fill the voids between coarse particles, thereby increasing stability.

Soil compressibility is the ease with which soil decreases in volume when subjected to a mechanical load (Ahmed and Siddiqua, 2016; Sridharan and Gurtug, 2005). The change in void ratio with increasing effective stress influences compressibility. For highly compressible soil, the change in void ratio will be greater. Compression influences consolidation and increases soil stability (Ahmed and Siddiqua, 2016). This occurs when compressional forces applied affect the effective stress and the soil's void ratio. Consolidation of tailings in a TDF reduces porosity because of the applied pressure from the tailings loaded during the construction of tailings dykes/raises (Vick, 1990). Consequently, moisture content is reduced by the expulsion of water from the pores/voids of tailings (Ahmed and Siddiqua, 2016). During tailings deposition, the constant pressure exerted by the tailing load compresses the grains, decreasing porosity and the void ratio. This process improves the soil's stability and strength. A study by Mondol et al. (2008) adds that the compaction of mudstone under a particular effective stress depends on its mineralogy, grain size/stiffness, grain framework, pore fluid, and pore pressure. This attests that compaction, consolidation, and compressibility depend on factors such as mineralogy, particle gradation, and pore pressure. The consolidation process increases the shear strength and dry density of materials, thereby enhancing material stability and reducing the risk of failure (Zhang et al., 2019; Nie et al., 2023).

2.2.4. Bulk density

Soil bulk density is defined as the ratio of the mass of oven-dried soil to its bulk volume at field moisture content (Askin T and Ozdemir, 2003). It is an indicator of soil compaction; it measures the degree to which the soil is tightly packed or dense (Nawaz et al., 2013). Compaction is defined as the densification and distortion of soil by which the total air-filled porosity is reduced (Greory et al., 2015). Soil compaction rearranges soil particles into a closely packed structure, thereby reducing soil volume and increasing soil density (Evans et al., 2021). Compaction and cementation increase the dry density, consequently increasing the inclusion of soil particles in the arrangement, the friction angle, and the cohesion (Kang et al., 2022). This tends to strengthen soil particles and thereby increase the shear strength of the soil

Geotechnical parameters such as bulk density, strength, and porosity can be used to quantify the soil compactness. Soil compaction directly influences the aforementioned soil geotechnical properties (Nawaz et al., 2013). An increase in soil density through compaction enhances soil stiffness, thereby reducing permeability and compressibility and, in turn, reducing shear stresses. Consequently, increasing the shear strength and bearing capacity of the soil during construction (Ebels et al., 2004). The stability of soil depends on its unit weight; unit weight is used to determine soil density (Guyer, 2013a). Conversely, poor compaction reduces bulk density; therefore, soil with low bulk density has higher permeability. In this case, seepage that occurs during excessive rainfall tends to decrease soil stability (Guyer, 2013a).

The required bulk density for a fine-grained clay soil ranges from 1.0 to 1.3 g/cm^3 (McCarty et al., 2015). Fine soil generally has a lower bulk density than coarse-grained soil, ranging from 1.4 to 1.8 g/cm^3 (McCarty et al., 2015). It is for this reason that most TSFs are unstable, as tailings are typically fine-grained and naturally exhibit lower stability compared to coarse-grained soils (Hu et al., 2017). Whereas soil with high bulk density tends to be more compacted and stable (Reddy, 2020). Furthermore, Askin and Ozdemir (2003) postulate that soil bulk density depends on the soil particle-size distribution, which, in turn, influences soil porosity and pore-water pressure. Consequently, these geotechnical factors are interconnected and exert a reciprocal influence on the stability of the TSF.

2.2.5. Moisture content

Moisture content is the percentage of water in soil or other earth materials, such as tailings**.** Soil moisture content is an indicator of the amount of water present in the soil mass, expressed as a percentage (Hossain et al., 2021). Moisture content is defined as the ratio of the mass of water present in pore spaces of the soil sample to the mass of the dry soil sample or the ratio of the volume of water in the soil to the volume of dry soil sample (Hossain et al., 2021). Increased soil moisture content diminishes its shear strength (Dhawele and Harle, 2017). According to Bidyaswari et al. (2017), slopes begin to deform as moisture content increases, intensifying slope collapse. This is because a higher moisture content reduces the van der Waals forces and frictional forces between soil particles, allowing them to slide across each other and shear (Yang et al., 2016). Moisture content softens soil, weakens the inter-particle bonding, and consequently decreases cohesion, friction angle, and shear strength (Kang et al., 2022).

The Brumadinho dam failure in 2019, which resulted in 270 fatalities, was caused by a slip surface failure triggered by excessive rainfall (Zhu et al., 2024). The primary reason for the worst incident of Fundao tailing dam failure in Marian in 2015 was the liquefaction of tailings sand and insufficient drainage (Mining Weekly, 2024). Liquefaction of soil is a process in which the strength and stiffness of soil are reduced by earthquake shaking and other rapid loading, causing it to behave more like a liquid (Ben-Zee et al., 2023). In this instance, the force from the earthquake has increased the pore water pressure between sand particles, pressing them tightly together and, as a result, causing them to lose their mechanical resistance and gain liquid characteristics (Carmo et al., 2017). The instability was influenced by excessive water, which reduced the undrained shear strength and ultimately led to TSF failure.

Moisture content increases the degree of saturation of the residual material and its pore-water pressure (Tiwari et al., 2016). A research study by Nie et al (2023) attests that an increase in water affects the friction angle of tailings and, consequently, their shear strength. Excessive rainfall can lead to high soil water content, reducing soil shear strength and causing deformation and failure of soil masses (Villavicencio et al., 2014; Wu et al., 2022).

A research study by Nie et al. (2023) attests that an increase in water affects the friction angle of tailings and, consequently, their shear strength. Rainfall may affect the seepage field of the tailings by influencing the level of the phreatic line (the lifeline of tailing dam stability) (Wu et al., 2022). This occurs when increased rainfall and flooding raise the phreatic line (saturation line). The residual materials become saturated, increasing the dam's weight and reducing its shear and effective strengths, leading to deformation (Lyu et al., 2019; Wu et al., 2022).

Jagerfotein dam ceased operating around 1970; however, in 2022, due to excessive rainfall caused by the Lanina cyclone, it collapsed (Mintek Industrial News, 2024). The seismic activity also contributed to the Jagerfotein dam failure through liquefaction, which caused the tailings material to behave more like a fluid, ultimately leading to the dam's rupture (Mintek Industrial News, 2024). The dam that collapsed in Brazil in 2019 is believed to have been largely caused by the continuous rainstorm, which reduced the stability of the tailing dam (Wu et al., 2022; Zhang et al., 2022a). Rainfall has also destabilised TSFs, leading to TSF failures in China and the Ajka red mud reservoir failure in Hungary (Nie et al., 2023). This shows a practical example of rainwater increasing moisture content, causing a sudden rise in pore-water pressure and, consequently, reducing the stability of the TSF.

Rainfall also affects the particle size distribution of tailings, thereby reducing the material's shear strength (Tiwari et al., 2016). This occurs when water infiltrates through the tailings and washes fine particles from the top to the bottom of the dam (Nie et al., 2013). As a result, the particle grading rearrangement caused by rain leads to an uneven spatial distribution of the mechanical properties of tailing, such as cohesion, internal friction angle, and density (Nie et al., 2023). A seasonal variation (due to rainfall) in soil moisture content affects soil shear strength, which may lead to the failure of tailing facilities (Jamaismie, 2019). Variation in moisture content also affects the total volume of soil. This is because an increase in moisture content causes contact with soil particles and an increase in shear stresses, which reduces shear strength and the stability of the tailing dam in general (Shehu and Abdulfatah, 2019).

2.2.6. Mineralogy and expansive characteristics of tailings

Mineral composition refers to the chemical constituents of a soil mass; a mineral is an aggregate of chemical elements. The mineral content of the tailings depends on the ore deposit's mineralogy (Adamo et al., 2020). Musbahh et al. (2024) have studied and documented the correlation among mineral content, compaction characteristics, and particle size. The authors substantiate that mineral content has a direct impact on compaction and Atterberg limit (plasticity, liquid limit, and plasticity index). Mineral tailings have the composition of a mined ore; therefore, the chemical composition of TSF will differ from one ore to the next. Various studies have investigated the relationship between mineral composition and stability. Quartz is the most abundant mineral found in many tailings (Wang et al., 2022). It has greater durability, enhancing its stability and reducing its susceptibility to settlement (Musbah et al., 2024). As a result, TSFs containing quartz minerals have increased the stability of tailings with quartz content. The mineral composition of soil influences its permeability and hydraulic conductivity, which, in turn, determine its stability (Zamara, 2024). The mineral composition also significantly influences bulk density and hydraulic conductivity. A practical example is Iron oxide mineral, which increases bulk density, reduces porosity, and hydraulic conductivity, resulting in a reduction in stability (Ati and Kareem, 2014)

The mineral composition of soil and the arrangement of its particles influence soil flexibility (the ability of soil material to change shape) and increase its plasticity, thereby reducing soil stability (Musbah et al., 2024). Flexible soil is that which contains a high percentage of expansive minerals, such as montmorillonite clay mineral, that could respond to a short-term moisture content variation (Musbah et al., 2024). A study by Elan et al. (2024) reveals that clay minerals, including montmorillonite, Smectite, illite, and kaolinite, are the main mineral constituents with a high water content. However, Montmorillonite is the most common clay mineral with swelling properties (Adamczuk et al., 2022). This water content leads to poor soil stability, which is influenced by low permeability, high plasticity, high compressibility, and a strong swelling characteristic of clay soil (Aksu et al., 2015). A study by Ural (2018) indicates that the presence of clay minerals in soil reduces compressive strength and increases shrinkage. Infrastructures such as schools, houses, and pavements were damaged in Iraq due to swelling clay minerals, which caused the expansion of foundation soils (Enad et al., 2024). The expansion/swelling characteristics of clay mineral-rich soils affect soil plasticity, thereby influencing its stability (Ikeagwuani and Nwonu, 2019). This occurs when soil volume changes significantly with water addition and drying (Enad et al., 2024).

The swelling properties of soil reduce the stability of soil structures and slopes and increase the risk of failure. Adding waste glass powder (WGP) reduces the swelling characteristic of soil containing clay minerals, thereby increasing its stability (Enad et al., 2024). The type of swelling soil expands upon wetting and shrinks upon drying, which renders it unfit as foundation soil (Behzad-Kalantari, 2012).

2.2.7. Shear strength (friction angle and cohesion)

Shear strength is a measure of the soil's capability to resist failure when the load that generates shear stress is exerted (Evans et al., 2021). Cohesion and frictional resistance between soil particles influence shear strength (Harabinova and Panulinova, 2020). Shear strength is a key geotechnical property that influences stability, amongst other geotechnical properties (Tian et al., 2022). It has a significant impact on both the foundation soil and the overall stability of tailings (Hussain et al., 2022; Lyu et al., 2019). Visagie and Bezuidenhout (2022) posit that a low shear strength of slope material causes instability of the TSF. Shear strength is a function of parameters such as cohesion and internal friction angle (El Hariri et al., 2023).

The strength of the tailings, which determines the stability of the TSF, depends primarily on the friction angle and its cohesion (Liu et al., 2012). The friction angle indicates the resistance to sliding between grains of tailings in a tailings mass. It determines how much shear stress the tailings can withstand before failure. It is used to determine the frictional shear resistance of the tailings slope to failure (Christian and Baecher, 2015). The friction angle has a significant impact on stability estimation (Fiolleau et al., 2023). Mud soil usually has a friction angle of 0° because the soil is in a liquid state and has no slope. Poor soil has a friction angle of 15°, whereas a friction angle of 30° is categorised as good soil. A soil friction angle above 30° improves shear strength and is stable. In contrast, a friction angle below 30° reduces overall shear strength and is considered unstable, posing a greater risk of slope failure (Watkins et al., 2010).

Cohesion is the ability of soil particles to adhere to one another and is most commonly found in soils with a higher content of fine particles, such as clay and silt. The internal friction angle is responsible for interlocking between particles as they slide during shearing; it represents the resistance to shear force/stress. These two parameters are responsible for resisting deformation and failure that is driven by shear stresses applied, thereby increasing the stability of soil (El Hariri et al., 2023). Cohesion is a strength parameter that determines the frictionless factor, Van der War force, and electrostatic force of a soil. These parameters aid in shear resistance and enhance soil stability (Lu and Likos, 2013). It is a measure of the intermolecular forces in soil structure (Budhu, 2010). Slope stability of cohesionless/non-cohesive soil (typically soil with a high coarse content of sand/gravel) depends on the internal friction angle, slope angle, unit weight of the soil, and pore pressure. On the contrary, the slope stability of cohesive soil (usually soil with a high content of fine clay and silt-sized particles) depends on the plasticity and elastic modulus (soil stiffness) between soil particles, soil strength, pore pressure, and slope height (Guyer, 2013b). Slopes composed of soil with a high friction angle have higher shear strength, can withstand shear stress, and remain stable (Harabinova and Panulinova, 2020). Sliding between particles in the slope of cohesive materials reduces shear strength and causes slope failure (Guyer, 2013a). Soil with low shear strength can cause instability in engineering structures (Oyidirn and Famakinwa, 2015; Mohamad et al., 2016). According to Mohamad et al. (2016), soil is considered to have low stability if its shear strength is less than 40kPa. On the contrary, soil is considered stable when its shear strength ranges between 75-150 kPa (Davisons and Springman 2000). The causes of failure of the tailing dams at Mount Polley, Canada, and Samarco in 2014 were undrained shearing of the tailing materials, which reduced their shear strength (Brown and Gillani, 2016). The failure of several buildings in Lagos (South-Western Nigeria) has been attributed to low shear strength, leading to ground instability (Oyidirn and Famakinwa, 2015).

An assessment of tailings shear strength in a TSF was undertaken to determine the FoS of the tailings dam. Brown and Gillani (2016) reported that the cause of the dam failure in Canada of Mount Polley dam and Mount Polley dam in Brazil was poor undrained shearing that occurred when pore water pressure reduced the tailing's shear strength and stability, leading to dam failure. Investigations conducted after the dam failure indicate that Mount Polley was constructed on a glacial lake composed largely of clay (Chambers, 2015). The shear stresses on foundation clay soil resulting from water and the load of the overlying TSF cause shear movement that makes the dam slide, rupture, and lead to TSF failure (Chambers, 2015). Likewise, moisture content, compaction, and particle shape are the three factors that influence the soil's internal friction angle (Kang et al., 2022). This occurs when a change in particle arrangement causes them to interlock, increasing their friction angle, stiffness, and strength. An increase in the moisture content of clay soil reduces the occlusion friction between particles and cohesion, thereby reducing the shear stress. This is one of the major factors influencing shear strength, along with soil cohesion and the internal friction angle (Roy and Bhalla, 2017).

2.2.7.1. The relationship between the Mohr-Coulomb theory of tailings and the shear strength of tailings

Mohr-Coulomb failure theory states that the failure of earth materials, such as soil/ rock, occurs when the shear stress on a plane reaches a critical value, based on the relationship between the normal and shear stresses of soil (Hoek and Brown 1997). It is utilised to determine the conditions at which the material will fail (Labuz and Zang, 2014). The Mohr-Coulomb failure envelope is represented as a straight line on a plot of normal stress versus shear stress. The materials' failure conditions, presented as a combination of normal and shear, plot on a straight line, termed a failure envelope (Labuz and Zang, 2014; Hoek, 1999). The failure envelop example is illustrated on Figure 4.1. It describes the prediction of soil shear strength based on the relationship between the normal stress at failure and the shear stress at the failure plane (Hoek 1999; Hoek and Brown, 2002). The combination of stresses below the failure envelope illustrates that the conditions of materials that have not led to failure until the plot reaches the failure line, which represents the point of stress combination where failure occurred (Hoek and Brown 1997; 1998).

The friction angle is the angle at which the shear stress and the normal stress intersect at the point of the failure envelope. The higher the frictional angle, the higher the shear strength and, therefore, the greater the capacity to resist various stresses that influence failure (Watkins et al., 2010).

2.2.7.2. Relationship between the Elastic modulus of soil and shear strength

The elastic modulus of soil is a physical property that determines the soil's stiffness. It is a property that influences soil shear strength. Elastic modulus is a function of soil type, soil compaction level, and burial depth (an increasing soil strength by increasing pressure) within the soil mass (Watkins et al., 2010). It represents the strain-stress relationship, which influences soil stiffness. Elastic modulus is a physical property used in the design of structures, such as tailings dams, to ensure a safe foundation and to further evaluate their stability (Waheed and Asmael, 2023). It is an important parameter used in the numerical modelling of slopes to determine the stability of structural slopes (Waheed and Asmael, 2023). The elastic modulus of granular/coarse soil was classified under the Unified Soil Classification System (USCS) by Obrzud and Truty (2012), based on Keldi. The elastic modulus classification of granular soil is presented in Table 2.2. The table presents the elastic modulus for well-graded gravel (GW), uniform sand/poorly graded sand (SP), Gravel sand (GM), well-graded sand (SW), and silty sand (SM).

Table 2.2: USCS classification of elastic modulus by Kezdi 1974 and Prat et al 1995 (Obrzud and Truty, 2012)

Typical USCS values of soil Elastic modulus				
Unified soil classification system (USCS)	Loose	Medium	Dense	Si unit
Well-graded gravel (GW), well-graded sand (SW)	30-80	80-160	160-320	MPa
Uniform sand/poorly-graded sand (SP)	10-30	30-50	50-80	MPa
Gravel sand (GM), Silty sand (SM)	7-12	12-20	20-30	MPa

2.2.8. Bearing capacity of foundation material

Bearing capacity refers to the ability of the underlying rock and soil layer to support the load of the overlying TSF. Poor foundations are those with underlying materials (rock and soil layers) incapable of supporting the load of a TSF (Adamo et al., 2020). The safe bearing capacity for clay soil should range from 75 to 100 kN/m² (Lees, 2021). The acceptable bearing capacity for all engineering structures ranges from 68 to 15 kN/m² (Oyidirn and Famakinwa, 2015). The internal friction angle is a key parameter used to calculate the shear strength and bearing capacity of foundation soil, and thus plays an important role in assessing stability. A higher internal friction angle usually indicates a soil that is highly resistant to deformation/failure, resulting in a more stable foundation.

Fine-grained materials are known to have lower bearing capacity than coarse-grained materials (Roy and Bhalla, 2017). Consequently, the TSF foundation that is constructed of tailings will have poor bearing capacity and be less stable compared to coarse-grained soil and other coarse materials. Chambers (2015) explained in his article on the review of causes of failure of the Mount Polley dam in Brazil in 2014 that the foundation soil was made of clay that lost its shear strength due to the increase in water content and overlying load of the TSF.

The weight of the overlying Mount Polley dam also increases the shear stress on the clay particles of the foundation soil underneath the dam, causing the dam to slide and rupture. (Brown and Gillani, 2016; Chambers, 2015; Zabolotnii et al., 2022). The capability of the underlying material to carry the load of TSF without failure depends on the strength parameters (cohesion and friction angle) of such materials (Evans et al., 2021). The loading of engineering structures during construction increases the driving forces while reducing the resisting forces, thereby weakening the soil's strength and leading to failure (Dong et al., 2020). The driving forces increase between tailing particles and foundation soil particles in response to the overlying TSF load, consequently reducing the bearing capacity of a foundation soil and stability of the entire TSF (Rad et al., 2024).

Conclusions drawn from the investigation into the causes of the Mount Polley dam failure in Canada identified TSF design-related errors and drainage problems (Morgenstern et al., 2015). The design error was made due to poor stability analysis of the foundation soil before dam construction (Brown and Gillani, 2016; Chambers, 2015). The foundation soil was later found to be unstable clay soil that lost cohesion under higher water content of tailings and stress due to a higher amount of TSF load, causing the base clay to slide, resulting in dam rupture and collapse (Zabolotnii et al., 2022).

2.3. Brief overview of tailings dams design and construction

The materials used in the construction of tailings dams are selected based on their physical characteristics, such as shear strength, to ensure stability (Hu et al., 2017). The design and height of the tailing dam rely on the strength of materials used for the embankment and the strength of the tailings (Branch, 1994). In the design process, it is crucial to consider construction methodologies, embankment design, and the positioning of internal seepage control drains. Material selection is predominantly influenced by attributes such as permeability and strength (Branch, 1994; Ferdosi et al., 2015). This section examines the design concerns for tailings dams, construction techniques for tailings storage facilities, their stability, and the impact of material qualities and tailings compaction.

2.3.1. Design of tailing dams

Poor design and inadequate TSF operational management are some of the major sources of TSF failure (Dixon-Hardy and Engels, 2007). It is therefore imperative to have a proper design of the TSF for stable and safe operational management, thereby reducing the chances of tailing dam failure. Challenges associated with tailings disposal and storage, such as tailing dam stability and failure, vary from one TSF to another. This follows the unique characteristics of tailings properties and environmental factors of each tailing dam (Dixon-Hardy and Engels, 2007).

The method of tailing disposal is selected during the design phase based on the type and properties of the tailings (strength-related parameters) to be deposited, as well as hydrological/meteorological conditions, and environmental conditions (Wu et al., 2023). Various geological and geotechnical site conditions influence TSF site selection during design and construction (Wu et al., 2023). The geotechnical parameters that affect site selection are particle size, permeability, and sand density (Wu et al., 2023). Other geotechnical properties that affect site selection include foundation soil bearing capacity, shear strength, and moisture content. of in-situ soil that influences the stability of TSF). Organic materials, weak and loose materials of high compressibility, and pervious sand are removed before the construction of a tailing dam. This is because these materials have low shear strength and deform easily under additional loads (Zardari, 2011).

Geological conditions, such as the mineralogy/ chemical composition of the tailings to be deposited in the TSF, influence the stability of the TSF. This is because various tailings have different mineralogy depending on the source ore mined, which influences their physical characteristics. The presence of clay minerals in ore deposits affects mineral processing and tailings disposal (Vietti and Steenkamp, 2023). Rainfall increases the seepage of TSF; therefore, the use of a consolidated tailings layer when constructing TSF to prevent seepage is vital (U.S Army Corps of Engineers, 2004). The allowable moisture content for foundation soil during TSF construction should range between 10% and 45% (Bhanbhro, 2014).

Various parameters, such as specific gravity, density, and moisture content, must be considered when selecting TSF construction materials. The specific gravity of materials plays a crucial role in selecting construction materials (SGU, 2024). This is because the ratio of the density of construction materials to the density of water content within these materials affects their strength properties (SGU, 2024). A study by Vietti and Steenkamp (2023) has compared the Jagerfotein TSF failure with the Kimberlite TSF. The study indicates that the dam failed due to a density change from high-density to low-density flow and accelerated ponding of water, resulting in seepage of the TSF external wall and over-wetting of the foundation. The foundation of the tailing dam requires a material with low to no permeability to prevent the higher rate of seepage that would compromise stability (SGU, 2024).

2.3.2. TSF construction methods and their impact on stability

Tailings storage facilities are often designed as raised dams, following one of three methods of construction (upstream, downstream, or centreline method) over a retention dam (Rana et al., 2021). This is because raised dams are continuously constructed over the entire life of a mine, which allows them to be expanded and monitored. They are monitored to ensure their stability throughout, unlike retention dams that are built to full height at the beginning of mine life. The method of construction is selected based on the direction of the dam embankment crest movement from the initial embankment point at the base of the dam as the lifts/levels are added (Adamo et al., 2020). The improper design of TSF and the poor selection of appropriate deposition methods lead to the instability and failure of TSF (Brown, 2019). Additionally, the level raising that occurs during dam construction may increase pore pressure on the tailings, thereby reducing the stability of the TSF (Zardari, 2011).

2.3.2.1. Upstream method

The construction of an upstream method begins with a starter dam, and then the raises/levels are added from the starter dam (Martin and McRoberts, 1999). This occurs through the deposition of tailings that construct the dam. The additional levels/lifts are constructed from the base embankment during the process of raising the dam's height (Grant-Stuart et al., 2020). In this method, the additional successive lifts move progressively upwards to the direction of the crest from the base starter dam/ outer toe (Vicks 1990; Grant-Stuart et al., 2020). The tailings are used to support the additional level/lifts as the height of the dam increases (Adamo et al, 2020). Consequently, the upstream method is more susceptible to failure (Martin and McRoberts, 1999). The failure of the upstream method is usually due to excessive pore pressure buildup and low hydraulic conductivity that occur when successive raises/levels are added rapidly (Zardari, 2011). Excess pore pressure and low hydraulic conductivity cause a low tailings consolidation, which reduces tailings stability and leads to TSF failure (Zardari, 2011)

Upstream methods are less stable than the other two construction methods and, consequently, are unsuitable for high-seismic-wave-prone areas (Adamo et al., 2020).

This method has a pervious starter dyke, thus promoting high seepage. This makes them more unstable than the downstream method (Martin and McRoberts, 1999). The figure below illustrates the construction of the upstream TSF method, as explained above. The initial deposit commences on the outer toe of the TSF/ starter dam, 2progressing upwards towards the tailing beach as the level of dyke is added.

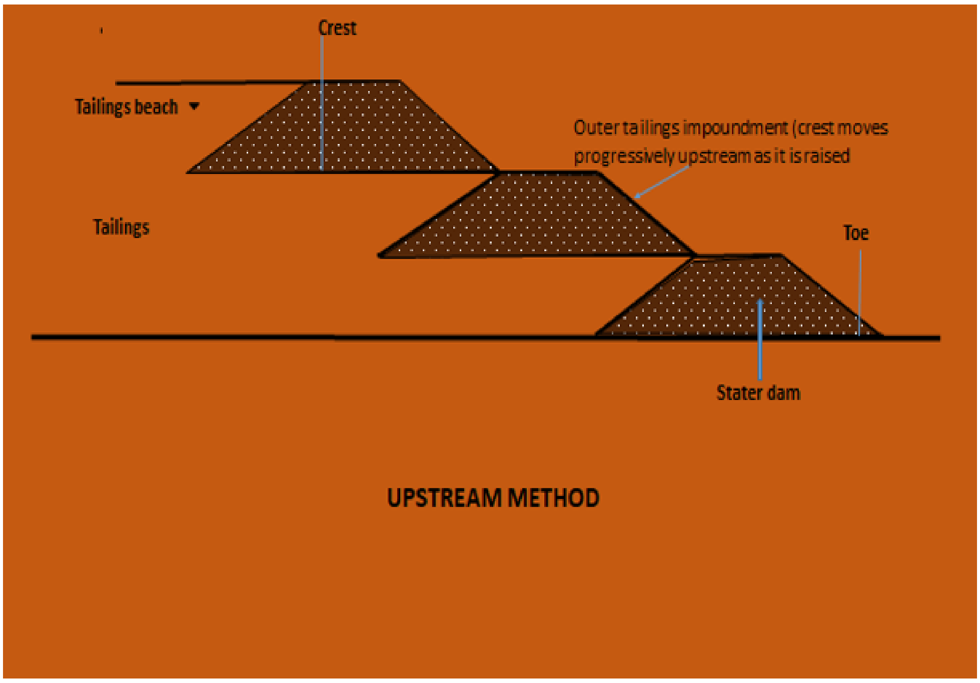

Figure 2.2: An upstream method of TSF construction (Modified after Vicks, 1990)

2.3.2.2. Downstream method

In the downstream method, the dam crest moves downstream as the level/lift of the dam is added. Thus, increasing the height of the dam towards the final outer toe line of TSF (Grant-Stuart et al., 2020). Materials are initially placed before dam construction, allowing the dam to be built on top of previously placed material (Vicks, 1990). This method has an impervious core and a drainage zone, which allow water to be contained through its internal drainage arrangements, thereby increasing its stability relative to the upstream dam (Adamo et al., 2020). Dykes are raised on the downstream slope of the existing dam (Bhanbhro, 2014). Figure 2.3 the construction procedure of the downstream method, where dykes are raised in a downstream direction toward the embankment from the starter dam.

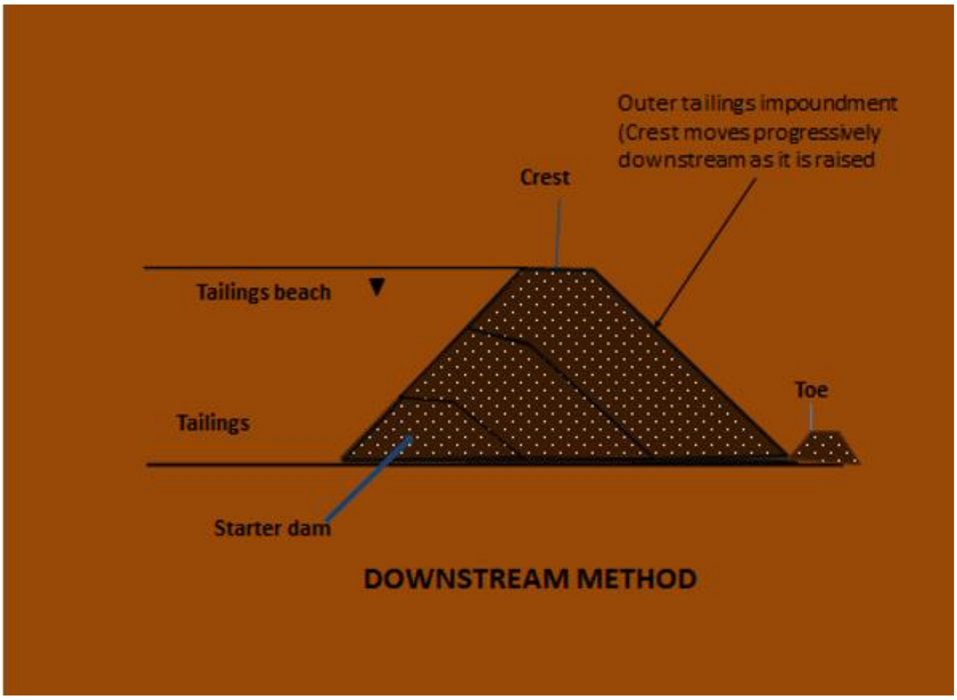

Figure 2.3: Downstream TSF construction method (Modified after Vicks, 1990).

2.3.2.3. Centreline method

In this method, the dam crest progresses only vertically as its height increases, whilst maintaining the same horizontal position of the dam crest (Adamo et al 2020; Grant-Stuart et al., 2020). The centreline is a progression of the downstream method with the centreline of the impoundment wall vertically raised (Grant-Stuart et al., 2020). Tailings are initially placed before the construction of a dam so that the dam is constructed on top of tailings previously deposited (Bhanbhro, 2014). Dykes are raised vertically on the crest of the existing dam and the downstream slope (Bhanbhro, 2014). Figure 2.4 illustrates a centreline procedure of TSF construction. The crest progresses vertically from the starter dam. The dam continues from a downstream dam and moves to the outer embankment as the dykes are added.

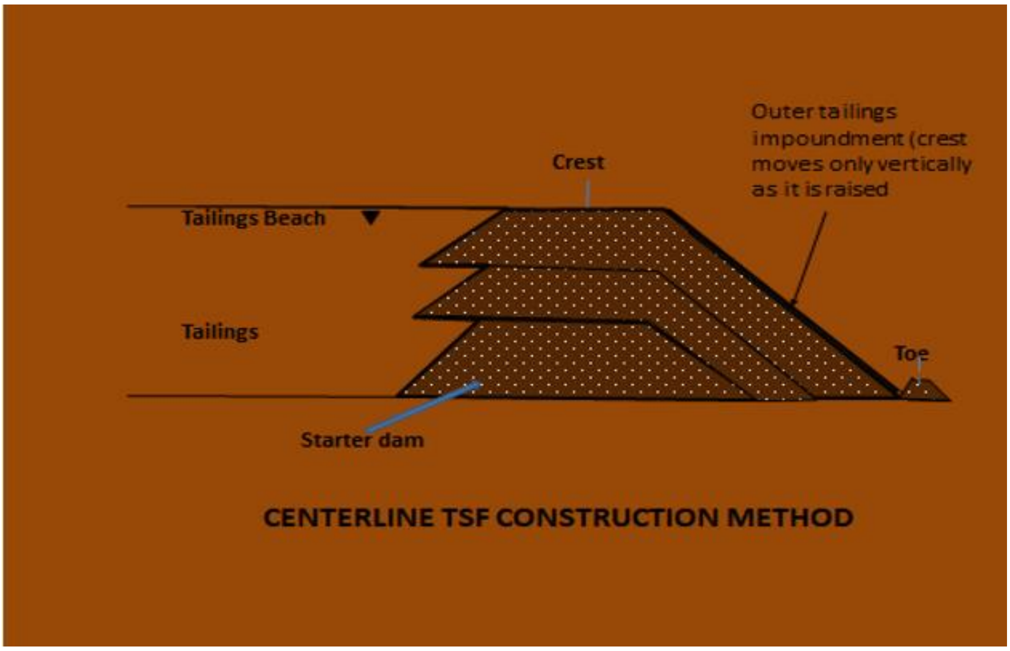

Figure 2.4: A centreline method of TSF construction (Modified after Vicks, 1990).

2.3.3. The effects of material used to construct tailing dams

The capacity of the foundation materials to withstand the external overlying load is a key factor to consider during TSF construction (Evans et al., 2021). The foundation materials need to be selected based on their bearing capacity and their shear strength for the construction of a stable TSF (Rad et al., 2024). It is therefore imperative to select a stable area before constructing an engineering structure, depending on the foundation material (Visagie and Bezuidenhout, 2022). The materials used for the foundation of the TSF during construction depend on the height the TSF will reach to maintain its stability (Branch, 1994). Therefore, if the dam height exceeds 30 meters, extensive preparation of the dam foundation is required, using materials that can withstand the load of the tailings to be deposited.

The design of TSF is governed by the grading of the tailings to be deposited (Branch, 1994). Unstable materials such as organic materials, highly compressible materials, loose and weak materials, and pockets of pervious sand are not suitable for the construction of TSF (Branch, 1994). This is because organic materials are soft materials and incapable of resisting stresses exerted by the overlying TSF load (Abdulkareem and Hassan, 2019). Organic, loose, and weak materials, as well as sand, increase water infiltration into the foundation soil, thereby reducing shear strength, bearing capacity, and stability (Abdulkareem and Hassan, 2019). Fine materials that consist largely of clay-sized particles are also not suitable for the construction of tailing dam embankments (Adamo et al, 2020). This is because of the low resistance to shear forces, and therefore they slide and fail when shear stresses are exerted (Zhang et al., 2022a)

2.4. Limit equilibrium analysis

The liquid equilibrium method (LME) is a geotechnical analysis technique for slope stability analysis that determines the FoS of a slope (Baba et al., 2012). LME consists of three methods of analysis: Bishop simplified, Janbu, and Spencer (Baba et al., 2012). LME determines the FoS by analysing the ratio of resisting forces to driving forces. The factor of safety of tailings is calculated using equation 2.1

$$\text{FoS}=\frac{resistive\ force\ (shear\ strength)}{driving\ force\ (shear\ stress)} \qquad 2.1$$

$$= \frac{c + \sigma\prime.\tan\phi}{\tau}$$

The modelling system divides the potential sliding mass into vertical slices. The method assumes a failure mechanism as circular, polygonal, or non-circular (Baba et al., 2012).

The factor of safety (FoS) is defined as the ratio of the resisting forces (stabilising forces) to the driving forces (destabilising forces) acting on the soil mass (Grant-Stuart et al., 2020). It is the relationship between the shear strength resisting failure movement and the shear stress applied to the slip surface influencing failure movement (Visagie and Bezuidenhout, 2022; Zheng, 2006). The minimum FoS against slope failure of a tailing dam in a static condition is 1.5, whereas in a dynamic condition, it is 1.1 according to South African legislation/standard (Grant-Stuart et al., 2020). Grant-Stuart et al. (2020) mentioned that a FoS of 1 indicates the onset of slope failure. Therefore, the slope with a FoS less than 1 is considered an unstable slope (Bidyashwari et al 2017)

The numerical simulations use the number of slices in a geometry to estimate the FoS. It is a unit-less property because it is the ratio of two forces (driving and resistive forces, which tend to cancel one another). A FoS that is greater than 1 indicates a stable slope, whereas a FoS that is less than 1 indicates an unstable slope. This is because a material with low strength to resist failure, compared to the stresses acting on the tailings structure, creates an unstable slope, contributing to the forces that drive the failure mechanism. This tends to reduce the stability of the TSF structure (Potgieter; Jacobsz, 2019).

2.5. An influence of the geotechnical parameters of soil on the Factor of Safety

Changes in soil geotechnical properties, such as water parameters (moisture content, Pore water pressure, permeability) and shear strength parameters (cohesion and friction angle), affect soil slope stability (Roy and Bhalla, 2017; Wang and Li, 2025). The change in slope stability occurs by affecting the equilibrium between the resistive and driving forces of failure (Al-Bared et al., 2019). In limit equilibrium analysis, the FoS represents the ratio of the strength of the soil material resisting failure to the stresses acting on the soil that drive failure (Harabinova and Panulinova, 2022). The FoS is increased and decreased by each of the geotechnical properties of soil differently. This section describes how each geotechnical property of soil affects the soil FoS, which, in turn, determines the stability of the slip slope.

2.5.1. Water parameters (moisture content, pore water pressure, and permeability)

An increase in soil cohesion increases the FoS of the soil slope by increasing the resistive force against the stress that poses failure. This is because cohesion increases the stickiness between soil particles, thereby enhancing the soil's resistance to sliding (Harabinová and Panulinová, 2020). Friction angle influences the FoS in the same way that soil cohesion does. An increase in the friction angle increases the FoS.

This is because the friction angle increases the strength that resists failure (Harabinová and Panulinová, 2020).

2.5.2. Shear strength parameters (cohesion and friction angle)

Porewater pressure also significantly affects the FoS; an increase in porewater pressure reduces the soil slope's safety factor. This is because the pore water pressure reduces the effective stress, which therefore affects the shear strength of the soil, causing the driving force to slope failure to surpass the strength of the soil (Arya et al., 2020; Perri et al., 2012). The unit weight moderately affects the safety factor of the slope (Xu, 2025). This suggests that it influences both the shear strength of soil and the shear stresses in soil, thereby determining the FoS, rather than other geotechnical parameters that affect either shear strength or shear stress. Generally, an increase in unit weight by a considerable amount reduces the FoS, whereas a decrease in unit weight by a significant amount reduces it (Xu, 2025). However, a slight change in soil unit weight does not result in a substantial change in the FoS. This is because an increase in unit weight represents an increase in Bulk density (mass/Volume) of tailings, which increases the gravitational forces that pull down the slope, reducing its stability (Xu, 2025).

2.6. Conclusion

This chapter reviewed the geotechnical properties of tailings affecting the stability of tailing dam facilities and how they influence the stability of TSF. Various methods of tailing dam construction were examined, and a brief explanation of how each method affects TSF stability was provided. The literature on how each geotechnical parameter of soil affects the soil slope stability was undertaken, which represents the same way the geotechnical parameters of tailings affect the tailings stability. The standards and methodology used to analyse each geotechnical parameter of tailings through experimental testing are outlined in the following chapter.

Chapter 3 Research Methodology

3.1. Introduction

This chapter describes the procedures and standards used for field sample collection. It also describes the methods used in the experimental analysis of geotechnical parameters of tailings that affect the stability of tailing storage facilities. The collected tailing sample was prepared and used for an experimental study of TSF stability. The geotechnical test procedures were followed to analyse geotechnical parameters, including moisture content, pore water pressure, shear strength, particle size distribution, and permeability. The experimental procedure was based on analysis standards, such as SANS and ASTM standards, to ensure accurate results. The limit equilibrium method (LEM) used for slope stability analysis was described in detail in this chapter.

3.2. Sample collection

Tailings samples were collected from the field in a tailing dam that is no longer actively being continuously pumped with tailings slurry. The samples were collected from the TSF of the copper mine located in Limpopo, specifically in the Phalaborwa area, as indicated in Figure 1.1 in Chapter 1. Due to current site restrictions, the samples were collected on the East and West sides of the TSF. The tailings were sampled as solid dry tailings, and a 100 kg sample was collected and sent to the University of South Africa's laboratory for further analysis of geotechnical parameters. The tailings sampling method used is grab sampling, which allows bulk sampling at one or more points across the tailings dam to obtain a representative sample of the TSF. Figure 3.1 shows the samples collected in sampling bags. The 100kg samples were stored in multiple bags to facilitate easy transport to the laboratory for analysis.

Figure 3.1: Illustrating the samples collected and stored in plastic sampling bags

3.2.1. Sampling procedure

The samples were collected using a shovel to scoop the tailings. The first step in the field was to mark the four points where tailings samples were collected. The shovel was used to dig the tailings into loose grains. This was done to ensure that the tailings could be stored easily and efficiently. The shovel was used to scoop the tailings, which were then poured into sample bags. The exact process of tailings sample collection was undertaken across all four points marked on the East and West sides of the TSF. The Sampling bags were then tightly closed using a cable tie to retain field moisture and were ready for experimental analysis. Figure 3.2 illustrates the sampling bags, which are collected and tightly sealed. This was done to retain field moisture and achieve accurate moisture results, which were analysed in the laboratory. The sampling bags are numbered according to the direction of the site where they were collected.

Figure 3.2: Samples in a tightly closed sampling plastic bag

3.3. Experimental procedures

The experimental procedures involve laboratory tests to analyse the geotechnical parameters of the tailings' samples. To ensure experimental accuracy, all laboratory testing was conducted in strict accordance with relevant standards. All testing apparatuses underwent routine calibration prior to the testing program to minimise systematic errors. To ensure the reproducibility of the experimental data, triplicate tests were performed for each geotechnical characterisation experiment.

3.3.1. Optimum moisture content (MOC) and Maximum dry density (MDD)

The determination of the maximum dry density and optimum moisture content was undertaken in accordance with the South African National Standard (SANS) 3001-GR30. The first step was to weigh the pan before pouring the tailings. Tailings samples were milled into fine-grained sizes that can pass a 20mm sieve. This was undertaken to achieve a desired particle size of the tailings sample that can be perfectly moistened. The tailings were placed in a pan, and the combined mass was measured with a scale and recorded to determine the mass of the tailings separately. Figure 3.1 illustrates the mass weighing of an empty pan and the weighing of tailings using a scale.

Figure 3.3: Measuring the weight of the pan and the tailings mass

The maximum sieve size diameter used is 20mm to achieve fine-grained tailings that can be easily moistened. The sample was divided into three specimens by riffling to provide the test sample. The three specimens had a range of moisture content, with the first below the optimum moisture content (OMC), the second above, and the third close to OMC.

The required volume of tap water was measured using a measuring cylinder. Thereafter, the water was poured into an empty sprinkler bottle, and the quantity was measured. The water from the sprinkler bottle was sprinkled onto the tailings whilst mixing them with water using a trowel until OMC was reached. The OMC was reached by sprinkling water onto the tailings sample until the tailings could be readily pressed together by hand into a lump without crumbling. A spongy feeling indicates that the moisture content is above OMC. The volume of water remaining in the sprinkler bottle was measured. This was done to calculate the volume of water required to be sprinkled into a tailings sample to reach its OMC. The sample was placed in a sealable container, covered with a cloth, and tightly sealed for 40 minutes to reach its OMC. Therefore, the OMC was recorded. The tailing specimen was immediately placed into a cylindrical mould and compacted.

The compacted dry density was estimated and recorded. The procedure was repeated for specimens two and three, and the average OMC and dry density were recorded. The optimum moisture content was alternatively estimated by plotting moisture content versus dry density. The tailings were compacted under various moisture contents in a proctor test. The point on the graph at the peak represents the maximum dry density, and the point where the moisture content reaches the peak MDD is called the optimum moisture content. The graph in Figure 3.4 illustrates the OMC where the MDD reaches its peak.

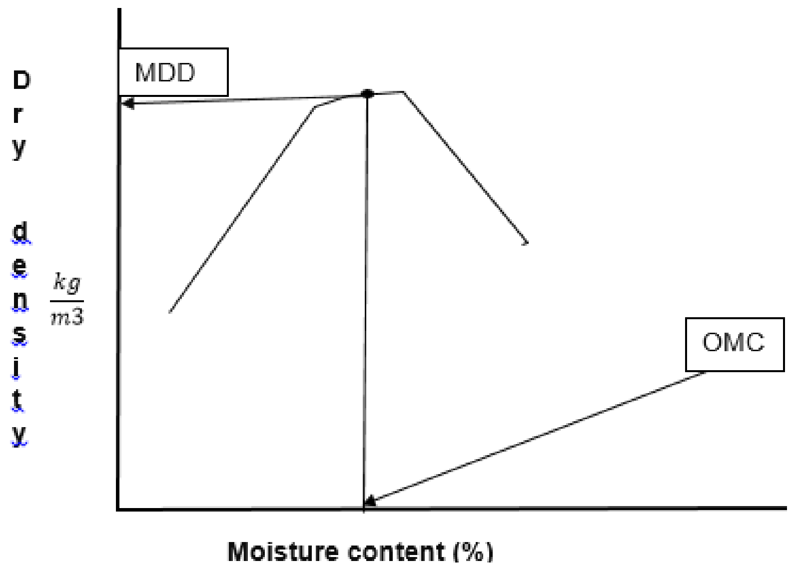

Figure 3.4: A graph illustrating the OMC at peak MDD

3.3.2. Atterberg limits tests

The Atterberg limits tests are the basic measure of consistency of fine-grained soil used to determine changes in moisture state from liquid to solid. These tests were initially developed by Atterberg in 1910 and modified in 1927 (Kalian, 2017). The liquid limit (LL) test and the plasticity test were the two Atterberg limit tests performed to determine the consistency of the tailings.

Determination of the liquid limit

The liquid limit test was conducted using the two-point method in accordance with SANS 3001-GR11. Figure 3.5 depicts the apparatus used for the liquid limit test, such as the Casagrande tool and the grooving tool.

Figure 3.5: Liquid limit apparatus: (a) numbered tin, (b) grooving tool, and (c) Casagrande tool.

Several steps were taken to prepare the Casagrande tool used for testing the liquid limit. The calibrated plate was used to adjust the bowl's height to ensure proper rotation of the Casagrande tool's handle. The calibrated plate was placed on the rubber base of the liquid limit device, and the bowl was allowed to rest on top of it. The hinged support was moved until the cam raised the bowl free of the plate on rotation.

Sample preparation was carried out after the equipment was set up. The material passing 0.425mm and 0.075mm sieves was prepared according to SANS 3001-GR1. A tailings mass of 60g was placed into a mixing dish and weighed. A small amount of tap water was added as specified in SANS 241 and 242 to a sample using a wash bottle to ensure proper mixing, forming a stiff consistency that flows together at 25 to 30 blows after grooving in a Liquid Limit device, as depicted in Figure 3.6. The tailings and water mixture was mixed for 10 minutes.

Figure 3.6: A mixing bowl with a tailings specimen and a washer bottle to form a tailing paste

The moist tailings were placed in the brass bowl of the LL device, filling it to the mark. The tailings were mixed slightly in the bowl to form a tailing paste, then flattened and spread in the Casagrande bowl. The tailings were flattened with a few strokes to avoid moisture being drawn to the surface of the brass. A groove was cut, separating the tailings pastes into two portions. The Casagrande tool was used to perform at least 15 strokes, and the liquid limit was determined and recorded. The liquid limit is determined by the number of strokes that were performed to close the groove between the two portions of tailing paste in a bowl.

Figure 3.7: An image illustrating a groove made using a Casagrande tool

Determination of Plasticity Limit

ASTM D4318 is the standard used for determining the plasticity limit. The sample was prepared by mixing the tailings with water to form a tailing mould into a ball shape. A flat table was used to make a tailing thread with the hands from a ball-shaped tailing mixture. The thread was constructed to 3mm before it crumbled to determine the tailings' moisture content. The plasticity limit of tailings was determined and recorded.

3.3.3. Triaxial tests for Shear strength and pore water pressure

A triaxial test was conducted to analyse the shear strength and porewater pressure under a consolidated undrained condition. The consolidation conditions were met to ensure the sample was compacted under pressure for accurate measurements of the stress that the tailings can withstand. Undrained conditions were met during the pressure buildup in a triaxial tube for pore water pressure analysis.

Shear strength parameters, such as adequate strength, were determined in accordance with British Standard (BS) 1377 Part 8, which is an ASTM standard for saturated soil under undrained, consolidated triaxial conditions. The pore water pressure was measured using the same test procedure as the pressure of undrained, saturated tailings build-up, after the consolidation stage. The test was conducted to determine shear strength parameters and measure pore water pressure under undrained, consolidated conditions. The standard used for the determination of pore-water pressure under the undrained consolidated undrained triaxial test is ASTM BS 1377-8.

The first step before the actual triaxial tests was sample preparation. The diameter and the height of a remoulded specimen were measured. A demoulded soil specimen, 38 mm in diameter and 76 mm in height, was used, and it was trimmed to the required dimensions. The sample was weighed, and its mass was recorded. The weight, height, and diameter of the tailings were used to calculate their initial volume. A filter paper and porous discs were placed on top of and below the specimen. The last step was to encase the specimen in a rubber membrane using a membrane stretcher, which was secured with an O-ring, and the specimen was then placed in a triaxial cell. Figure 3.8 shows a demoulded tailing specimen being weighed on a scale to determine its mass just before saturation, for easier comparison of the mass before and after saturation.

Figure 3.8: A tailing specimen prepared and weighed mass

After the sample was prepared, it underwent a saturation stage. The purpose of the saturation stage is to fill the voids in the tailings with water, thereby creating a pressure buildup within the tailings' pore spaces. A small confining pressure of 20 kPa was applied, with the back pressure incrementally increased. The cell and back pressure were maintained at a pressure difference of 5-10 kPa. A B-value, also known as Skempton's pore pressure parameter, was allowed to reach 0.95, where a B-value is equivalent to the ratio of $\Delta u/\Delta\sigma$ (change in pore pressure over change in cell pressure)

The consolidation stage followed the saturation stage, which involves exerting confining pressure on the sample while keeping the back pressure constant to bring it into an in-situ stress condition. The desired adequate confining pressure (σ'_3) was applied to the tailing specimen, and the specimen was allowed to drain (valves open). This was done to consolidate the specimen under isotropic conditions, with careful monitoring of volume change and pore pressure to ensure the final stage of consolidation was achieved. The tailings' grain size determined the consolidation duration.

The Shearing stage is the final stage of a triaxial test, maintained under undrained conditions. This is the failure-inducing stage, in which the axial load is increased in a tailing specimen while maintaining a constant confining pressure until it fails. The drainage valves were closed to prevent water from escaping. Axial load was applied at a constant strain rate (typically 0.1 to 0.5). Figure 3.9 depicts triaxial testing equipment used to analyse shear test parameters under undrained, consolidated conditions.

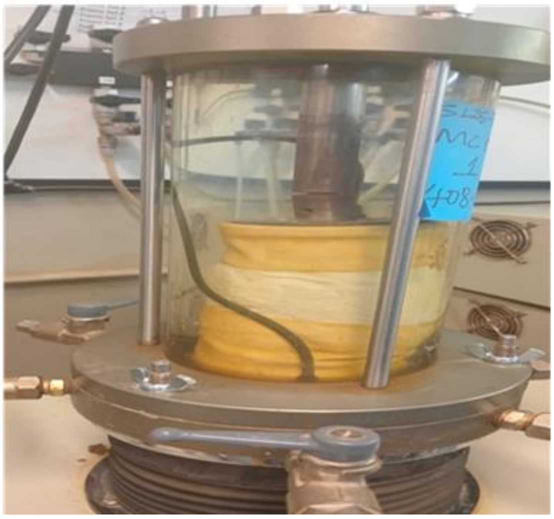

Figure 3.9.: Illustrating a triaxial test equipment

The device recorded axial load, Axial strain, and Pore water pressure, and the test continued until a peak deviator stress was reached. Three tests were conducted at varying confining pressures to determine effective stress parameters. The details on sample identification (type, size, condition), saturation information (B-value, back pressure), confining pressure (σ_3), and shear rate were documented. The shear strength was calculated using Equations 3.1.

$$\tau = c + \sigma'.\tan \phi \qquad 3.1$$

Where τ : shear strength; σ': effective normal stress, and ϕ friction angle

Graphs of the stress-strain curve, pore pressure versus strain, Mohr circles, and the values of c and ϕ were drawn from the information recorded on deviator stress and pore pressure at failure. These graphs will be presented in Chapter Four.

3.3.4. Pore water pressure of tailings

The tailings pore water pressure was determined using a theoretical hydrostatic calculation using Equation 3.2. The unit weight of water and the water depth were used to calculate the pore water pressure. The depth of water was measured.

$$u = \gamma_w \cdot h \qquad 3.2$$

where *"u"* denotes the pore water pressure; γw: the unit weight of water, and h is the height of the water column. To determine the depth of water in the field, the reference elevation was established in a tailing dam, and the piezometer was calibrated (zeroed). The piezometer was then inserted in a borehole drilled. The then depth was recorded, and the calculations were made.

3.3.5. Permeability/ hydraulic conductivity

Permeability was determined using a constant-head falling-head test in accordance with ASTM D2434-68, as the tailings have a coarse texture. The apparatus, including permeameters, Monometer outlines, monometer outlets, a porous disk, a specimen compacter, and vibrator tubes, was used. The aforementioned apparatus was prepared to meet specific conditions before the test commenced.

The permeameter specimen cylinders with a minimum diameter of approximately 8 or 12 times the medium fine sand particles size. The permeameter was fitted with a porous disk at the bottom, which had a permeability greater than that of the soil specimen, to prevent particle movement. The length of the manometer outlets for measuring the loss of head is equivalent to the diameter of the cylinder and a porous disk with a spring attached to the top plate. The diameter of a special cylindrical spout of 25 mm for 9.5 mm max size particles and 13 mm for 2.00 mm max size particles was measured, and the spouts were fitted in a large funnel. A vibrating tamper was equipped with a 51 mm-diameter tamping foot. Additionally, a sliding tamper was equipped with the same size tamping foot and included a rod for sliding weights of 100 g, specifically designed for use with sand. This rod allows for an adjustable drop height, which can be set to 102 mm for sand applications. Figure 3.10 illustrates a manometer used for permeability testing.

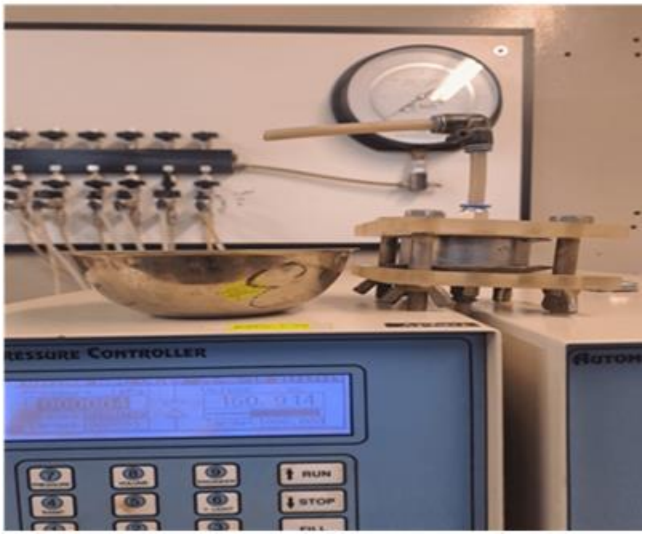

Figure 3.10: A manometer with tubes and a recording device

Other conditions were met to prepare for the laminar flow of water through granular soils under constant-head conditions. The flow was maintained continuously, with no change in tailing volume throughout the test. The flow was made with the tailing voids saturated with water, and no air bubbles in the tailing voids. Flow was undertaken in the steady state with no changes in hydraulic gradient, and direct proportionality of flow velocity with hydraulic gradient below specific values, at which turbulent flow starts. A sample for testing, approximately twice the amount required to fill the permeameter chamber, was selected by the quartering method. Sample preparation involved air-drying a representative granular tailing sample containing less than 10% of the material passing the 0.075mm sieve, equivalent to an amount sufficient to satisfy the requirements of sieve analysis. Any particles larger than 19 mm were separated by sieving and excluded from the permeability test. However, the percentage of oversize material was recorded and selected using the quartering method.

The cross-sectional area of the specimen was calculated. A small portion of the sample selected was taken to determine water content. The weight of the remaining air-dried sample was taken and recorded for unit weight determinations. The prepared soil was placed in uniform, thin layers of equal thickness after compaction to a maximum particle size of 15 mm.

The tailings were thoroughly mixed in the pan for each successive layer to minimise segregation that could occur when removing tailings from the pan. A scoop was used to evenly distribute the tailings by sliding a scoopful in a nearly horizontal position along the inside surface of the device down to the bottom layer. The scoop was then tilted and drawn toward the center in a single, smooth motion. This technique allowed the soil to flow from the scoop in a windrow without segregation. The permeability cylinder was rotated sufficiently for the next scoopful, ensuring that the process continued around the inside perimeter to create a uniformly compacted layer with a thickness matching the maximum particle size.

Successive layers of tailings were compacted to the relative density of 2116kg/m^3 by appropriate procedures, as follows, to a height of about 2 cm above the upper manometer outlet. The Minimum Density and the Maximum Density are 0% and 100% Relative Density, respectively. Compaction was performed using a vibrating tamper to thoroughly compact each layer of tailings and distribute the light tamping action uniformly over the surface of the layer in a regular pattern. The pressure of contact and the duration of the vibrating action were such that each spot should not cause soil to escape from beneath the edges of the tamping foot, thereby tending to loosen the layer. A sufficient number of coverages were made to produce maximum density, as evidenced by practically no visible motion of surface particles adjacent to the edges of the tamping foot. Each layer was compacted by sliding a weight tamper, which was thoroughly tamped with blows to distribute the weight uniformly across the layer. The drop height was adjusted to provide sufficient coverage and achieve maximum density. The permeability test tool is illustrated in Figure 3.11.

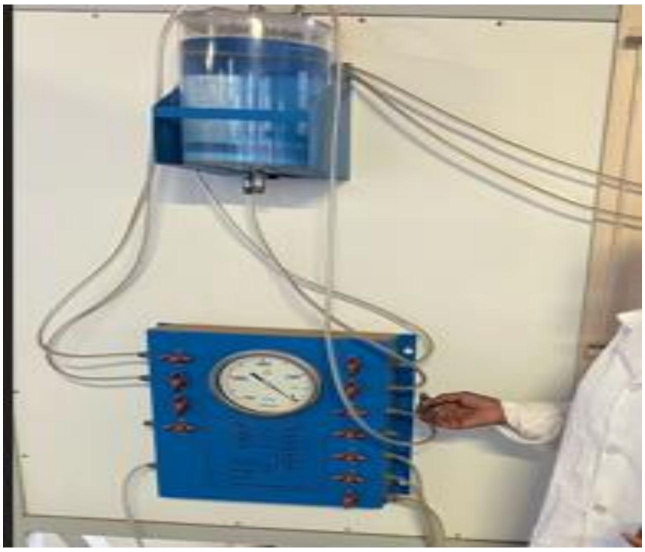

Figure 3.11: A permeability test procedure

The flow quantity measurements were delayed and heated until a stable head condition was achieved. This was done without appreciable drift in water manometer levels. The time t, the head h (the difference in level between the manometers), the flow rate Q, and the water temperature were measured and recorded. The test runs at heads were repeated, increasing the head by 0.5 cm, to accurately establish the region of laminar flow and the velocity, which is directly proportional to the hydraulic gradient. Turbulent flow conditions were reached when departures from the linear relation became apparent at 1-cm intervals of head. After the permeability test, the sample was inspected to ensure there were no visible defects, such as cracks or preferential flow paths, which could have affected the test results. Calculations of the coefficient of permeability were made thereafter. The calculation was made following the hydraulic conductivity equations as follows:

$$K=\frac{Q}{IA} \quad 3.3$$

$$I=\frac{\Delta h}{L} \quad 3.4$$

$$V=\frac{Q}{At} \quad 3.5$$

$$Q=\text{KA}\frac{h}{I} \quad 3.6$$

3.3.6. Particle size distribution (PSD)

Sieve analysis is the test conducted to determine the size distribution of tailings particles. Hydrometer analysis was performed after sieve analysis to quantify the results obtained through particle size distribution analysis. Sieve analysis was undertaken in accordance with SANS 3001-GR2.

A sieve set complying with SANS 3310-1, featuring diameter sieve sizes of 100μm, 75μm, 63μm, 50μm, 28μm, and 20μm, along with a pan and cover, was used. The sieves were arranged in order of size in accordance with SANS 3001:2002, starting with 100μm, 75μm, 63μm, 37.5μm, 28μm, and 20μm, and, lastly, the pan and lid. Figure 3.12 depicts the sieve arrangement according to the required standard sizes for the PSD analysis test.

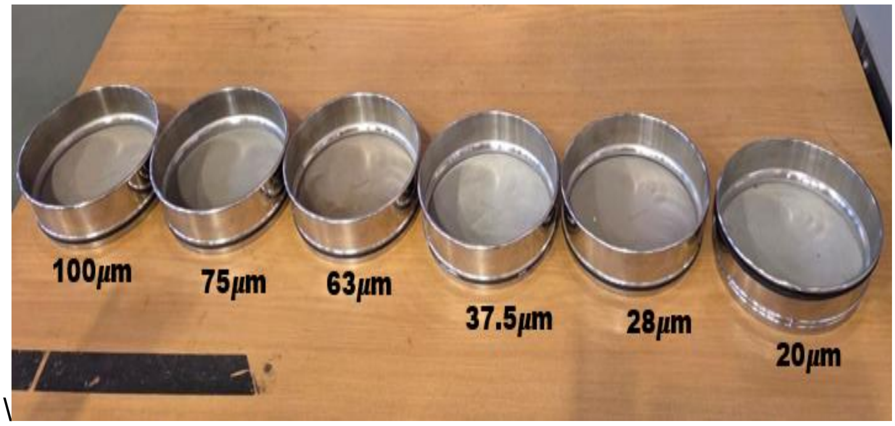

Figure 3.12.: Sieve size arrangement according to SANS 3001 gr2

The sample was prepared by drying the field tailing sample (Figure 3.13). Tailings containing field moisture were dried overnight (24 hours) to remove excess moisture, enabling easy handling in an oven.

Figure 3.13: Drying the tailings in the oven overnight

The sample was weighed, and the mass was recorded to the nearest 1 g. The test sample was then sieved using a mechanical shaker. Excess fine particles adhering to the aggregate were removed with a hard-bristle brush. The tailings remaining in each sieve were weighed and their mass recorded to the nearest 1g. The fraction of the test sample passing a 20 μm sieve was then riffled several times until the required tailings size was obtained. The tailings passing the 20 μm sieve were sieved again through the 14 μm and 5 μm sieves using a pan and a cover. Any fine material adhering to the sieve's sides was removed using a brush. The tailing passing 5 μm was further sieved using 2 μm. The readings were taken, and the percentage passing was calculated. The percentage retained for each sieve is initially calculated, followed by the cumulative percentage, and lastly, the % passing.

The calculation of the percentage of passings was done using equations 3.7 to 3.9

$$\% \text{ retained} = \frac{weight\ retained\ on\ that\ sieve}{total\ sample\ weight} \quad 3.7$$

% cumulative sum of %retained on that sieve and all coarse sieves 3.8

% passings= 100%- cumulative retained percentage 3.9

3.3.7. California bearing ratio (CBR)

The purpose of the CBR test was to determine the bearing capacity of tailings to carry the overburden load of tailings deposited on top of them. The standard used for CBR analysis is SANS 3001.GR40: 2013. A cylindrical mould made of corrosion-resistant steel, with an inner diameter of 152 mm and a height of 152 mm, is used for CBR analysis in the laboratory. The mould also includes a detachable extension collar that is at least 70 mm high and a base plate. Figure 3.14 depicts a cylindrical mould filled with a tailing specimen

Figure 3.14: An image of a cylindrical mould with tailings

A circular spacer plate, made of corrosion-resistant steel, 25 mm thick, and of a diameter that just fits inside the mould, was selected. A compression testing machine, with a total capacity of at least 55 kN, capable of penetrating at a rate of 1.0

mm/minute, and equipped with a force-indicating device, was used. The sieves that comply with SANS 3310-1 or SANS 3310-2 were selected as applicable, which are 200 mm in diameter with nominal aperture sizes of 5 mm and 2 mm. A dial gauge, with a travel of at least 25 mm, reading to two decimal places of a millimetre, was also prepared.

The sample was prepared for the CBR test. The required sample size was measured, and the sample was graded accordingly. The sample was then placed in a sealed container as described in SANS 3001-GR30 for MOC and MDD.

The first step of the CBR test involved measuring the moisture content of the tailings. Two representative samples of approximately 1000 g were taken from the test sample using a scoop to determine the initial moisture content, as described in SANS 3001-GR20. The optimum moisture content determined in SANS 3001-GR30 was used. Data from the maximum dry density (MDD) test procedure mentioned in SANS 3001-GR30 above, and the test sample's initial moisture content. The calculated equivalent water volume (VW) was added to achieve the optimum moisture content (OMC). A measuring cylinder was used to measure the water volume, which was then poured into an empty sprinkler bottle.

The test sample was removed from the sealed container and placed in the mixing basin. The remaining water from the sprinkler bottle was added gradually to the sample, whilst mixing thoroughly with the trowel to ensure a homogeneous mixture. The test sample was covered with a moist cloth and allowed to stand for 40 minutes. The test sample provides sufficient material for the compaction of three specimens, including moisture determination. The second step involved compacting the tailings into three specimens. The test material for the compaction of three specimens, A, B, and C, was prepared. A test sample with OMC moisture content was prepared. The three specimens were compacted using the standard MDD effort and two reduced efforts to produce a range of densities from 93% to 100% of the MDD. If the moisture content after soaking is required, the mass of the wire gauze was determined, and the soaking base plate was perforated.

Specimen A

The compaction test procedure for specimen A involved several steps. First, the test sample was thoroughly mixed to ensure an even moisture content. Next, a mould was weighed, and the mass (MMA) was recorded to the nearest gram (1 g). A paper disc was placed in the mould on the spacer plate, and specimen A was compacted with a total of 55 blows for each of the five layers. Additionally, a representative sample of approximately 1000 grams was taken from the remaining test sample in the large mixing basin, and the moisture content (WC2) was determined.

Specimen B

The test procedure for specimen B began with thoroughly mixing the remaining test sample before its preparation. The mould was then weighed, and the mass was recorded. A paper disc was placed in the mould on the spacer plate, and specimen B was compacted. The compaction process involved applying 22 blows per layer. Additionally, a sample of approximately 1000 grams was taken from the remaining test sample in the large mixing basin, and the moisture content (WC2) was subsequently determined.

Specimen C

The test procedure for specimen No. C involved thoroughly mixing the remaining test sample before preparing specimen C. The mould was weighed, and the mass (MMB) was recorded to the nearest gram. A paper disc was placed in the mould on top of the spacer plate, and then specimen B was compacted. The compaction process consisted of applying 11 blows for each of the five layers.

Each specimen (A, B, and C) was prepared, and the density after compaction was determined as described previously. Any material adhering to the collar was removed with a spatula. The next step involved loosening the collar by gently turning it and then carefully removing it from the mould, taking care not to disturb the material above the mould. After removing the collar, it was important to ensure the material protruded by 5-15 mm above it. Any excess material was then carefully cut off using a steel straightedge. The straightedge was held nearly flat while scraping along the top edge of the mould to ensure the compacted material was level with the mould's top. Finally, a sieving test was conducted on the excess material remaining in the basin. A 5 mm sieve was used to spread the material that passed through the sieve over the trimmed surface of the specimen.

An old straight-edge was used to hammer down the spread material, levelling off the top surface of the specimen evenly. This procedure was repeated until a smooth surface, even with the top of the mould, was achieved. The process was then repeated using material screened through a 2 mm sieve for tailings to create a dense final surface. After compacting, the mould containing the specimen was removed from the spacer and base plate. The mass of the specimen was weighed and recorded to the nearest gram.

The third step involved soaking and swelling of the tailing's specimen. The following steps were carried out: a paper disc, wire gauze, and a perforated soaking base plate were placed on the prepared and levelled surface of each specimen. The lock nuts were tightened to attach the perforated soaking base plate to the mould, and then the mould was inverted. This was done so that the surface of the specimen, which had been in contact with the spacer plate, was now facing upwards and positioned on the surface to be penetrated. Next, a circular soaking weight with an adjustable stem was placed on the paper disc, which sat on the surface of the compacted specimen. The assembled mould containing the specimen was then transferred to the soaking tank, where the specimen was submerged in the soaking weight. The level of Class II water in the soaking tank rose to approximately 10 mm above the top of the mould, ensuring that the top surface of the soaking weight remained above the water level in the tank.

The tripod was placed on the rim of the mould, with the dial gauge resting on the stem of the soaking weight to measure the swell. One tripod foot was placed on the reference mark. The tripod was slightly moved until a maximum reading was obtained. A reference mark on the mould rim was placed to maintain the tripod's position during all readings. An initial dial gauge reading was taken, and the stem was adjusted on the soaking weight to give an initial reading. Recording of the value as the initial swell reading was undertaken to the nearest two decimal places, and the dial gauge was checked as set up to verify if it has sufficient travel to measure a swell of up to 10 mm. The second swell reading was taken 96 hours after the first.

The bearing test was the last step, which involved the actual California bearing testing of the specimen. After the soaking period, the mould assembly was removed from the wet tank. The excess water was poured off by holding the mould at a downward angle for 30 seconds, whilst keeping the soaking weight in place. The mould was placed upright on a grid or layer of stone chips, allowing free drainage for 15 minutes.

The next step was to remove the soaking weight and place the mould, containing the specimen and perforated soaking base plate, in the compression testing machine. The ring-shaped surcharge weight was then placed on the surface of the specimen to be penetrated. The specimens were penetrated at a steady rate of 1,0 mm/min to a total penetration depth of 9 mm. The aforementioned procedure was performed on all three specimens. The penetration procedure was automatically executed by selecting the required penetration rate and reading intervals. Penetration data was recorded as the last step of the procedure

3.4. X-ray fluorescence (XRF)

The purpose of the test was to determine the mineralogical composition of the tailings**.** An X-ray fluorescence tool that emits X-ray radiation to detect the mineral constituents in a material was used to detect the occurrence of minerals in the tailing specimen.

The first step was to sieve the dried tailings through a 0.125mm sieve to achieve fine-grained tailings. The sample was divided into three specimens, and 3g of each sieved tailings specimen was weighed using a scale. Weighing involves measuring the pan's weight and adding 3g to it. Three specimens of tailings were prepared by placing three grams of fine tailings passing a 0.125mm sieve into an XRF container. The XRF container was tightly sealed with a plastic and a ring seal for proper X-ray beam radiation penetration and circulation of atoms within the tailing’s specimen. Figure 3.15 shows the tailings specimen being placed into an XRF container in preparation for an XRF test for mineral composition analysis.

Figure 3.15: Illustrating the placement of tailings into the XRF test container in preparation for the XRF test

The XRF tool was switched on, and the mineralogy test option was selected; therefore, the XRF test was performed as depicted. The test procedure involved holding the XRF tool, pointing it directly at the XRF container containing the tailings specimen, and pulling the trigger to irradiate the tailings specimen with the X-ray beam. The XRF test conducted is illustrated in Figure 3.16

Figure 3.16: XRF test results for mineral composition analysis on tailings

The elements of the tailings' specimen were digitally displayed on the tool, and the tailings' mineralogy was recorded. The test was repeated for the remaining two specimens, and the results were recorded and compared.

3.5. Limit equilibrium analysis

Limit equilibrium was performed using Slide 2 RocScience software. The geotechnical analysis method used for slope stability analysis is the limit equilibrium method. This method was selected due to its time efficiency when modelling, compared with other numerical methods such as Finite Difference method (FDM), Finite Element method

(FEM), and Boundary Element Method (BEM). The Limit Equilibrium Method (LEM) provides accurate factor-of-safety results, which align with the objectives of this study. The analytical method was undertaken specifically to determine the FoS of the TSF and to quantify the results of experimental analyses of other parameters that determine deformation, such as the triaxial tests in Chapter 4. The LEM is the proper tool for determining the FoS as compared to the aforementioned numerical modelling method. The model was run using three Limit Equilibrium Methods to obtain accurate results. The three Limit Equilibrium methods used include Bishop's simplified method, Janbu's simplified method, and Spencer's method. The tailings are assumed to obey the Mohr-Coulomb (MC) criterion of the LEM. The FoS was determined based on input parameters obtained from the experimental analysis. Each parameter was subsequently increased and decreased by two to observe fluctuations in the FoS. The model was run, and therefore, the FoS under the increased parameter values was determined. A similar process was repeated, with the geotechnical parameters reduced to compare the FoS when each parameter is low versus when it is high. This process was undertaken to study the impact of variation in the values of each geotechnical parameter of tailings on the FoS. The input parameters, including tailing cohesion, friction angle, unit weight of tailings, and pore water pressure, were utilised. The 2-dimensional geometry was drawn using Slide 2, incorporating the dimensions of the actual tailing dam, including the length and height of the benches and the TSF's overall elevation. The elevation of the tailing dam is 60 m, the height of each bench in a tailing dam is 18 m, whereas the width of each bench is 25 m. The steps undertaken to perform the simulation are illustrated in the flowchart in Figure 3.17.

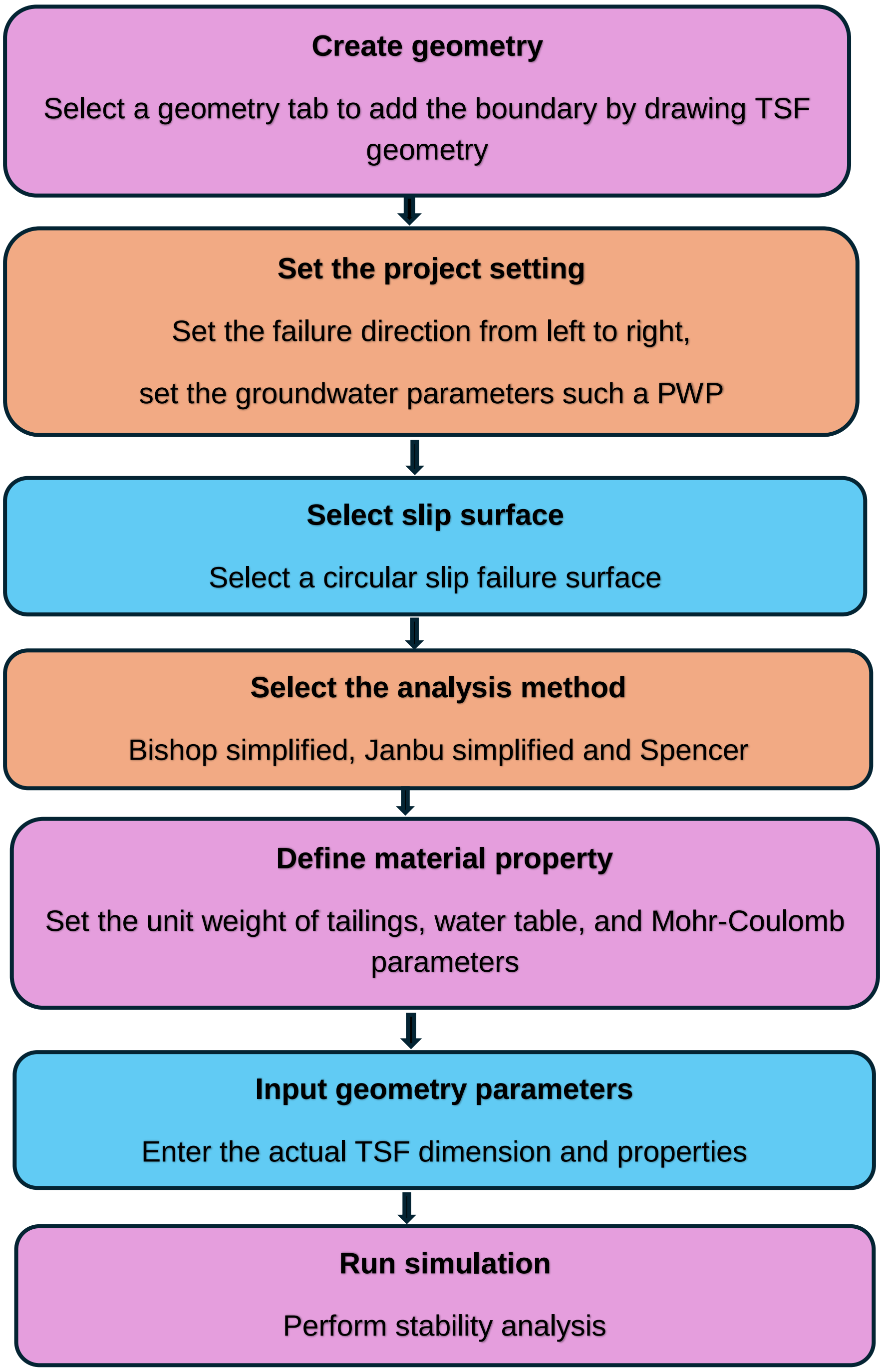

Figure 3.17: A flow chart summarising the procedure for LEM analysis

The steps undertaken in the LEM analysis are thoroughly explained in the flowcharts shown in Figure 3.17. The steps undertaken in the analysis are as follows:

1. Creating a geometry by selecting the geometry tab, then adding a boundary. This allows for a free sketching of the TSF geometry.
2. The geometry was drawn following the actual dimensions of the TSF

3. Set the project settings. The project settings involve general settings (failure direction). The failure direction is set from right to left because the geometry was drawn left-to-right. The pore water pressure was put on the groundwater icon under project settings
4. Set the surface of the geometry to determine the slip surface failure type. The circular failure was selected.
5. Set the method of analysis into Bishop simplified, Janbu simplified, and Spencer simplified to specify the LEM of analysis.
6. The material properties were defined on the Define Material Tab. The properties defined include surface water properties (unit weight of tailings, water table). The selected failure criterion is Mohr-Coulomb, with shear strength parameters (cohesion, friction angle) added.
7. The geometry was sketched with the dimensions of an actual tailing dam; all the parameters were specified according to the values of each parameter from experimental analysis. The analysis method was also set. After all, the model was set up, computed in accordance with all the LEMs, and interpreted to obtain the FoS.

The model was rerun to assess the impact of each tailing's geotechnical property on the FoS of the TSF slope. Results for the FoS were recorded after each change in the tailings' geotechnical properties.

3.6. Challenges of the study

Several challenges were encountered during the data collection for the study. The analysis of shear strength parameters required the use of a shear box; however, due to limited access to the tool, the triaxial test machine was utilised instead. This choice was made because the triaxial test offered greater flexibility, enabling simultaneous analysis of parameters such as pore water pressure (PWP) and shear strength. Additionally, obtaining the necessary permission letter from the mine for ethical clearance took longer than expected, resulting in delays to the study. Securing permission to access the tailing dam for sample collection also presented a significant challenge.

3.7. Concluding remarks

This chapter has entailed the procedures followed in the experimental analysis of each geotechnical property. The standards used to analyse each geotechnical property were identified, and the steps followed were detailed. The geotechnical parameters identified in the previous chapter were analysed using various test methods to achieve the second objective mentioned in Chapter One. The results of each experimental test are presented in Chapter Four, which follows this chapter.

Chapter 4 Effect of geotechnical properties of tailings on the stability of TSF

4.1 Introduction

This chapter presents and interprets the findings of laboratory analysis. The discussion focuses on how each geotechnical parameter of the tested tailings affects its stability. The debate is presented in comparison with the literature in Chapter Two to understand the correlation between the literature and the findings of this study. The relationships among various parameters were articulated. The findings presented in this chapter are based on the standard laboratory standards followed during the experimental analysis. Results on geotechnical properties are presented in graphs, charts, and tables. The geotechnical properties tested include optimum moisture content (OMC), maximum dry density (MDD), Pore water pressure (PWP), Atterberg limits, particle size distribution (PSD), shear strength, California bearing ratio (CBR), and permeability (Hydraulic conductivity). This chapter highlights the effect that each of these parameters has on the stability of the tailing dam. Other parameters, such as the elastic modulus, Poisson's ratio, and unit weight of tailings, were calculated to quantify TSF stability results based on geotechnical properties.

4.2. Geotechnical parameters affecting the stability of TSF

4.2.1. Shear strength

The shear strength of the soil was tested using triaxial testing to determine the maximum load/force the tailing specimen can sustain before deformation. Shear strength parameters from the laboratory experiment results were recorded and illustrated in a Mohr-Coulomb chart in Figure (4.1) and a Table (4.2) respectively. The Tables present the shear strength parameters determined in three undrained consolidated triaxial tests.

Figure 4.1 illustrates the relationship between normal and shear stresses, presented in Mohr circles of Coulomb. The small triangular, star and circles surrounding the three circles of Mohr columb on graph were added to differentiate between the three specimens.

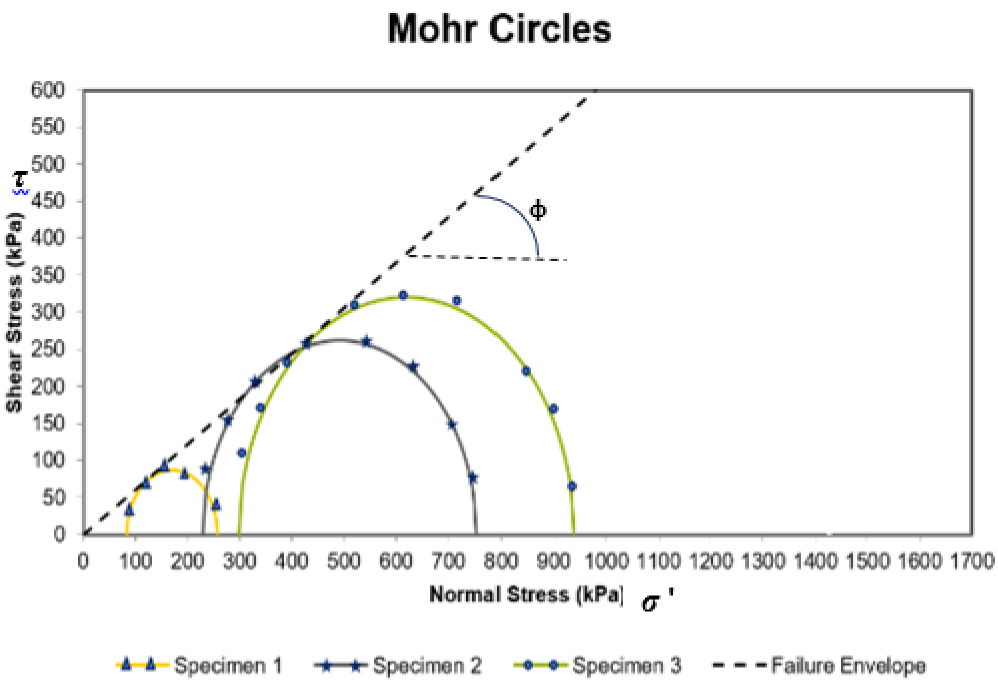

Figure 4.1: A Mohr-Coulomb circle chart depicting a relationship between vertical (normal) and horizontal (shear) stress

Shear strength parameters were determined using consolidated undrained triaxial tests on three specimens. Results showed a friction angle of 31.5° and zero cohesion, classifying the tailings as cohesionless silt-sand (SM) under the Unified Soil Classification System chart. Figure 4.1 (Mohr-Coulomb circle) illustrates the failure envelopes for the three specimens. Specimen 1 failed at approximately 120 kPa normal stress and 90 kPa shear stress, Specimen 2 at 300 kPa for both normal and shear stress, and Specimen 3 at 400 kPa normal stress and 250 kPa shear stress. In all cases, the failure envelope intercepts the y-axis at the origin, confirming that the material is cohesionless. The measured friction angle of 31.5° lies within the typical range for silty sands (30°–34%), indicating moderate shear resistance (Ubani, 2022). This suggests that while the tailings have sufficient strength to resist sliding under moderate loads, their stability relies mainly on interparticle friction rather than cohesion. Cohesionless material contains particles that do not adhere to each other because they lack the bonding agent (clay/electrostatic, or Van der Waals forces) between them. Consequently, stability may be reduced significantly under conditions of increased pore pressure or saturation (Hu et al., 2015; Shanmugam, 2016).

The diagonal failure envelope describes the direct, proportional relationship between tailings failure and the stresses acting on the tailings. The normal stress was exerted from 90 kPa to 260 kPa, as depicted on the x-axis (normal stress) from the Mohr-Coulomb curve in Figure 4.1, which produced a failure envelope. The failure in specimen one, represented by 1st circle, began at the normal stress of 100 kPa and the shear stress of 65 kPa. The failure is shown at the point where the 1st circle intersects the dotted failure envelope line. The shear stress exerted by the principal stresses on the material caused the tailings grains to slide against each other, leading to failure, as depicted on the failure envelope.

Specimen number two represents a failure that began at a normal stress of 300 kPa and a shear stress of 200 kPa. The failure in specimen number two is defined as the initial point at which the second circle touches the failure envelope line. Normal stress was exerted from 240 kPa up to 750 kPa. Whereas in specimen number three, the failure envelope began at 400 kPa normal stress and 255 kPa shear stress. The normal stress on specimen number three was exerted from 300 kPa to 940 kPa. The envelope line begins to touch the y-axis, indicating the shear stress at zero, which characterises a cohesionless material (where cohesion equals zero). The tailings are non-plastic.

Shear strength parameters were tested in accordance with the Mohr-Coulomb failure theory and the standards described in Chapter 3. Table 4.1 depicts the shear strength parameters that were used to calculate shear strength. Shear strength was calculated using equation 3.1 in Chapter 3.

Table 4.1: Depicts shear strength parameters

Shear strength parameters in Mohr-Coulomb failure	values	Si units
cohesion	0.0	kPa
Internal friction angle	31.50	°
effective stress	77.76	kPa

The strength of soil depends primarily on its frictional angle and cohesion. The friction angle determines the shear stress at which the soil fails (Liu et al., 2012). The friction angle is used to determine the friction shear.

4.2.2. The relationship between pore water pressure and axial strain

Three tailings specimens were analysed to understand the relationship between pore water pressure in the tailings and axial strain. Figure 4.1 shows the results of each specimen on the response of the pore water pressure when the axial load/strain was exerted on it. The small triangles, stars, and circles along the graph lines have been added to clearly differentiate between the three specimens.

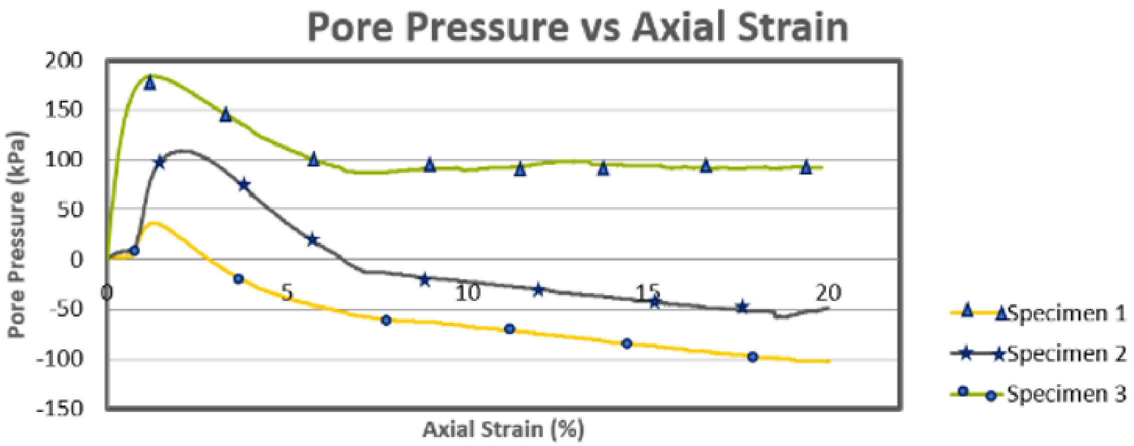

Figure 4.2: Illustrating the relationship between axial strain and pore water pressure

The relationship between the load applied to a tailings sample during triaxial testing and the resulting stress is illustrated in Figure 4.2. This figure shows how axial (vertical/longitudinal) strain affects the pressure within the pore spaces between tailings particles. Specifically, it depicts the relationship between pore pressure and vertical strain, ranging from 0 to 3 vertical strain and from 0 kPa to 180 kPa pore pressure at the beginning of the test. As vertical strain increases in the specimen, pore pressure also increases, indicating that pore water pressure is directly proportional to vertical strain. This increase in pore water pressure is due to compression between tailings particles during an undrained consolidation test. This results in close particle packing, increasing grain-to-grain contact, and reducing pore space. Close packing reduces the volume of water between pore spaces, thereby increasing pore water pressure. The entire process of transferring stress to the pore is referred to as effective stress consolidation (Hueso, 2017).

At the beginning of the test, pore water gradually escapes, dissipating the pore water pressure initially increased by the applied vertical strain.2 As the test progresses, the graph in Figure 4.2 shows a decrease in pore pressure, dropping to negative kPa values as strain increases. This trend is attributed to ongoing water escape from the pore spaces, leading to a sudden reduction in pore water pressure. Notably, there is a sharp decrease in pore pressure between the 2 and 6 strain. Additionally, Figure 4.2 illustrates a stable relationship between tailings strain and pore pressure over 6% to 20% axial strain. This indicates that there is no further change in pore water pressure, indicating that the system has reached a stable undrained state. The parameters used to calculate the pore-water pressure in tailings are shown in Table 4.2.

Table 4.2: Tailings pore water pressure parameters

pore water pressure parameters		
unit weight	values	SI unit
γ_w	9.81	kN/m^3
γ	20.76	kN/m^3
Depth of TSF (h)	60	M
waterhed	5	kPa
PWP	588.6	kPa

The tailings pore water pressure under undrained, consolidated conditions is 588.6 kPa. The pore water pressure of tailings was calculated using equation 3.2 in chapter 3. The tailings have a high PWP, indicating they are saturated. The tailings exhibit high pore water pressure, which tends to reduce their effective stress and thereby their ability to resist load (Oruabena et al., 2018). This PWP will then reduce the shear strength of tailings, thereby reducing tailings and TSF stability and posing a threat of TSF failure (Wu et al., 2025). A general tailings pore-water pressure of 588.6 kPa indicates a saturated condition, reduced stability, and a high risk of failure (Oruabena et al., 2018).

An increase in pore water pressure decreases the effective stress between tailings particles, which therefore reduces the overall strength of tailings and their stability. A decrease in tailings strength reduces the tailings stability, which consequently increases the chances of TSF failure, as mentioned in the literature in chapter two.

4.2.3. Effects of moisture content on the stability of tailings

Moisture content fluctuations affect soil plasticity and swelling characteristics, particularly in the presence of fine particles. The plasticity, cohesion, and swelling characteristics of soil have an impact on the soil's stiffness, deformation strength, and, consequently, its stability.

4.2.3.1. Expansive and plasticity behaviour of tailings

Figure 4.3 (a) illustrates the expansive character of the tailings, which can be used to determine soil stability, while Figure 4.3 (b) illustrates the plasticity behaviour of the tailings.

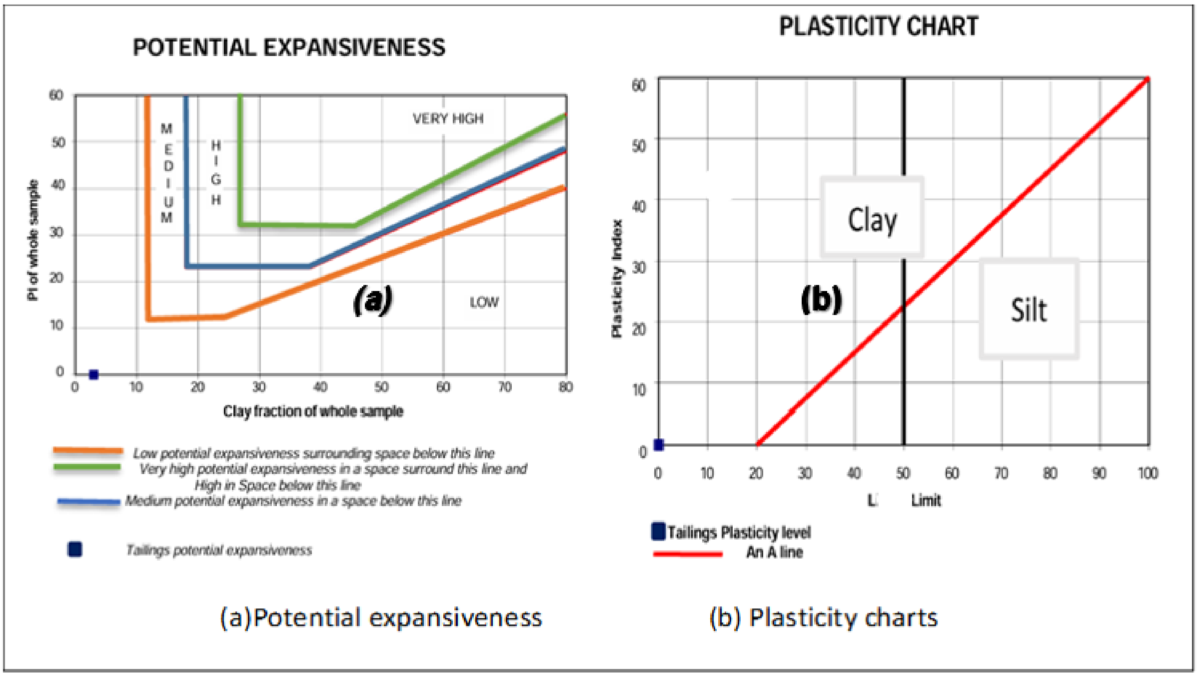

Figure 4.3: Tailing heave characteristics

The blue dot on a potential expansiveness chart indicates the overall potential for tailings expansion. This blue dot corresponds to a tailings sample with a 3% clay fraction and a Plasticity Index (PI) of 0%. The low clay fraction signifies that the tailings are cohesionless and have a low PI. As a result, the tailings exhibit minimal swelling and shrinkage, indicating a low potential for expansion (Barbosa et al., 2023). This stability remains regardless of moisture content, whether from rainwater or any additional water added to the tailings (Firoozi et al., 2017). The absence of cohesion enhances the shear strength of the tailings due to increased frictional interlocking among the tailings particles, thereby stabilising the tailings storage facility (TSF) (Keaton, 2018). Consequently, the tailings dam remains stable despite variations in moisture content.

Figure 4.3b presents a plasticity chart of the tested tailings, modified from the Casagrande chart. The charts reveal that the tailings exhibit low plasticity and low cohesion, as indicated by a low liquid limit and a plasticity index of zero. This suggests that the tailings are stable, contributing to a stable Tailings Storage Facility (TSF). The plasticity index represents the range of water content over which the soil exhibits plastic behavior, meaning the particles adhere to one another. The liquid limit is the moisture content at which the soil transitions fr8om a liquid to a plastic state. In the chart, the blue dot indicates the category of the tested sample, which exhibits a zero liquid limit and a zero-plasticity index. The low plasticity is attributed to the relatively low clay and silt content in the tailing sample, which has a significant sand fraction, as determined by sieve analysis. According to the Unified Soil Classification System (USCS) established by the American Society for Testing and Materials, the tailings are classified as silt-clay (SM). The findings from the Particle Size Distribution (PSD) analysis were corroborated by hydrometer analysis.

Figure 4.3b depicts the direct relationship between liquid limit (LL) and plasticity index (PI) of fine-grained soil for the general analysis of soil plasticity. An increase in liquid limit increases the plastic index of tailings; however, below 20% LL, PI remains constant. The tailing plasticity is represented by the blue dot, which depicts tailings with PL and LL equal to zero, resulting in a plasticity index of 0. The plasticity index was determined using the calculation following equation 3.3 in chapter 3. The blue dot is located under an A line, indicating low tailings plasticity and an overall low expansive characteristic.

Soil with a high clay content exhibits expansive behaviour, swelling when saturated with water and shrinking when it dries (Lees, 2021). The low-clay fraction of tailings exhibits low to no plasticity, and therefore, fluctuations in moisture content will have no impact on their swelling and shrinkage properties. The low clay content has a negligible influence on the tailings heave, and it will maintain favourable stability conditions for the tailings and thereby the stability of TSF. This is because soil with less clay content is less compressible, which minimises volume change under loading and therefore remains stable under cyclic loading (Firoozi et al., 2017)

4.2.4. Effects of particle size distribution (PSD)/ on TSF stability

The greater percentage of particle size fraction in the tailings, as determined through a sieve analysis test, is the sand-size tailings particles. The table and the particle size gradation curve below indicate that 89% of the tailing's particles are sand-sized, 7% are silt-sized, 3% are clay-sized, and the gravel-sized particles comprise only 1%. The tailings consist of a large fraction of sand and a smaller fraction of clay, gravel, and silt, which may negatively affect their stability. This is because particle gradation plays a greater role in tailings stability. A well-graded material consists of a mixture of fine and coarse materials, where the fine materials act as a binding agent between the coarse materials (Vahidi-nia et al., 2024). This will enhance the stability of coarse material, unlike tailings, which consist mainly of coarse (sand-sized) particles that easily slide over one another under shear stress due to their cohesionless nature (Abu et al., 2025).

Figure 4.4 shows a particle-size distribution curve from a sieve analysis test used to determine the cumulative percentage passing of the tailings.

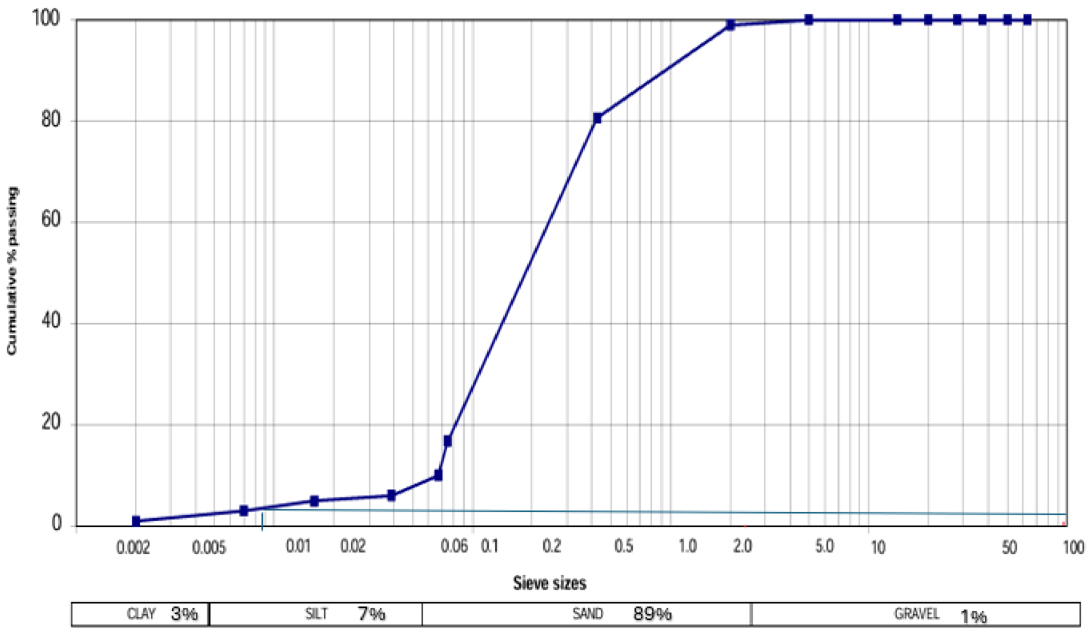

Figure 4.4: Depicts the tailings particle size distribution curve

The tailings exhibit a grading modulus of 1.04, which indicates a moderate proportion of fine to sand-sized particles. This value suggests that the material is fairly graded and reasonably well distributed across particle sizes. The presence of a moderate amount of fine material is beneficial, as it improves stability and compaction characteristics. As previously stated, according to the USCS, the tailings are classified as silt–sand (S/M) and are predominantly cohesionless, with sand-sized particles predominating. Therefore, the relatively large pore spaces associated with sand-sized grains promote adequate drainage, allowing water to pass through easily (Paltseva, 2024; Wolschick et al., 2021). When favourable drainage conditions are maintained, the stability of the tailings and the tailings storage facility (TSF) is enhanced. Moreover, under the COLTO classification system, the tailings fall within the G7 category, which reflects a coarse-grained texture and a cohesionless, non-plastic behaviour. This classification indicates low compressibility; however, the lack of cohesion may limit compaction efficiency (Kolay, 2005), potentially adversely affecting overall stability if moisture content and drainage conditions are not adequately managed.

4.2.5. The determination of Tailings bearing capacity using the tailings California bearing ratio (CBR)

A high soil bearing capacity value indicates a soil with high stiffness, typically due to high compaction. Soil with high CBR has a high elastic modulus. This is because stiff soil usually has higher strength and is stable. Table 4.3 illustrates the CBR value under the influence of various compactions for three different moulds in the triaxial test.

Table 4.3: CBR (%) values from three different tailings moulds named A-C

CBR SANS 300-GR-40	
MOULD A	
Moulding moisture content (%)	3.3
Dry density (kg/m^3)	2119
Relative compaction	100.0
CBR (%)	24
%swell	0.0
MOULD B	
Dry density (kg/m^3)	2010
Relative compaction	94.8
CBR (%)	18
%swell	0.0
MOULD C	
Dry density (kg/m^3)	1904
Relative compaction	89.8
CBR (%)	13
%swell	0.0

Mould A has a CBR value of 24% at 100% compaction, resulting in a dry density of 2119 kg/m³. Mould B, on the other hand, has a CBR value of 18% at 94.8% compaction, with a dry density of 2010 kg/m³. Mould C shows a CBR value of 13% at a compaction pore pressure of 89.8%, resulting in a dry density of 1904 kg/m³. The dry density values were determined from the compaction forces applied during triaxial testing, which affect the tailings volume and, consequently, density variations. The observed decrease in density, moisture, and compaction from Mould A to Mould C correlates with a reduction in CBR value. All three moulds exhibit zero swelling. According to COLTO standards, the analysed tailings fall under the G7 classification. G7 material tested at a compaction of 93% of MDD with a CBR of 15% or more is considered strong. Conversely, any G7 material below 15% at 93% MDD is regarded as weak due to its insufficient load-bearing capacity. Table 4.3 indicates a CBR value of 16% at 93% dry density, exceeding the 15% threshold and classifying it as a medium-strength material under COLTO standards. The CBR value of the tailings increased from 13% to 24% with greater compaction effort. This improvement occurs because increased compaction reduces the volume of tailings, thereby increasing their density and enhancing their CBR value. The tailings exhibit a medium-low average bearing capacity, resulting in good stiffness under compaction. High stiffness in the tailings suggests a high elastic modulus, indicating strong material properties that contribute to stability under load.

4.2.6. Permeability/hydraulic conductivity of tailings

This section discusses the results of a constant permeability test and their relation to the stability of Tailings and TSF. The parameters used to calculate hydraulic conductivity are depicted in Table 4.4.

Table 4.4: Permeability/ hydraulic conductivity parameters of tailings samples

Parameters	**value**	**Units**
Moisture content	3.5	%
Flow (ΔV)	170.6	M^3/s^2
Max dry density	2116	kg/m^3
Time	00:34:47	h:m:s
water Head	5.0	kPa
K	1.49×10^{-4}	cm/s

The tailings pore water pressure test was conducted using an undrained triaxial test on a tailings sample with a moisture content of 3.5%. The hydraulic conductivity was calculated using Equations 3.3 to 3.5 in Chapter 3, yielding a calculated hydraulic value of 1.49×10^{-5} cm/s. According to Swiss standards, the coefficient of permeability for stable soil should range between 1×10^{-6} and 1×10^{-4} cm/s. The measured hydraulic conductivity of the tailings falls within this range, influenced by the tailings grains, which are classified as silty sand (USCS).
This permeability value indicates that the tailings are sufficiently permeable, allowing water to pass through their pores, as outlined in Swiss standards in Chapter 3. Furthermore, this permeability helps maintain the tailing pore-water pressure at a level that does not negatively affect the stability of the TSF. During slurry deposition into the TSF, the pore water pressure may dissipate relatively quickly in permeable (coarse) tailings, leading to an increase in effective stress and shear strength. However, in fine-grained tailings with low permeability, pore pressure dissipation is slow, which can reduce stability under undrained conditions. The permeability of the tailings was compared to the standards outlined in the permeability guideline (SN 670 010b) developed by the Swiss in the early 1990s, presented in Table 2.1 in Chapter Two.

4.2.7. Maximum dry density (MDD) and unit weight of tailings

The density of tailings measures the mass of tailings per unit volume of tailings specimen. Table 4.5 illustrates the MDD and the parameters used to calculate the unit weight of tailings. MDD is influenced by compaction and reflects the soil's stiffness. Well-compacted tailings are typically dense, making them stiff and high in strength. Denser tailings have tightly packed particles, which increase stiffness and reduce hydraulic conductivity, thereby enhancing TSF stability (Musbah et al., 2024; Shaheb et al., 2021). The maximum dry density of tailings, determined through experimental analysis under compaction, is 2116 kg/m³ at an optimum moisture content of 3.5%. The maximum dry density is the highest density achievable during compaction when there is sufficient water (optimum moisture content) to facilitate particle packing (Ali et al., 2024).

The tailings exhibit a unit weight of 20.76 kN/m³, indicating that they consist of dense, saturated granular soil composed of well-graded sand-sized particles. A well-graded sand usually has a higher unit weight due to its dense packing. This tends to increase tailings compaction and compressibility, reducing percolation of water and improving the overall stability of the TSF (Shaheb et al., 2021). The unit weight of the tailings influences their compaction characteristics, which, in turn, affects their stiffness and strength. A unit weight of 20.76 kN/m³ indicates that the tailings are stable (Musbah et al., 2024). However, other geotechnical parameters, such as moisture content and shear strength, can also affects stability.

Table 4.5: unit weight variables

Unit weight parameters	Value	SI Unit
MDD	2116	kg/m^3
g	9.81	m/s^2
γ	20.76	kN/m^3

4.2.8. Elastic modulus of tailings

Table 4.6 depicts the physical parameters used to calculate the elastic modulus of tailings. Effective and vertical strain are the two parameters used to calculate the elastic modulus of tailings. The tailings have an effective stress of 77,76 kPa and a vertical strain of 0.25, obtained from triaxial tests of tailings shear-strength parameters. These parameters were used to calculate the elastic modulus of tailings using Equation 3.5 in Chapter 3.

Table 4.6 Shear strength and elastic modulus parameters

Calculated parameters		
Parameters	Values	units
σ' av	77.76	kPa
c	0.0	kPa
ϕ	31.5	°
τ	47.66	kPa
ε_{axial} av	0.61	
E	0,31	MPa
$\varepsilon_{lateral}$ av	0.25	

The tailings have an elastic modulus of 0.31 MPa. Earth materials that have a stable elastic modulus are those that are stiff enough to resist elastic deformation. The tailings have a low elastic modulus compared to the elastic modulus of USCS silty sand-sized soil. The low elastic modulus resembles a low stiffness tailing that can easily be deformed even under the slightest load (strain) that can be applied to it. This tends to reduce the stability of tailings and poses a risk to the stability of the TSF. The classification of the elastic modulus of tailings was made by Kezdi (1974) and Prat et al. (1995), who classified the elastic modulus of silty sand soil as ranging between 7 and 12MPa (refer to Table 2.1).

4.3. Impact of Poisson's ratio on the tailings' compressibility behaviour

The parameters used to calculate the poison's ratio are presented in Table 4.7. Poisson's ratio was calculated using equation 4.1.

$$P_{v}=\frac{\varepsilon_{lateral}}{\varepsilon_{axial}} \qquad 4.1$$

The tailings have a Poisson's ratio of 0.41, which represents slightly low compressible material. The poisons ratio of this value indicates material that can be easily laterally deformed under vertical strain and expands under axial strain (Essien et al., 2014).

Table 4.7: values used for calculating Poisson's ratio

Parameters	**Values**	**SI unit**
σ' ava	77.76	kPa
c	0.00	kPa
ϕ	31.5	°
τ	47.66	kPa
ε_{axial} av	0.61	
E	0.31	MPa
$\varepsilon_{lateral}$ av	0.25	
P_{v}	0.41	

The tailings exhibit a high Poisson's ratio, as noted by Kumar Thota et al. (2021). Poisson's ratio for soil ranges from 0 (the minimum) to 0.5 (the maximum). Soils with a high Passion's ratio tend to exhibit significant lateral deformation relative to axial strain. The tailings with a Poisson's ratio of 0.41 are therefore likely to display a near-incompressible behaviour with notable lateral strain under loading.

Highly compressible materials easily deform, which reduces their strength. The tailings have low effective stress, a low friction angle, and low compressibility, which collectively contribute to the overall reduction in tailings shear strength. The tailings have a sand-like texture and therefore exhibit lower compressibility compared to clay and silt. However, tailings of the SM grain size are usually compressible. The compressible tailings have responded to the strain/load applied during consolidation, indicating a volume change.

Figure 4.5 shows the influence of lateral axial strain/load during the consolidation stage of tailings on the triaxial test. The graph illustrates the relationship between the volume change of tailings over time of consolidation. The sample was divided into three specimens to monitor how each specimen behaves under the influence of the applied load/strain. The graph illustrates the volume change over time for all specimens, ultimately resulting in a negative value. These indicate an intensive reduction in tailings volume over time under applied load or strain.

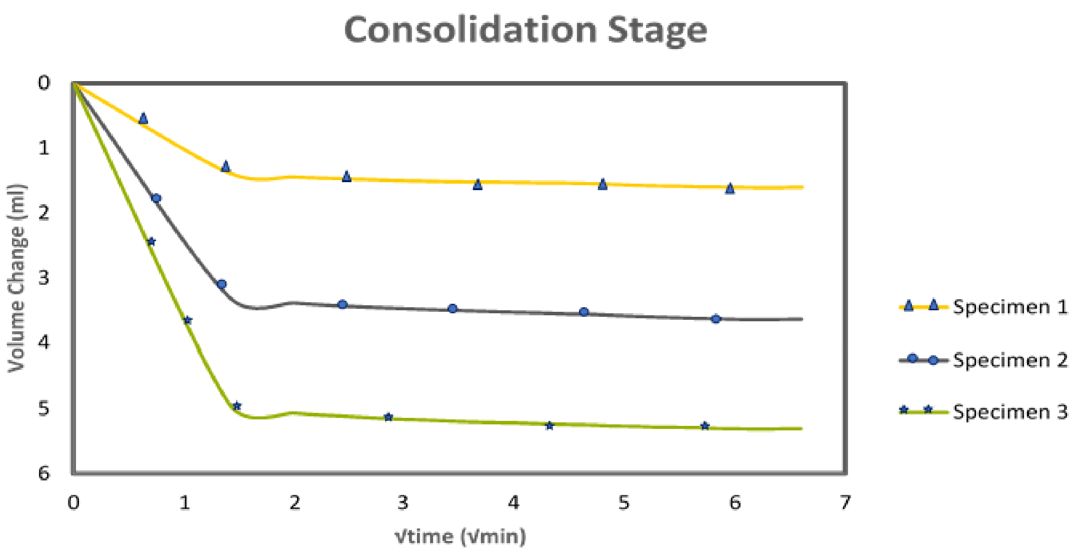

Figure 4.5: Depicts a volume change of tailings in time throughout consolidation

4.4. Analysis of mineral composition of tailings

The mineralogical content of the tailings is known to influence their mechanical behaviour; therefore, the mineral constituents were detected using XRF. Minerals that are over one percent include quicklime (calcium oxide), hematite, quartz, diphosphorus pentoxide, and manganese oxide. Table 4.8 presents the mineral constituents of tailings that exceed 1%. The XRF results for Specimen 2 show only Fe_2O_3, which is more than 1%.

Table 4.8: depicting high content minerals of tailings

specimen 1		specimen 2		specimen 3		average%
mineral	%	mineral	%	mineral	%	
Fe_2O_3	21.032	Fe_2O_3	12.83	Fe_2O_3	16.414	16.76
CaO	25.494	CaO	24.677	CaO	25.004	16.83
P_2O_5	1.807	P_2O_5	1.077	P_2O_5	1.724	1.18
SiO_2	4.013	SiO_2	2.987	SiO_2	3.332	2.44
MgO	5.539	MgO	5.101	MgO	5.165	3.57

The tailings consist of a large content of quicklime, which accounts for 16.8%, followed by hematite at 16.76%. manganese oxide has 3.57, with quartz content present in the tailings of 2.4 %. Diphosphorus pentoxide content in the tailings tested is at a low content of 1.1. XRF results revealed a diverse mineralogy; however, most elements and minerals exhibited very low concentrations, and therefore only those above 1% were recorded in Table 4.8. This is because the other minerals appear in very low content that is as low as 0.007 and therefore does not make much impact on the overall mineralogy of the tailings. Quartz is known for its durability characteristics and resistance to weathering during rainy seasons (Kumar et al., 2024). A higher quartz content in tailings can increase the internal friction angle and shear strength due to the hardness, angularity, and resistance to crushing of quartz particles, which enhances inter-particle friction and interlocking.

Diphosphorus pentoxide is a dehydrating agent, which absorbs water, and changes it into phosphoric acid, which acts as a binding agent between the tailing's grains. This process reduces the swelling and shrinkage characteristics of tailings. Calcium oxide and hematite act as a binding agent between tailings particles. Calcium oxide has the capacity to break clay structures within tailings and flocculate the clay particles that bind tailings particles together (Jawad et al., 2014). This may increase compressibility, as clay acts as a binding agent, enhancing electrostatic bonds between tailing particles.

4.5 Concluding remarks

This chapter discussed the geotechnical behaviour of the tailings based on grading characteristics, moisture content, pore water pressure, and shear strength parameters, among others. The results indicate that the tailings are predominantly cohesionless, with 89% of the particles sand-sized. This has mainly contributed to TSF's moderate stability. The experimental test results have shown different impacts on the tailings. Various geotechnical parameters, such as PWP, moisture content, and permeability, affect the shear strength of tailings, thereby determining the stability of the tailing dam. These findings provide a basis for the numerical stability assessment of the tailing's storage facility, which is addressed in the following chapter.

Chapter 5 Limit equilibrium assessment of the stability of tailings storage facilities.

5.1. Introduction

This chapter presents the results and discusses the limit equilibrium analysis of the tailings dam's stability. This was done through employing a slope stability software called RocScience Slide2. Limit equilibrium analysis was performed to determine the FoS using the methodology outlined in Chapter 3. The model's input parameters are the geotechnical factors presented and discussed in Chapter 4. The simulation focuses on the parameters that most significantly control shear strength and stress conditions within the tailings, namely cohesion, unit weight, friction angle, and pore water pressure. These parameters were varied systematically in the LEM analysis to assess their individual and combined effects on slope stability and overall TSF performance.

Table 5.1 presents the input parameters and their amended values. Each parameter was increased by 2, and the model was run to calculate the FoS. Subsequently, the value of each parameter was reduced by 2, and the model was rerun to determine the FoS. The parameters were assumed to have decreased by 2 to assess the effect of each parameter at its lower value (as per lab results) on the FoS. The value of each parameter was later increased by a constant value of 2 to assess the impact of a value higher than the original value of each parameter. The results for all three models, corresponding to each parameter, are presented in Figures 5.1-5.5.

Table 5.1: Input geotechnical parameters used for the simulation

Parameter	Original	C increase	C decrease	γ increase	γ decrease	ϕ increase	ϕ decrease	PWP increase	PWP decrease	SI unit
C	4	6	2	0	0	0	0	0	0	kPa
γ	20.76	20.76	20.76	22.76	18.76	20.76	20.76	20.76	20.76	kN/m3
ϕ	31.50	31.50	31.50	31.50	31.50	33.50	29.50	31.50	31.50	°
PWP	588.6	588.6	588.6	588.6	588.6	588.6	588.6	590.6	586.6	kPa

The LEM analysis was initially performed using the original values of each geotechnical parameter presented in Table 5.1. Figure 5.1 reveals that the FoS for the original parameters, obtained from experimental analysis, is 0.63. The FoS is less than 1, which represents the unstable slip slope (Bidyashwari et al 2017)

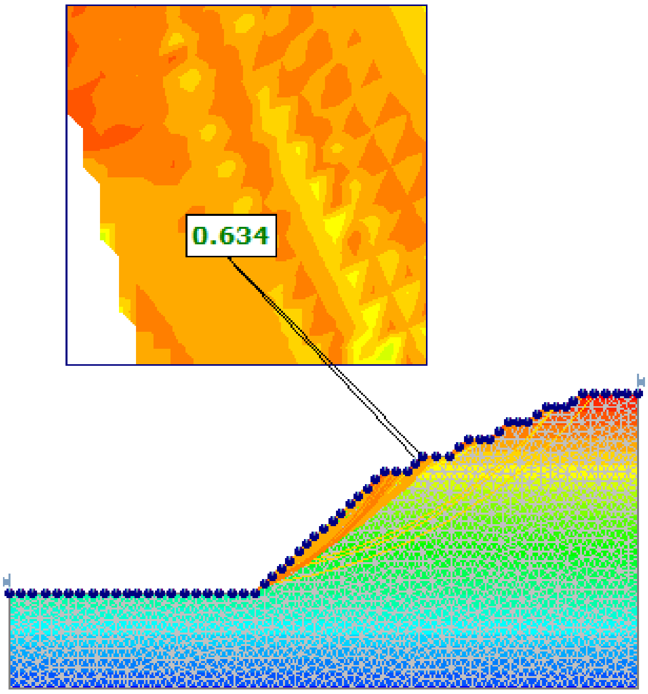

Figure 5.1: LEM results obtained from the original values

Bidyashwari et al. (2017) and Wu et al. (2025) have shown in their studies that a FoS less than 1 indicates an unstable slope. In contrast, a FoS greater than 1 indicates a stable slope. The TSF has a FoS of less than one, which represents that a driving force that is produced by the shear stresses acting on the tailings dam slope is greater than the resistive forces (Wu et al., 2025). When shear strength parameters such as cohesion and friction angle are low, the tailings material's resistance to failure decreases, increasing its susceptibility to failure. On the contrary, when the water parameters, such as pore water pressure and the unit weight of tailings, are higher, it reduces the effective stress of tailings, which is an inter-particles pressure that directly influences the shear strength, thereby reducing the FoS. It is worth noting that although the limit equilibrium analysis yielded a FoS of 0.63, large-scale instability was not observed in the field. This apparent discrepancy may be attributed to limitations associated with representing the complex in-situ behaviour of tailings using laboratory-derived material properties and simplified limit equilibrium assumptions. While the laboratory tests indicated negligible cohesion, the in-situ tailings may derive additional shear resistance from factors such as particle interlocking, density variations, and unsaturated conditions within portions of the deposit. Furthermore, the calculated FoS represents a theoretical stability condition and may not fully reflect the current field response of the TSF. Consequently, the results should be interpreted as indicating a potentially unstable condition that warrants attention, rather than as evidence that failure has already occurred.

5.2. Effect of cohesion on the safety factor

To examine the impact of cohesion on slope stability, the cohesion values obtained from laboratory analysis were varied. Figure 5.2. illustrates the numerical simulation analysis of the TSF slopes and the corresponding fluctuation in the FoS with cohesion variation. The actual value of cohesion of tailings that was analysed through experimental analysis is 0 kPa (referred to as the original cohesion value). The cohesion value was assumed to have decreased initially (marked by fig 5.2b) and later increased (marked by Figure 5.2c) to understand the impact of cohesion variation on the FoS. A similar approach was followed, where Figure 5.2(a) shows the original cohesion value, Figure 5.2(b) depicts a two-fold decrease in cohesion, and Figure 5.2(c) depicts an increase in tailings cohesion.

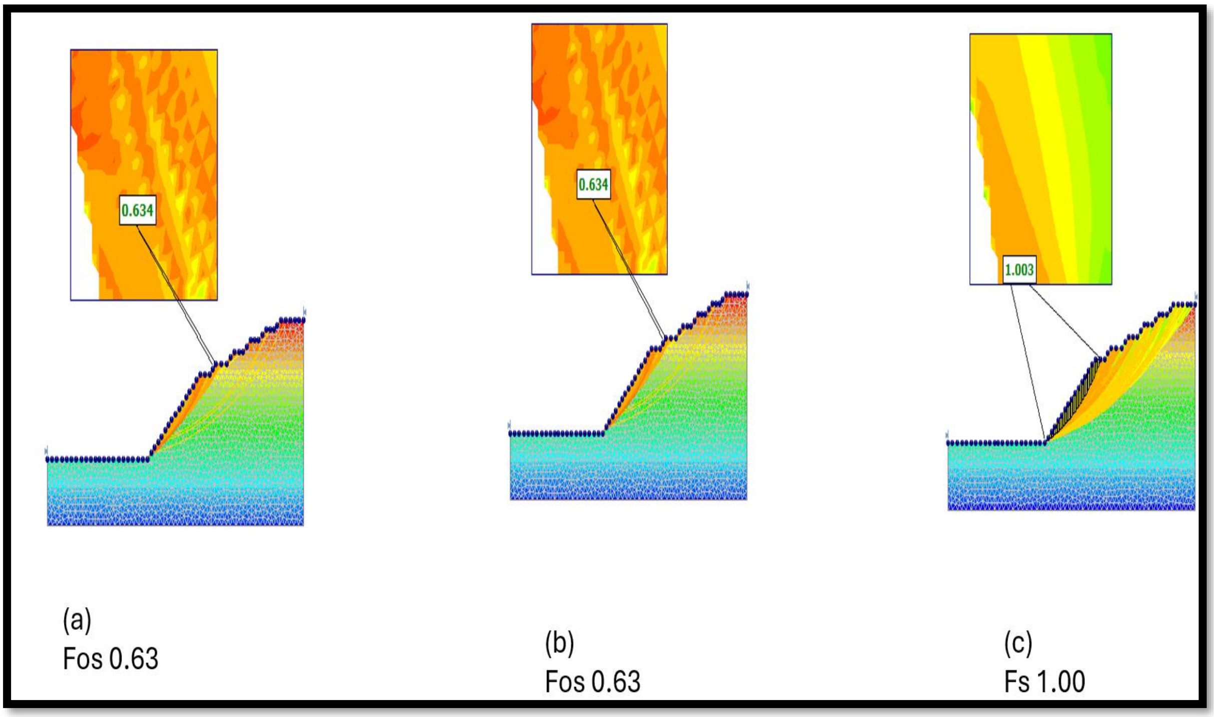

Figure 5.2.: Depicting the cohesion variation influence on the FoS

The FoS of the original value of cohesion of 0 kPa is 0.63 in Figure 5.2. (a). The FoS increases to 1.02 when cohesion is increased to 2 kPa in Figure 5.2.(c). Furthermore, in Figure 5.2.(b), the FoS remains 0.63 because it cannot be decreased below zero, as negative cohesion is invalid. Instead, soil can be cohesionless/non-cohesive (Gautam, 2018).

Generally, a FoS of one or above indicates a stable slope, whereas a FoS less than 1 indicates an unstable slope that has a chance of failure (Wu et al., 2025). The tailing material analysed has a FoS of 0.63 on the original cohesion of the tailings material (Figure 5.2.a), indicating instability of the TSF slope. An increase in cohesion also increases the FoS as depicted in Figure 5.2(c). An increase in the FoS with increasing cohesion is due to the stiffness of tailings particles, resulting from the interlocking of grains and electrostatic bonds that cause particles to adhere to each other (Gautam, 2018). The FoS is greater than 1 (Figure 5.2c), indicating a stable condition and reduced risk of failure.

5.3. Impact of unit weight on the factor of safety

A change in unit weight of tailings shows a negligible impact on the FoS. The liquid-equilibrium analysis results for the FoS, with unit weight variation, are illustrated in Figure 5.3.

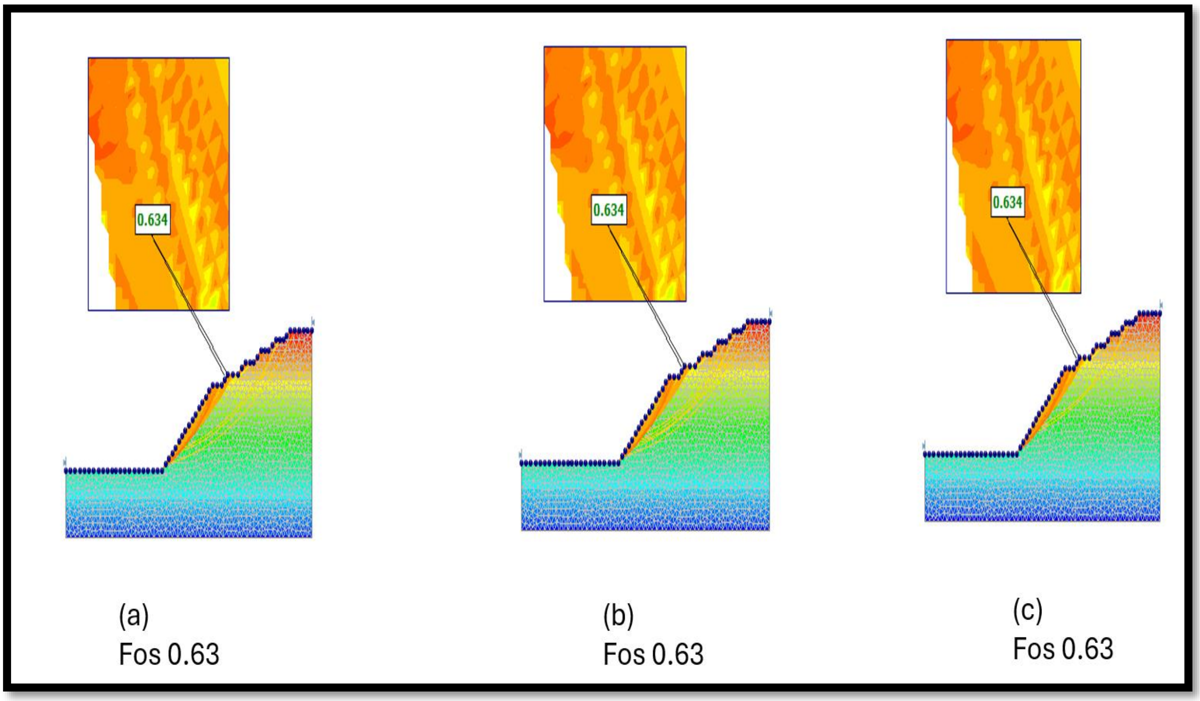

Figure 5.3: Depicts the impact of tailings unit weight on the FoS

The FoS of the TSF slope depicted in Figure 5.3 (a) is 0.63. As the unit weight increases, the FoS in Figure 5.3(b) remains at 0.63. The decrease in unit weight did not change the FoS; it remained 0.63. Moreover, a decrease in unit weight by 2 values did not affect the FoS, instead the value of FoS remained less than 0.63. The unit weight moderately affects the slope's safety factor, as its influence largely depends on the bulk density of the tailings material (Xu, 2025). This is because an increase in unit weight represents an increase in the bulk density (mass/Volume) of tailings, which increases the gravitational forces pulling the slope down, reducing its stability (Xu, 2025).

5.4. Impact of friction angle on the factor of safety

Friction angle has a significant influence on the stability of TSF. Figure 5.4 illustrates the relationship between the friction angle and the FoS of the TSF slope. The FoS decreased from 0.63 to 0.59 when the friction angle was reduced from 31.50 to 29.50°, as depicted in Figure 5.4(b). In Figure 5.4 (c), the FoS has increased to 0.69 when the friction angle increased from 31.50° to 33.5°, as illustrated in Figure 5.4 (c).

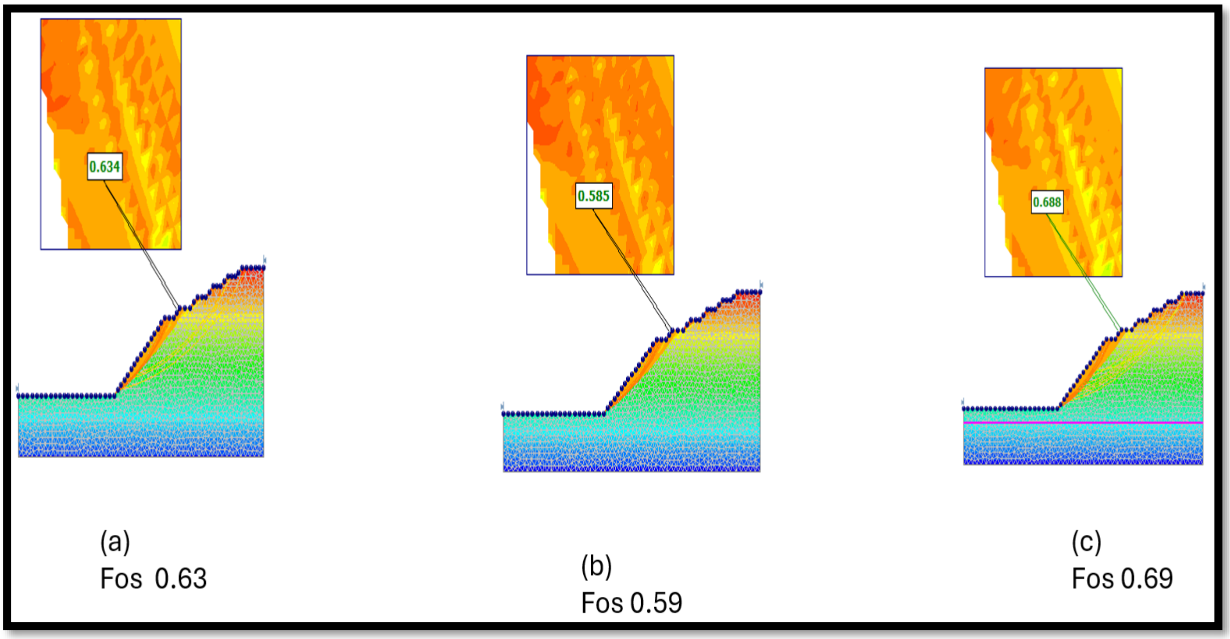

Figure 5.4: The influence of friction angle variation on the FoS

Figure 5.4 depicts that the friction angle is directly proportional to the strength of the tailing material. When the friction angle increases, the strength of the tailings material exceeds the stresses driving the material to failure. This increases FoS and stabilises the TSF slope. The friction angle influences the stability of TSF as depicted in Figure 5.4. Increasing the friction angle increases the shear strength of the tailings, thereby improving the stability of the TSF slope. Conversely, a decrease in the friction angle lowers the shear strength and reduces the TSF's stability as assessed by the FoS. A higher friction angle increases inter-particle friction and promotes greater angular contact between tailing particles, allowing them to resist sliding more effectively (Cárdenas-Barrantes and Ovalle, 2025). Hence, the increase in FoS as the friction angle increases.

5.5. Effect of PWP on the factor of safety

The pore water pressure was modified to understand the impact of PWP variation on the FoS of the tailing dam slope. Figure 5.5 shows the relationship between the pore water pressure and the FoS. The models are arranged in the same manner as the other analyses of other tailings' geotechnical properties.

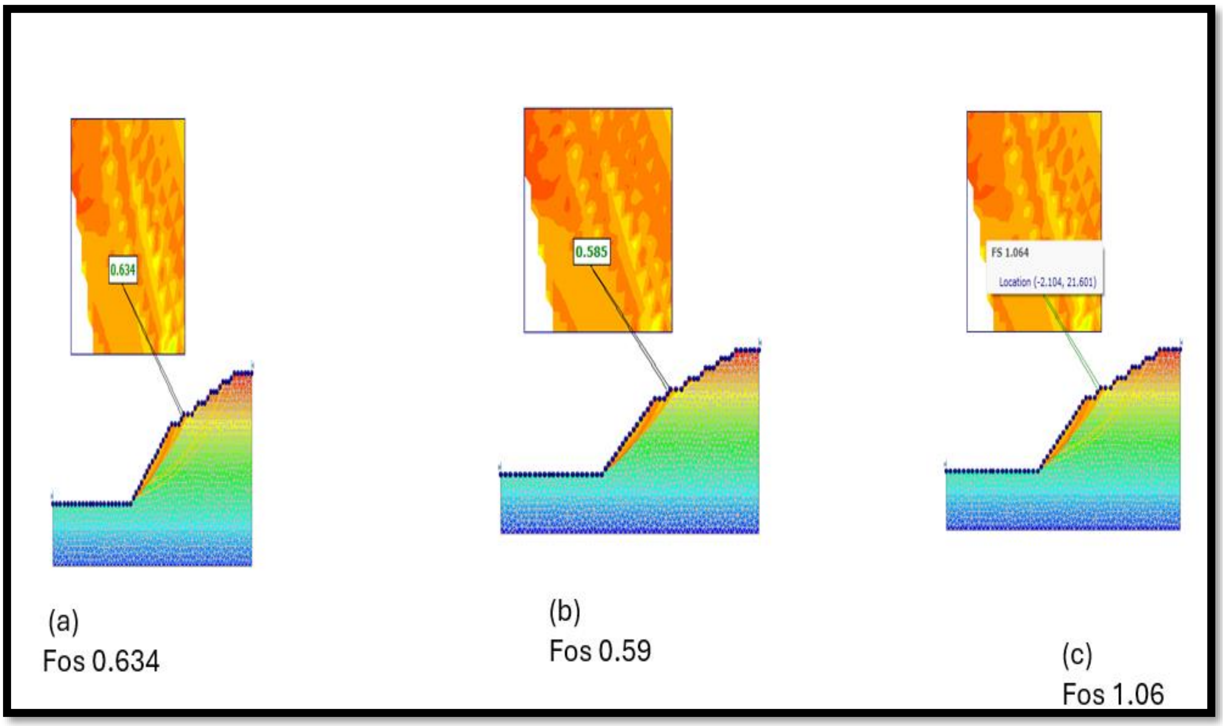

Figure 5.5: The relationship between tailings PWP and the FoS

The FoS decreased to 0.59 as pore water pressure increased (Figure 5.5b). A high pore water pressure reduces the effective normal stress that is responsible for decreasing the frictional resistance between tailings particles and the tailings shear strength, thereby reducing the FoS (Arya et al., 2020; Troncone et al., 2019). When the pore water pressure is reduced, the FoS increased to 1.06 as shown in Figure 5.5c. A decrease in pore water pressure reduces the driving forces/shear stresses, increasing the effective normal stress and the frictional resistance between tailings particles, thereby increasing the safety factor of the TSF slope (Arya et al., 2020). The

PWP is inversely proportional to the FoS, as illustrated in Figure 5.5. As the FoS decreases, stability decreases due to increased pore water pressure. The results show that an increase in pore water pressure reduces the shear strength of earth materials (soil, tailings, rock, etc.) and, consequently, the stability of the slope (Brown and Gillani, 2016). This is because low PWP reduces effective stress, thus reducing the frictional interlocking between particles and shear tailings strength (Arya et al., 2020; Troncone et al., 2019).

5.6 Concluding remarks

This chapter presented a LEM analysis of TSF stability using RocScience Slide2, based on geotechnical parameters determined through laboratory testing and field characterisation. The slope stability analyses indicated that the TSF slope is unstable under the original material and hydraulic conditions, with a FoS of 0.63, which is below the generally accepted stability threshold. A systematic analysis was conducted to evaluate the influence of key geotechnical parameters on slope stability. The results showed that cohesion, friction angle, and pore water pressure have a pronounced effect on the FoS, whereas variations in unit weight have a negligible effect. An increase in cohesion and friction angle improved slope stability by enhancing the shear strength of the tailings material. Conversely, increased pore water pressure significantly reduced the FoS by lowering effective stress and frictional resistance, confirming its critical role in TSF instability.

Overall, the LEM results highlight the sensitivity of the TSF slope to shear strength parameters and hydraulic conditions. These findings of this chapter form the foundation for the conclusions and recommendations presented in Chapter 6.

Chapter 6 Conclusion and Recommendation

6.1. Introduction

This study aimed to analyse the effect of tailings' geotechnical properties on the stability of tailing storage facilities. The main geotechnical properties examined include moisture content, pore water pressure (PWP), shear strength, hydraulic conductivity, elastic modulus, maximum dry density (MDD), permeability/density ratio (PSD), and the bearing capacity of the tailings. The conclusions are drawn by synthesising the results of the geotechnical characterisation and numerical stability analyses conducted for the tailings storage facility. The chapter highlights the main outcomes of the research, reflects on the study's limitations, and provides recommendations to improve the safety of the tailings dam and to guide future research.

6.2 Summary of findings

This section summarises the study's core findings in accordance with the research objectives. Each objective is revisited, and the extent to which it was addressed through laboratory testing and numerical modelling is highlighted.

6.2.1. To determine the key geotechnical factors of tailings contributing to the failure of tailings dams.

This objective was achieved through laboratory testing and literature analysis, which identified shear strength as the primary geotechnical factor controlling tailings dam stability. The study demonstrated that shear strength is strongly influenced by moisture content, permeability, pore water pressure, cohesion, friction angle, and effective stress, all of which directly affect shear strength. This makes shear strength the key parameter that influences the stability of a tailing dam. Elevated pore water pressure and increased moisture content were found to reduce shear strength and increase susceptibility to instability, consistent with mechanisms reported in the literature.

6.2.2. To evaluate the impact of various geotechnical properties of tailings material on the stability of tailings dam facilities.

The results indicate that the geotechnical properties of the analysed tailings have both stabilising and destabilising effects on TSF performance. The tailings were classified as silty sand (SM) with low clay content, zero cohesion, and a relatively high friction angle of 31.5°, resulting in high shear strength and low compressibility. These characteristics contribute positively to TSF stability. However, high pore water pressure of 975 kPa was identified as a potential destabilising factor due to its reduction of effective stress. The tailings permeability of 1.49×10^{-4} cm has a significant influence on the build-up of high pore pressure within the tailings. Overall, the findings confirm that TSF stability is governed by the interaction of multiple geotechnical parameters rather than a single property.

6.2.3. To assess the stability of tailings dam slopes using the limit equilibrium analytical method by quantifying the FoS under varying geotechnical conditions.

The FoS of the tailing dam slope, estimated through the numerical modelling, is 0.63, which is less than 1 (indicating an unstable slope). The factor of 0,63 represents a tailing dam slope with low stability and a high risk of failure. The FoS was low due to the low cohesion of the cohesionless material (0 kPa) and the high pore water pressure.

6.3. Conclusion

The geotechnical parameters of tailings have a greater effect on the stability of the tailings dam. A decrease in soil shear strength reduces the stability of a tailing dam, thereby increasing the risk of failure. Water parameters are the key factor that drives shear stresses acting on the tailing materials, and the increase in water parameters reduces the shear strength. In conclusion, water parameters such as moisture and PWP need to be maintained below their maximum required levels, as defined by USCS, ASTM, etc., to ensure a tailing with stable geotechnical properties and a tailing dam. The experimental analysis has shown that shear strength has more impact on the stability of TSF. Numerical modelling has demonstrated that increasing shear strength parameters (cohesion and friction angle) enhances the FoS and stability of TSF. An increase in pore water pressure reduces the stability of TSF, whereas a decrease in pore water pressure increases the stability of TSF. The tailing dam analysis shows a low FoS, indicating instability.

The study's findings support the literature review on the impact of geotechnical parameters on soil. The contribution factor to soil stability is similar to that for tailings stability. The study has contributed to the understanding of the stability of the tailing dam based on the geotechnical properties of the tailing

6.4 Limitations

The study focused on the analysis of the geotechnical parameters of tailings from a copper tailings dam, due to time constraints that prevented coverage of the geotechnical impact of tailings from various other ores. Therefore, the results are limited to only the geotechnical properties of a copper tailing ore. Factors such as liquefaction have not been thoroughly studied. There is limited information on how the liquefaction process occurs and on the geological factors that trigger it. Additionally, there is a lack of knowledge on how to assess the likelihood of seismic activity leading to liquefaction before it occurs. This lack of information hinders the ability to warn mine workers and nearby residents about potential safety risks. For example, the collapse of the Fundão dam was attributed to liquefaction; however, the specific triggers of the seismic waves that caused the liquefaction were not well investigated. Furthermore, the bearing capacity of the foundation soil underlying the tailing storage and its impact on stability are not well documented. This study solely covered the bearing capacity of a tailing in a tailing dam, which was analysed due to financial constraints attached to studying the bearing capacity of foundation soil. Lastly, the scope of this study was restricted to the evaluation of the FoS of the TSF. Since the objective was a stability assessment rather than a deformation failure analysis, a limit equilibrium method was employed.

6.5 Recommendation

This study strongly recommends the proper monitoring of pore water pressure, particularly in areas where the highest pore water pressure of tailings may occur, as this can contribute to sliding between tailings grains and lead to TSF instability, making the TSF susceptible to failure. The study also recommends further research on the liquefaction process and the stabilisation of clay soil to increase its cohesion, friction angle, and plasticity. Furthermore, it recommends cost-effective measures to determine excess water content in TSF, warning of an excess water level before failure, and implementing mitigating measures to reduce the risk of TSF failure due to such excess water. Future studies should consider remote methods to maintain the geotechnical properties of tailings, such as installing sensors around dams to monitor them. Technological solutions must be developed to monitor and control water parameters in a dam during rainy seasons, as well as those that immediately reduce water when slurry is continuously deposited into the TSF. There must be new technological innovations in computer-operated tailing dam stability control machines.

This study recommends comprehensive research focused on the effects of seismic waves produced by earthquakes on the bearing capacity of foundation soils and the stability of structures, including tailings storage facilities (TSF) and other infrastructure. This includes examining how geological factors influence seismic waves that may trigger liquefaction, as well as developing effective prevention methods. This will provide detailed results on the effects of tailings' geotechnical properties on the stability of tailing dam facilities. The findings will be useful during TSF design and constant monitoring of the active TSF. A three-dimensional analysis is highly recommended as a further study to quantify the FoS of the TSF slope.

The TSF design should include embankment stability, drainage, and a seepage flow management/control plan. The dam embankment must be stable under dynamic and static dam loading, and seepage through the foundation soil must be controlled and collected during TSF operation. The TSF foundation design should consist of a low-barrier drainage system that controls water drainage both below and above the barrier. The barrier above the liner ensures drawdown of the phreatic surface, reducing the seepage gradient and the likelihood of liquefaction of the tailings material. In contrast, the barrier beneath the liner serves as a detector layer. This will increase the shear strength and stability of foundation soil, thereby reducing the risk of undrained shear failure. It is advisable to use foundation soil that has low moisture content to increase foundation slope stability. Moisture content should be monitored to prevent excess moisture and ensure a stable foundation for the tailing dam.

Tailings texture needs to be improved by mixing the coarse (sandy) tailings with fine-texture material to increase its cohesion and thus the FoS. More compactions can be undertaken in the tailing dam continuously after each slurry disposal to increase the slope's FoS to a stable value greater than 1. Slope grading is needed to improve the slope safety factor.

7. References

Abdulkareem, S.K., Hassan, S., 2019. Organic and Peat Engineering Properties, and their Suitability for Construction Projects. Engineering Department, the American University of Iraq, Sulaimani. *[Online]*, Available at: https://www.researchgate.net/publication/. [accessed 27 March 2024].

Abu Qamar, M.A.I., Hamad, A.G., Alshannaq, A.A., Tamimi, M.F. and Al-Qura'an, M.I., 2025. Role of Particle Size and Element Characteristics on Shear Response at Sandy Soil-textured Surface interfaces, Vol.15, no.1, p.42365. https://doi.org/10.1038/s41598-025-26385-3.

Adamczuk, A., Gryta, A., Skic, K., Boguta, P., Jozefaciuk, G., 2022. Effect of Different Minerals on Water Stability and Wettability of Soil Silt Aggregates. *Materials*, vol. 15, no. 16, pp. 5569. https://doi.org/10.3390/ma15165569.

Adamo. N., Al-Ansari, N., Sissakian, V., Laue, J., Knutsson, S., 2020. Dam Safety: The Question of Tailings Dams. *Journal of Earth Sciences and Geotechnical Engineering,* vol.11, no.1, pp. 1792-9660. http://doi.org//10.47260/jesge/1111.

Ahmed, S. I., Siddiqua, S., 2016. Compressibility Behaviour of Soils: A Statistical Approach. *Geotechnical and Geological Engineering*, vol. 34, no. 6, pp. 2063-2070. https://doi.org/10.1007/s10706-016-9996-7.

Aksu, I., Bazilevskaya, E., Karpyn, Z.T., 2015. Swelling of Clay Minerals in Unconsolidated Porous Media and Its Impact on Permeability. *GeoResJ,* vol. 7, pp. 1-13. https://doi.org/10.1016/j.grj.2015.02.003.

Al-Bared, M.A.M., Harahap, I.S.H., Marto, A., Mustaffa, Z., Ali, M.O.A. and AlSubal, S., 2019. Stability of cut slope and degradation of rock slope forming materials–a review. *Malaysian Construction Research Journal*, vol.6, no.1, pp.215-228.

Ali, H.F.H., Omer, B., Mohammed, A.S. and Faraj, R.H., 2024. Predicting The Maximum Dry Density and Optimum Moisture content from Soil index properties using Efficient Soft Computing Techniques. *Neural Computing and Applications*, vol.36, no.19, pp.11339-11369. https://doi.org/10.1007/s00521-024-09734-7.

Ali, U., Kikumoto, M., Ciantia, M., Cui. Y·, Previtali, M., 2023. Systematic Effect of Particle Roundness/angularity on Macro- and Microscopic Behavior of Granular Materials. *Granular Matter*, vol. 25, no. 51, pp. 1-16. https://doi.org/10.1007/s10035-023-01341-y.

Arya, I.W., Wiraga, I.W., Dwipa, I.G.A.G.S., Pramana, I.M.W., 2020. Effect of Pore Water Pressure on Soil Crack Against Safety Factor of slope Stability. *Jornal of physics*, Vol, 1450, No.1, p.012014. https://doi:10.1088/1742-6596/1450/1/012014.

Aşkin, T., Özdemir, N., 2003. Soil Bulk Density as Related to Soil Particle size distribution and organic matter content. *Poljoprivreda/Agriculture*, vol. 9, no. 2, pp. 52-55, https://doi.org/10.18047/poljo.

Ati, A.S., Kareem. B.M., 2014. Effect of Shape, Size of Pores on Saturated Hydraulic Conductivity of Some Iraqi Soils. *Journal of Zankoy Sulaimani- Part A*, Special Issue, vol. 16, pp. 157-175.

Austruy, S., 2024. The importance of achieving soil compaction. Douglass partners. A report. *[Online]* Available at: https://www.douglaspartners.com.au/. [Accessed 5 October 2024].

Baba, K., Bahi. L., Ouadif, L., Akhssas, A., 2012. Slope Stability Analysis Evaluation by Limit Equilibrium and Finite Element methods applied to a railway in the Moroccan Rif. *Open Journal of Civil Engineering*, Vol. 2. No. 1, Pp. 27-32. https://doi.org/10.4236/ojce.2012.21005.

Basson, I., Lourens, P., Paetzold, H.D., Thomas, S., Brazier, R., Molabe, P., 2017. Structural analysis and 3D modelling of major mineralizing structures at the Phalaborwa copper deposit. *Ore Geology Reviews*, 83, pp.30-42.

Barbosa, V.H., Marques, M.E., Guimarães, A.C., 2023. Predicting soil Swelling Potential Using Soil Classification Properties. *Geotechnical and Geological Engineering,* vol.41,no.8 ,pp.4445-4457, https//doi/.10.1007/s10706-023-02525-2.

Kalantari, Behzad. "Foundations on Expansive Soils: A Review., 2012. *Research Journal of Applied Sciences, Engineering and Technology*, vol. 4, no.18, pp. 3231-3237.

Ben-Zeev. S., Goren. L., Toussaint. R., Aharonov. E., 2023. Drainage Explains Soil Liquefaction beyond the Earthquake near-field. *Nature communications*, vol. 14, no. 1, p.5791. https://doi.org/10.1038/s41467-023-41405-4.

Boadu, K.F., 2000. Hydraulic Conductivity of Soil from Grain-size distribution. New models. *Journal of Geotechnical and Geoenvironmental Engineering*, vol. 126, no. 8, pp. 739-746. https://doi.org/10.1061/(ASCE)1090-0241(2000)126:8(739).

Bhanbhro, R., 2014. Mechanical Properties of Tailings: basic description of a tailings material from Sweden. Doctoral dissertation, Department of Civil, Environmental and Natural Resources Engineering Division of Mining and Geotechnical *Engineering Luleå University of Technology*. Available [Online] at https://www.diva-portal.org/smash/get/diva2:989943/FULLTEXT01. [Accessed 02 March 2024].

Bidyashwari, H., Kushwahal, R.S., Chandra, M. and Okendro, M., 2017. Physical Properties of Soil and its Implications for Slope Stability of Nungbi Khunou, NH-150, Manipur. *International Journal of Geosciences*. vol.8, no. 11, pp.1332-1343. https://doi.org/10.4236/ijg.2017.811077.

Branch, S.W., 1994. Design and Evaluation of Tailings Dams. Technical report, *EPA*. gov.

Brown, B. Gillani, I., 2016. Common Errors in the Slope Stability Analyses of Tailings Dams. In APSSIM 2016: Proceedings of the First Asia Pacific Slope Stability in Mining Conference. *Australian Centre for Geomechanics*. Pp 545-556. https://doi.org/10.36487/ACG_rep/1604_36_Brown.

Brown, B. S., 2019. What Are The Real Risks For Tailings Facilities. Proceedings of the first international conference on my name risk, Perth Australia, vol. 9, no, 12. https://doi.org/10.36487/ACG_rep/1905_0.2_Brown.

Budhu, M. 2010. Soil Mechanics and Foundation.3rd edition. Library of congress cataloging-in-publication data. John willey and sons, Inc. ISBN. 978-0-470-55684-9

Cacciuttolo, C., Pastor, A., Valderrama, P., Atencio, E., 2023. Process Water Management and Seepage Control in Tailings Storage Facilities: Engineered Environmental Solutions Applied in Chile and Peru. *Water*, v. 15, no.1, pp 196. https://doi.org/10.3390/w15010196.

Çal, S. Barik, K., 2020. Hydraulic Conductivity Values of Soils in Different Soil Processing Conditions. *Alinteri Journal of Agriculture Sciences*, vol. 35, no, 1, pp. 132-138. https://doi.org/10.28955/alinterizbd.740904 .

Cameron, K.C, and Buchan, G.D, 2005. Porosity and Pore Size Distribution. *Encyclopaedia of Soil Science*, 2nd ed. pp.1350-1353. https://doi.org/10.1201/noe0849338304.ch284 .

Cárdenas-Barrantes, M., Ovalle, C., 2025. Effect of Friction on the Angle of Repose of Elongated Particles. *Powder Technology*, vol. 458, p.120974. https://doi.org/10.1016/j.powtec.2025.120974.

Carmo, F. F. do, Kamino, L. H. Y., Junior, R. T., Campos, I. C. de, Carmo, F. F. do, Silvino, G., Pinto, C. E. F., 2017. Fundão Tailings Dam Failures: the environment tragedy of the largest technological disaster of Brazilian mining in global context. *Perspectives in Ecology and Conservation*, vol. 15, no.3, pp, 145–151. http://dx.doi.org/10.1016/j.pecon.

Chambers. D.M., 2015. A Review of the "Report on Mount Polley Tailings Storage Facility Breach, Independent Expert Engineering Investigation Panel". *Centre for Science in Public Participation*. Investigation and Review Panel, Province of British Columbia.

Chen, J.; Zhang, Y.; Yang, Y.; Yang, B.; Huang, B.; Ji, X., 2023. Influence of Coarse Grain Content on the Mechanical Properties of Red Sandstone Soil. *Sustainabilit*y. Vol.15, no.4, p, 3117. https://doi.org/10.3390/su15043117 .

Chen, P., Wei, C., Liu, J., Ma, T., 2013. Strength Theory Model of Unsaturated Soils with Suction Stress. *Journal of applied mathematics.* Mathematical and Numerical Modeling in Geotechnical Engineering. https://doi.org/10.1155/2013/756854.

Clarkson, L., Williams, D., 2021. An Overview of Conventional Tailings Dam Geotechnical Failure Mechanisms. *Mining, Metallurgy and Exploration*, vol. 38, no. 3, pp. 1305–1328 https://doi.org/10.1007/s42461-021-00381-3.

Christian, J.T. and Baecher, G.B., 2015. DW Taylor and the Foundations of Modern Soil Mechanics. *Journal of Geotechnical and Geo-environmental Engineering*, vol.141. no. 2, p.02514001.

Davison, L, and Springman, S. 2000. Basic Mechanics of soil. Geotechnical reference package. *University of the west of England.*

Dareeju, B., Rowles, T., Xu, Y., Dissanayake, A., 2021. Selection of Undrained Shear Strength Parameters of Residual Soils and their Application in Stability Analysis. [online] Available at: https://www.knightpiesold.com/ [Accessed 11 March 2025].

Decrée, S., Cawthorn, G., Deloule, E., Mercadier, J., Frimmel, H. Baele, J.M., 2020. Unravelling the Processes Controlling Apatite formation in the Phalaborwa Complex (South Africa) based on Combined Cathodoluminescence, LA-ICPMS and in-situ O and Sr isotope analyses. *Contributions to Mineralogy and Petrology*, vo.175, no.4, p.34.

Dhawale, V.R., Harle, S. M. 2016. Influence of Different Soil Properties on Shear 15 34 Strength of Soil: A Review. *American Journal of Applied Scientific Research*. Vol. 2, No. 6, 2016, pp. 87-90. https://doi.org/10.11648/j.ajasr.20160206.19.

Dimitrova, R.S., Yanful, E.K., 2012. Factors Affecting the Shear Strength of Mine Tailings/clay Mixtures with Varying Clay Content and Clay Mineralogy. *Engineering Geology*, 125, pp.11-25.

Dixon-Hardy, D. W., Engels, J. M. 2007. Methods for the Disposal and Storage of Mine Tailings. *Land Contamination and Reclamation*, vol.15, no. 3, pp.301–317. https://doi.org/10.2462/09670513.832.

Du, J., Shen, X., Li, C., Zhu, W., Feng, G., 2023. Effect of Dry-wet cycles on the Strength and Deformation of the Red-bed Rockfill Material in Western Yunnan. *Frontiers in Earth Science*, vol. 11, p.1192269. https://doi.org/10.3389/feart.2023.1192269.

Duong, T.V., Tang, A.M., Cui, Y.J., Trinh, V.N., Dupla, J.C., Calon, N., Canou, J., Robinet, A., 2013. Effects of Fines and Water Contents on the Mechanical Behavior of Interlayer Soil in Ancient Railway sub-structure. *Soils and foundations*, vol. 53, no.6, pp.868-878. https://sci-hub.se/10.1016/j.sandf.2013.10.006.

Ebels, L.J., Lorio, R. Ver Merwe, C., 2004. The Importance of Compaction from a Historical Perspective. *Document Transformation Technologies*. ISBN Number: 1-920-01723-2.

El Hariri, A., Ahmed, A. E. E., Kiss, P., 2023. Sandy Loam Soil Shear Strength Parameters and Its Colour. *Applied Sciences*, Vol. 13, no. 6, P. 3847. https://doi.org/10.3390/app13063847.

Enad, A. A., Ahmed, S. M., Mohammed, A. K., Mohammed, A. S., 2024. Influence of Feldspar Addition on the Geotechnical Properties of Expansive Soil in Rahhaliya, Iraq. *Journal of Composite and Advanced Materials*. vol. 34, no. 2, pp. 143–148. https://doi.org/10.18280/rcma.340203.

Essien, U.E., Akankpo, A.O., Igboekwe, M.U., 2014. Poisson's Ratio of Surface Soils and Shallow Sediments Determined from Seismic Compressional and Shear Wave Velocities. *International Journal of Geosciences*, vol. 5, no.12, 1540-1546. http://dx.doi.org/10.4236/ijg.2014.512125.

Evans, J.C., Ruffing, D., Elton, D., 2021. Fundamentals of Ground Improvement. Consolidation chapter. *Crc press*, tailor and Francis group. Pp. 119–148. https://doi.org/10.1201/9780367816995-5.

Ferdosi, B., James, M., Aubertin, M., 2015. Effect of Waste Rock Inclusions on the Seismic Stability of an Upstream Raised Tailings Impoundment: a numerical investigation. *Canadian Geotechnical Journal*, vol. 52, no. 12, pp.1930-1944. https://doi.org/10.1139/cgj-2014-0447.

Firoozi, A.A., Guney Olgun, C., Firoozi, A.A. and Baghini, M.S., 2017., Fundamentals of soil stabilization. *International Journal of Geo-Engineering*, vol. *8*, no.1, p.26.

Flint, L.E. and Flint, A.L., 2002. 2.3 Porosity. *Methods of soil analysis: Part 4 physical methods*, vol. *5*, no.4, pp.241-254. https://doi.org/10.2136/sssabookser5.4.c11.

Gautam, T.P.,2018. Cohesive Soils. In: Bobrowsky, P.T., Marker, B. Encyclopedia of Engineering Geology. *Encyclopedia of Earth Sciences Series. Springer*, Cham. https://doi.org/10.1007/978-3-319-73568-9_60.

Guyer, J.P., 2013a. An Introduction to Bearing Capacity Analysis. Instructor Fellow ASCE, Fellow AEI.coarse no G02-004. P. 26. ISBN-10 : 1490341129. ISBN-13: 978-1490341125.

Guyer, J.P., 2013b. An Introduction to Slope Stability Analysis. Continuing Education and Development, Inc. 44240 Clubhouse Drive El Macero, vol. 95618 no. 530, pp758-6637.

Grant-stuart, D. J., 2020. Your Tailings Dam. The South African National Committee on Large Dams*. [Online]* available at:

https://sancold.org.za/wp-content/uploads/2024/05/SANCOLD-Your-Tailings-Dam-2020.pdf *. [Online]* [Accessed 30 May 2025].

Gregory, A. S., Ritz, K., McGrath, S. P., Quinton, J. N., Goulding, K. W. T., Jones, R. J. A., Whitmore, A. P., 2015. A Review of the Impacts of Degradation Threats on Soil Properties in the UK. *Soil Use and Management*, vol. 31, pp. 1–15.https://doi.org/10.1111/sum.12212.

Haque. E., Hossain S., Hasan I., 2013. Evaluation of Some Geo Mechanical Parameters of the Soil Samples from Ganakbari Area, Dhaka, Bangladesh. Journal of Science and Technology. Vol. 3, no. 8.

Harabinová, S. and Panulinová, E., 2020. Impact of Shear Strength Parameters on Slope Stability. In *MATEC web of conferences*. Vol. 310, p. 00040 https://doi.org/10.1051/matecconf/202031000040.

Harabinova, S. and Panulinova, E., 2022. Numerical Analysis of Slope Stability. *Materials Science and Engineering* . Vol. 1252, No. 1, p. 012084. IOP Publishing. https://doi:10.1088/1757-899X/1252/1/012084.

He. Y., Yu. Z., Zhang. Z., Chen. B., Zhang. K., 2022., Effect of Rainfall on the Mechanical Behaviour of Residual Soil landslide. *geohazards and georisks*. Research article.Vol,10. https://doi.org/10.3389/feart.2022.925636

Hossain, M.D., Islam, M.D., Badhon, F.F., Imtiaz, T., 2021. Properties and Behavior of Soil-Online Lab Manual. ISBN 978-1-64816-971-7. *[Online]* Available at: https://uta.pressbooks.pub/soilmechanics/chapter/chapter-1. [accessed 25 November 2024].

Hatje, V., Pedreira, R.M.A. de Rezende,C. E., Schettini, F., Cotrim, G., Haigh, S.K., Canaver D., Hackspacher, P., 2017. The Environmental Impact of One of the Largest

Tailing Dams Failure Worldwide. *Science report 7*. vol.63, no. 6, pp.435–440. https://doi.org/10.1038/s41598-017-11143-x.

Hu. F., Xu. C., Li. H., Li. S., Yu. Z., Li. Y., He. X., 2015. Particles Interaction Forces and Their Effects on Soil Aggregates Breakdown, Soil and Tillage Research. Vol 147, Pp. 1-9, ISSN 0167-1987, https://doi.org/10.1016/j.still.2014.11.006.

Hu, L., Wu, H., Zhang, L., Zhang, P., Wen, Q., 2017. Geotechnical Properties of Mine Tailings. *Journal of Materials in Civil Engineering*, vol. 29, no. 2, pp. 04016220. https://doi.org/10.1061/(ASCE)mt.1943-5533.0001736.

Hueso, G., 2017. Pore Water Pressure Behaviour and Evolution in Clays and its Influence in the Consolidation Process. Thesis submitted for examination for the degree of Master´s Programme in Building Technology. *[Online],* Available at: https://aaltodoc.aalto.fi/server/api/core/bitstreams/ [accessed 20 Dec 2025]

Hussaina, K., Bina, O., Hussain, J., Sayed, M.I., Syed, Y.A., Hussaina, S., 2022. Geotechnical Parameter Assessment and Bearing Capacity for Foundation Soil Design. ESMACU research article. ISSN: 2521-5035 (Print) ISSN: 2521-5043 *[Online]* Earth Sciences Malaysia (ESMY). Vol. 6, no.2, pp. 136-145. http://doi.org/10.26480/esmy.

Ikeagwuani, C.C., Nwonu, D.C., 2019. Emerging trends in expansive soil stabilisation: A review. *Journal of rock mechanics and geotechnical engineering*, vol. 11, no. 2, pp.423-440. https://doi.org/10.1016/j.jrmge.2018.08.013.

Islam, S., 2021. A study on the Mechanical Behaviour of Three Different Fine-grained Mine Tailings. *Journal of King Saud University – Engineering Sciences*. Vol.35, no. 5, pp. 335–341. https://doi.org/10.1016/j.jksues.2021.04.001.

Jawad, I.T., Taha, M.R., Majeed, Z.H., Khan, T.A., 2014. Soil Stabilization Using Lime: Advantages, Disadvantages and Proposing a Potential Alternative. *Research Journal of Applied Sciences, Engineering and Technology*, Vol. *8*, no.4, pp.510-520.

Jayalekshmi. S, Elamathi, V., 2017. A Study on the Consolidation and Permeability Behaviour of Soils of State of Tamil Nadu, India S. IOP Conf. Series: *Materials Science and Engineering*. vol. 1006, no. 1, p. 012017. https://doi.org/10.1088/1757-899x/1006/1/012017.

Jeschke, M., and Lutt. N., 2019. Soil Compaction in Agricultural Production. Crop insight. Pioneer Agronomy Sciences. *Corteva agriscience*. vol. 28, no. 10.

Jones, G.A., 2017. An Empirical Preliminary Prediction of Heave. *Journal of the South African Institution of Civil Engineering*, vol.*59, no.*4, pp.64-66.

Kalantari, B., 2012. Foundations on Expansive Soils: a review. *Research journal of applied sciences, engineering, and technology*. ISSN: 2040-7467. vol. 4, no.18, pp. 3231-3237.

Kang, Q., Xia, Y., Li, X., Zhang, W. Feng, C., 2022. Study on the Effect of Moisture Content and Dry Density on Shear Strength of Silty Clay based on Direct Shear test. *Advances in Civil Engineering*, vol. *2022*, no.1, p.2213363. https://doi.org/10.1155/2022/2213363.

Kezdi, A. 1974. Handbook of Soil Mechanics. *Elsevie*r, Amsterdam.

Kolay, P.K. and Wadiah, N., 2005. Effect of Fine Content on Compaction Characteristics of Sandy Soil. In *National civil engineering conference (NACEC), Kuittho*, pp. 718-725. https://doi.org/10.271387349.

Koohmishi, M., & Azarhoosh, A., 2020. Assessment of Permeability of Granular Drainage Layer Considering Particle size and Air void distribution. *Construction and Building Materials.* Vol.270, p.121373. https://doi.org/10.1016/j.conbuildmat.2020.121373.

Koperska W., Stachowiak M., Duda-Mróz N., Stefaniak P., Jachnik B., Bursa B., Stefanek P., 2022. The Tailings Storage facility (TSF) Stability Monitoring System using Advanced big data Analytics on the Example of the Żelazny Most Facility. *Archives of Civil Engineering*, vol. 68, no.2, pp. 297 – 311. https://doi.org/10.24425/ace.2022.140643.

Kossoff, D.; Dubbin, W.E. ; Alfredsson, M.; Edwards, S.J.; Macklin M.G.; and Hudson-Edwards, K.A., 2014. Mine tailings dams: Characteristics, failure, environmental impacts, and remediation. Vol. 51, no 2014, Pp. 229-245. http://dx.doi.org/10.1016/j.apgeochem.2014.09.010.

Kumar, M.K., Rupali, S. Senthil, K., 2024. An Experimental Study on Stabilization of Silty Soils Using Quartz Powder. In Indian Geotechnical Conference. *Springer Nature Singapore.*

Kumar Thota, S., Duc Cao, T. Vahedifard, F., 2021. Poisson's Ratio Characteristic Curve of Unsaturated Soils. *Journal of Geo-environmental Engineering*, vol.147, no.1, p.04020149.

Kuschke, O.H., Tonking, M., 1971. Geology and Mining Operations at Palabora Mining Company Limited, Phalaborwa, NE Transvaal. *Journal of the Southern African Institute of Mining and Metallurgy*, Vol. *72, vol.* 1, pp.12-23.

Lees, A., 2020. Pore Water Pressure and the Importance of Drainage *[online],* Available at: https://www.tensarinternational.com/resources/articles/pore-water-pressure. [Accessed 23 Dec 2025].

Lees. A., 2021. Bearing Capacity of Soil - Types and Calculations. A division of CMC. Pp. 1-8. *[Online]* Available at: https://www.tensarinternational.com/ [Accessed 2 November 2024].

Lees. A., 2024. What is Particle size Distribution in Soil? An article. Tensar. *[Online]* Available at: https://www.tensar.co.uk/resources/articles/. [Accessed 8 Feb 2025]

Li P., Hou, Y.B, Cai, M.F., 2019. Factors Influencing the Pumpability of Unclassified Tailings Slurry and its Interval Division. Int J Miner Metall Mater vol. 26, no. 4, pp. 417–429. https://doi.org/10.1007/s12613-019-1750-8.

Liu, H.M., Yang, C.H., Zhang, C., Mao, H.J., 2012. Study on Static and Dynamic Strength Characteristics of Tailings Silty Sand and its Engineering Application. *Safety science*, vol.*50*, vol.4, pp.828-834.

Liu, Q. Q., Li, J. C., 2015. Effects of Water Seepage on the Stability of Soil-slopes. Procedia IUTAM,vol. 17, pp. 29–39. https://doi.org/10.1016/j.piutam.2015.06.006.

Lu, N., Linkos, W., 2013. Origin of Cohesion and its Dependence on Saturation for Granular media. Pp. 1669-1675. https://doi.org/10.106`/9780784412992.197.

Lumbroso, D., Mark Davison, M., Body, R. Petkovšek, G, Wallingford, H.R., 2020. Modelling the Brumadinho Tailings Dam Failure, the Subsequent loss of Life and how it could have been reduced Darren. *Preprint*. Vol. 21, no.1. pp. 21-37. https://doi.org/10.5194/nhess-2020-159.

Lyu, Z., Chai, J., Xai, Z., Qin, Y., Cao, J., 2019. A Comprehensive Review on Reasons for Tailings Dam Failures Based on Case. A review article*. Hindawi Advances in Civil Engineering.* vol. 2019, no.1, p.1-18. https://doi.org/10.1155/2019/4159306.

McCarty, L.B., Hubbard, L.R., Quisenberry, V.L., 2015. Applied Soil Physical Properties, Drainage, and Irrigation Strategies. Switzerland: *Springer International Publishing.* ISBN 978-3-319-24224-8. 1st ed. pp. 73–137. https://doi.org/10.1007/978-3-319-24226-2_2.

Mac-Robert, C., 2022. Burst Mining Dam in South Africa: What Must be Done to Prevent Another Disaster. Mining weekly, Stellenbosch University article. Cramer media's engineering news. An online Report. Available *[online]* at https://www.engineeringnews.co.za/article/. [Accessed 03 February 2024].

Mahinroosta, R., Oshtaghi, V., 2021. The Effect of Particle Shape on the Deformation and Stress Reduction of a Gravel Soil due to Wetting. *Scientific Reports,* vol.11, no.1, p.16583. https://doi.org/10.1038/s41598-021-95731-y.

Marais P., Kemp, D., Watt, P., Cloete, J., Harris, J., A, M. , 2024. The Catastrophic Failure of the Jagersfontein Tailings Dam: An industrial disaster 150 years in the making. *International Journal of Disaster Risk Reduction.* Vol. 109, pp. 104585. https://doi.org/10.1016/j.ijdrr.2024.104585.

Martin, T.E. and McRoberts, E.C., 1999. Some Considerations in the Stability Analysis of Upstream Tailings Dams. In Proceedings of the sixth international conference on tailings and mine waste. vol. 99, pp. 287-302.

Meng, X., Duan, H., Liu, M., Li, G., Yang, Z., Shi, W. and Ling, X., 2025. A Semi-Empirical Method for Predicting Soil Void Ratio from CPTu Data via Soil Density Correlation. *Applied Sciences*, vol. 15,no.16, p.9167. 7.

https://doi.org/10.3390/app15169167.

Mintek industrial News., 2024. Jagersfontein Tailings Dam Failure. Minetek Industry News & Insights. *[Online]* Available at: https://minetek.com/en-au/resource-hub/news/jagersfontein-tailings-dam-failure/ [accessed 12 march 2025].

Mohamad, N. O., Razali, C. E., Hadi, A. A. A., Som, P. P., Eng, B. C., Rusli, M. B., Mohamad, F. R., 2016. Challenges in Construction Over Soft Soil - Case Studies in Malaysia. IOP Conference Series: *Materials Science and Engineering*, Vol 136, Soft Soil Engineering International Conference. https://doi.org/10.1088/1757-899x/136/1/012002.

Mokwa, R.L., Trimble, N.R., 2008. Permeability of Coarse-Grain soil from void Space and Pore Distribution. In *GeoCongress 2008:* Characterization, Monitoring, and Modeling of GeoSystems. pp. 428-435. https://doi.org/10.1061/40972. Vol.311, no.54.

Mondol, N.M. Bjørlykke, K., Jahren. J., 2008. Experimental Compaction of Clays: Relationship Between Permeability and Petrophysical Properties in mudstones. Department of Geosciences, University of Oslo. *An article in Petroleum Geoscience,* Vol. 14 no.2008, pp. 319–337. http://doi.org/10.1144/1354-079308-773.

Morton, K.L., 2021. The Use of Accurate Pore Pressure Monitoring for Risk Reduction in Tailings Dams. *Mine Water Environ* vol. 40, no. 1, and p.42–49. https://doi.org/10.1007/s10230-020-00736-0.

Morgenstern, N.R., Vick .S.G., Van Zyl. D., 2015. Report on Mount Polley Tailings Storage Facility Breach. Independent Expert Engineering Investigation and Review Panel, Province of British Columbia. *[online]*. Available at: https://www.mountpolleyreviewpanel.ca/final-report/ [accessed 12 March 2025]. pp 30-37.

Munro, J. Harris, C., 2023. A High-δ18O Mantle Source for the 2.06 Ga Phalaborwa Igneous Complex, South Africa?. *Journal of Petrology*, vol. *64*, no.9.

Musbahh, A., Mohammed, M., Alfghia, A., 2024. The Effect of Mineral Composition and Quantity of Fines on the Atterberg Limits and Compaction Characteristics of Soils. Department of Civil Engineering. Open journal of civil engineering. vol. 14, no.2. https://doi.org/10.4236/ojce.2024.142014.

Nawaz, M.F., Bourrié, G., Trolard, F., 2013. Soil Compaction Impact and Modelling. A review. *Agrononomy. Sustainable*. Development. Vol. 33, pp. 291–309. https://doi.org/10.1007/s13593-011-0071-8.

Nie, W., Li, C., Hu, J., Saffari, P., Wang, W. and Luo, M., 2023. Spatial Variation of physical and Mechanical Properties of Tailings under Different Rainfall intensities and the interaction pattern. *Geomechanics and Geophysics for Geo-Energy and Geo-Resources.* Vol. 9, no. 1. p. 86.https://doi.org/10.1007/s40948-023-00625-0.

Obrzud R., Truty, A., 2012. The Hardening Soil Modelling- A practical guidebook. Soil.PC 100701. A report, revised 31.01.2012.

Oruabena B., George D , Okiridu M. U , Odoh C. B.,2018. Pore Pressure Response of Soils Under Dynamic and Static Loading Conditions. A research paper: School of Engineering Technology, Department of Civil engineering, Federal Polytechnic Ekowe, Bayelsa State, Nigeria. *International Journal of Civil and Structural Engineering Research* [Online] Vol. 5, no. 2, Pp 11-15. ISSN 2348-7607 Available [online] at [https://www.researchpublish.com/].

Owen, J. R., Kemp, D., Lèbre, É. Svobodova, K., Pérez Murillo, G., 2019. Catastrophic Tailings Dam Failures and Disaster risk disclosure. International *Journal of Disaster Risk Reduction*, https://doi.org/10.1016/j.ijdrr.2019.101361.

Oyediran, I.A. and Famakinwa, J.O., 2015. Geotechnical Basis for Building Instability and Failure: case study from Lagos, Nigeria. *In Engineering Geology for Society and Territory- Urban Geology.* Sustainable Planning and Landscape Exploitation. Springer International Publishing. Vol. 5. pp. 365-370. *Springer,* Cham. https://doi.org/10.1007/978-3-319-09048-1-70.

Ozcan, N.T., Ulusay, R. and Isik, N.S., 2013. A study on Geotechnical Characterization and Stability of Downstream Slope of a Tailings Dam to Improve its Storage Capacity (Turkey). *Environmental Earth Sciences*, vol. 69, pp.1871-1890. https://doi.org/10.1007/s12665-012-2016-1.

Padovani, F.A. and Bretas, T., 2023. Tailings Dam's Safety Assessment Considering Undrained Foundation Failure. In TMIC 2022. Slope Stability Conference. *Atlantis Press*. pp. 44-52. https://doi.org/10.2991/978-94-6463-104-3_5.

Paltseva, A., 2024. What Is the Total Pore Space in the Soil?. In *The Urban Soil Guide: A Field and Lab Manual*, Cham: *Springer Nature Switzerland*. pp. 35-39.https://doi.org/10.1007/978-3-031-50777-9_6.

Palu, M.C. and Julien, P.Y., 2019. Modeling the Sediment Load of the Doce River after the Fundão tailings dam collapse, Brazil. *Journal of Hydraulic Engineering*, vol.145, no.5, p.05019002. https://doi.org/10.1061/(asce)hy.1943-7900.0001582.

Pan, Z., Zhang, C., Ma, C., Ma, L., Gan, S., 2021. Study on the Permeability Characteristics of Tailings with Different Particle Sizes and Variation of the Saturation Line of Tailings Dam. Paper presented at the 55th U.S. *Rock Mechanics/Geomechanics Symposium.* no. ARMA-2021-1044 *[online]* available at: https://onepetro.org/ARMAUSRMS/proceedings. [accessed 12 March 2025].

Park, T., Kimb, H, Tanvirc, T.M., Lee. J and Moon. S., 2017. Influence of Coarse Particles on the Physical Properties and Quick Undrained Shear Strength of Fine-grained Soils. Department of Civil and Environmental Engineering. *Geomechanics and Engineering,* Vol. 14, No. 1, pp. 99-105. https://doi.org/10.12989/gae.2018.14.1.099.

Perri, J.F., Shewbridge, S.E., Cobos-Roa, D.A. and Green, R.K., 2012. Steady state Seepage Pore Water Pressures' influence in the slope stability analysis of levees. In *GeoCongress 2012: State of the Art and Practice in Geotechnical Engineering* .pp. 604-613. https://doi.org/10.1061/9780784412121.063.

Piciullo, L. Storrosten, E.B., Liu, Z., Nadim,F., Lacasse, S., 2022. A New Look at the Statistics of Tailings Dam Failures. *Engineering Geology*. vol. 303, pp. 106657. https://doi.org/10.1016/j.enggeo.2022.106657.

Rad, H.T., Jalali, F.M., Gheibi, M., Khaksar, R.Y., Annuk, A., Moezzi. R., 2024. Enhancing Load-Bearing Capacity of Weak Soils Using Geosynthetics: A Finite Element Analysis. vol. 4, no.4, pp. 777-805. https://doi.org/10.3390/mining4040044.

Rana, N. M., Ghahramani, N., Evans, S. G., McDougall, S., Small, A., Take, W. A., 2012. Catastrophic Mass Flows Resulting from Tailings Impoundment Failures. *Engineering Geology*, vol. 292, p.106252. https://doi.org/10.1016/j.enggeo.2021.106262.

Reid, M.E., 2013. Pore-Water Pressure In: Bobrowsky, P.T. Encyclopedia of Natural Hazards. Encyclopedia of Earth Sciences Series. *Springer*, Dordrecht. https://doi.org/10.1007/978-1-4020-4399-4_272.

Resources Victoria., 2021. Understanding Porosity and Permeability. Victoria state government. Department of Energy, Environment and Climate Action. *[online]*available at https://resources.vic.gov.au/projects/[accessed 19 february 2025].

Roy, S., Bhalla .S.K., 2017. Role of Geotechnical Properties of Soil on Civil Engineering Structures. *Resources and Environment*. Scientific and Academic Publishing. , vol. 7, no.4, pp. 103-109. http://doi.org/10.5923/j.re.20170704.03.

Shaheb, M.R., Venkatesh, R. Shearer, S.A., 2021. A Review on the Effect of Soil Compaction and its Management for Sustainable Crop Production. *J. Biodiverty system. Engineering.* No. 46, pp. 417–439. https://doi.org/10.1007/s42853-021-00117-7.

Shanmugam, G., 2016. Slides, Slumps, Debris flows, Turbidity Currents, and Bottom Currents. *Reference Module in Earth Systems and Environmental Sciences*, *4*.

Shehu, A.B., Abdulfatah, A.Y., 2019. Effect of Varying Moisture Content (Ground Water) on Settlement of Foundations. *Journal of Environmental Engineering and Studies.* e-ISSN: 2582-3132, vol. 4, no. 3.

Shinohara, K., Oida, M., Goldman, B., 2000. Effect of Particle Shape on angle of Internal Friction by Triaxial Compression Test. *Powder Technology*. Vol. 107 2000 p.131–136. http://doi.org/0.1016/S0032-5910(99)00179-5.

SGU Geological Survey of Sweden., 2024. Chapter 12: Tailing Storage Facility. Accessibility report for ITP308, available *[online]* at http://www.sgu.s.e/. [Accessed 13 may 2025].

Silva Rotta, L.H., Alcantara, E., Park, E., Negri, R.G., 2020. The 2019 Brumadinho Tailings Dam Collapse:Possible cause and Impacts of the Worst Human and Environmental Disaster in Brazil*. International journal of applied earth observation and geoinformation.* Vol. 90, no.2020, p.102119. https://doi.org/10.1016/j.jag.2020.102119.

Sivakugan, N., 2000. Soil Classification: chapter 3. *[online]* available at: https://www.geoengineer.org.[accessed 21 November 2024].

Spies, L.H., 2020. Design of a Lined Platinum Tailings Storage Facility in South Africa. *Journal of the Southern African Institute of Mining and Metallurgy*, vol. 120, no, 7, pp.399-404. http://dx.doi.org/10.17159/2411- 9717/1185/2020.

Starck, S., Beushausen, H., Alexander, M., and Torrent, R., 2017. Complementarity of in situ and Laboratory-based Concrete Permeability Measurements. *Materials and structures*, vol. 50, no.3, p.177.https://doi.org/10.1155/2022/7895880.

Stark, T.D., Moya, L., Lin, J., 2022. Rates and Causes of Tailings Dam Failures. *Advances in Civil Engineering*, vol. 2022, no.1, pp.1-20. https://doi.org/10.1155/2022/7895880.

Sridharan, A., Gurtug, Y., 2005. Compressibility characteristics of soils. Geotechnical a Geological Engineering. Vol. 23,pp. 615–634. https://doi.org/10.1007/s10706-004-9112-2.

Tanyıldızı, M., Uz, V.E. and Gökalp, İ., 2023. Utilization of Waste Materials in the Stabilization of Expansive Pavement Subgrade: An extensive review. *Construction and Building Materials*, no.*398*, p.132435.

Tian, S. He, Y· Bai, R· Chen, J · Wang, G., 2022. Experimental Study on Consolidation and Strength Properties of Tailings with Different Particle Size distribution characteristics. Natural Hazards: *Journal of the International Society for the Prevention and Mitigation of Natural Hazards.* No.2022, vol, 114.pp3683–3699. https://doi.org/10.1007/s11069-022-05537-y.

Tiwari, B., Tran, D., Ajmera, B., Carrilo, Y., Stapleton, J., Khan, M., Mohiuddin. S., 2016. Effect of Slope Steepness, Void Ratio, and Intensity of Rainfall on Seepage Velocity and the Stability of Slopes. *Geotechnical and Structural Engineering Congress*. https://doi.org/10.1061/9780784479742.048.

Toderaș, M., Florea, V.A. and Itu, R.B., 2023. Stability Analysis of the Tailings Dam for the Purpose of Closing, Greening, and Ensuring Its Safety—Study Case. *Sustainability*, vol.*15*.9, p.7606. https://doi.org/10.3390/su15097606.

Troncone, A., Conte, E. and Pugliese, L., 2019. Analysis of the Slope Response to an Increase in Pore Water Pressure using the Material point Method. *Water*, vol.*11.no.*7, p.1446.6. https://doi.org/10.3390/w11071446.

Ural, N., 2018. The Importance of Clay in Geotechnical Engineering. Current Topics in the Utilization of Clay in Industrial and Medical Applications. https://doi.org/10.5772/intechopen.75817.

US EPA., 1994. Technical report design and evaluation of tailings dams. Environmental Protection Agency Office of Solid Waste. *[online]* Available at :https://archive.epa.gov/epawaste/. [accessed 12 march 2025].

Vahidi-Nia, F., Bayesteh, H. and Khodaparast, M., 2024. Effect of Particle size Ratio and Fines Content on Drained/undrained Behavior of Binary Granular Soil According to Confining pressure and Packing density: a DEM simulation. *Computational Particle Mechanics*, Vol.*11*, no.1, pp.141-167.https://doi.org/10.1007/s40571-023-00614-w.

Vick, S.G., 1990. Planning, Design, and Analysis of Tailings Dams. ISBN 0-921095-12-0 (Previously published by John Wiley & Sons under ISBN 0-471-89829-5). Publisher, LTD Vancouver, B.C. Canada.

Vietti, A.J., Steenkamp, N.C., 2023. Effect of Clay Minerals on deposition and safety of tailings storage facilities. Next generation tailings.[online] Available at: https://www.saimm.co.za/. [accessed on 22 November 2024].

Villavicencio, G., Espinace, R., Palma, J., Fourie, A., Valenzuela, P., 2014. Failures of Sand Tailings Dams in a Highly Seismic Country. *Canadian Geotechnical Journal*, vol. 51. No. 4, pp. 449–464. https://doi.org/10.1139/cgj-2013-0142.

Visagie, J.D. and Bezuidenhout, T., 2022. A Limit Equilibrium Approach to the Use of Stability Bunds in the Design of HDPE-lined tailings storage facilities. *Journal of the Southern African Institute of Mining and Metallurgy*, vol. 122, no. 6, pp. 275-282. http://dx.doi.org/10.17159/2411- 9717/1787/2022.

Wang, H.; Liu, Z.; Xie, Y.; Li, Y., 2024. Study on the Influence of Moisture Content and Void Ratio on the Disintegration of Red Clay. *Applied Science*. vol, 14, p3652. https://doi.org/ 10.3390/app1409365.

Wang, M. and Li, L., 2025. Slope Stability Analysis Considering Degradation of Soil Properties Induced by Intermittent Rainfall. Water, vol. 17, no. 6, p.814.

https://doi.org/10.3390/w17060814.

Wang, Y.; Li, K.; Li, J.; Tang, S., 2021. Influence of Soil Particle Size on the Engineering Properties and Microstructure of a Red Clay. *Applied Science*. vol. 11, no.22, p. 10887. https://doi.org/10.3390/app112210887.

Wen, R., Tan, C., Wu, Y., Wang, C., 2018. Grain Size Effect on the Mechanical Behavior of Cohesionless Coarse-Grained Soils with the Discrete Element Method. *Advances in Civil Engineering*, vol. 2018, no.1, p.4608930. https://doi.org/10.1155/2018/4608930.

Weser. J., 2020. The importance of soil compaction in construction. Mintek team. Mintek resources. A report. *[Online]* Available at: https://mintekresources.com/importance-of-soil-compaction-in-construction/ [accessed 14 Nov 2024].

Wiklund, V., 2018. Fines Content and Density Effects on tailings behaviour a Laboratory study on geotechnical properties: A Laboratory Study on Geotechnical Properties. Lulea University of Technology, MEng Dissertation. *[Online]* Available at: http://www.diva-portal.org/smash/get/diva2:1264678/FULLTEXT01.pdf. [accessed 23 november 2024].

Wu, F.Y., Yang, Y.H., Li, Q.L., Mitchell, R.H., Dawson, J.B., Brandl, G. and Yuhara, M., 2011. In situ determination of U–Pb ages and Sr–Nd–Hf isotopic constraints on the petrogenesis of the Phalaborwa carbonatite Complex, South Africa. *Lithos*, vol.127, no1-2, pp.309-322. https://doi.org/10.1016/j.lithos.2011.09.005.

Wu, L., Chen, X., LI, H., Pan, Y., 2023. Mining Waste Utilization: Case Studies and Good Practices. In book: Managing Mining and Minerals Processing Wastes. Concepts, Design and Applications. *Elsevier*. pp, 251-269. https://doi.org/10.1016/B978-0-323-91283-9.00012-2.

Wu, P., Liang, B., Jin, J., Zhou, K., Guo, B., Yang, Z., 2022. Solution and Stability Analysis of Sliding Surface of Tailings Pond under Rainstorm. *Sustainability*. Vol. 14, no. 5, p. 3081. https://www.mdpi.com/2071-1050/14/5/3081.

Xu, Z., Xu, N., and Wang, H., 2019. Effects of Particle Shapes and Sizes on the Minimum Void Ratios of Sand. Research Article. *Hindawi Advances in Civil Engineering*. Vol, 2019, no. 1, p. 5732656. https://doi.org/10.1155/2019/57326566.

Xue, J., 2025. Analysis of Factors Affecting Slope Stability Based on the Finite Element Strength Reduction Method. *Academic Journal of Science and Technology* ISSN: 2771-3032 | Vol. 17, No. 2. https://doi.org/10.54097/4z35nj47.

Yan, X., Zhan, W., Hu, Z., Yu, Y. Xiao, D., 2021. Experimental Study on the Effect of Compaction Work and Defect on the Strength of Soil-Rock Mixture Subgrade. *Advances in Materials Science and Engineering*, vol. 2021, no.1, p.5533590. https://doi.org/10.1155/2021/5533590.

Yang, L.; Hu, J.; Bai, K., 2016. Capillary and Van Der Waals Force Between Microparticles with Different Sizes in Humid Air. Journal Adhesive. Science Technology. Vol. 30, no. 5, 566−578. https://doi.org/10.1080/01694243.2015.1111834.

Zabolotnii, E., Morgenstern, N.R., Wilson, G.W., 2022. Mechanism of Failure of the Mount Polley Tailings Storage Facility.an article Department of Civil and Environmental Engineering, University of Alberta, 9211 116 St., Edmonton, AB T6G 1H9, Canada. Canadian science publishing. *Geotechnical Journal*. vol. 59, no. 8, pp. 1503–1518. https://doi.org/10.1139/cgj-2021-0036.

Zamara, K., 2024. Soil Permeability: Definition, Tests, and Formulae. Tensar. *[online]* Available at: https://www.tensarinternational.com/resources/articles/the-permeability-of-soils-explained [accessed on 13 Dec 2024].

Zardari. M. A., 2011. Stability of Tailings Dams Focus on Limit Equilibrium Analysis. Licentiate thesis. Luleå University of Technology, Department of Civil, Environmental and Natural Resources , Engineering Division of Mining and Geotechnical Engineering.ISSN: 1402-1757 ISBN 978-91-7439-245-6.*[online]* Available at: https://ltu.diva-portal.org/smash/record.jsf?pid=diva2%3A991436&dswid=-5189 [accessed on 13 Nov 2024].

Zhang, C., Ji, E., Wang, B. and Wang, H., 2023. Research on the Relationship Between Soil Shear Stress Level and Safety Factor. *Advances in Materials Science and Engineering*, vol. 2023, no,1, p.9775240. https://doi.org/10.1155/2023/9775240.

Zhang, C., Pan, Z., Yin, H., Ma, C., Ma, L., Li, X., 2022a. Influence of clay mineral content on mechanical properties and micro fabric of tailings.

www.nature.com/scientificreports. *Scientific Reports* vol. 12. No. 1, p.10700. https://doi.org/10.1038/s41598-022-15063-3.

Zhang, J., Lu, S., Feng, T., Yi, B., Liu, J., 2022b. Research on Reuse of Silty Fine Sand in Backfill Grouting Material and Optimization of Backfill Grouting Material Proportions. Tunnelling and Underground Space Technology. vol. 130, p. 104751. https://doi.org/10.1016/j.tust.2022.104751.

Zhang, J., Soltani, A., Deng, A., Jaksa, M. B. 2019. Mechanical Behavior of Micaceous Clays. *Journal of Rock Mechanics and Geotechnical Engineering*, vol. 11. No. 5, p. 1044–1054. https://doi.org/10.1016/j.jrmge.2019.04.001.

Zhong, H., Zhu, Z., Zhao, J., Wei, L., Zhang, Y., Li, J., Wang, J., Yao, W., 2024. Influence of Fine Content and Mean Diameter Ratio on the Minimum and Maximum Void Ratios of Sand–Fine Mixtures: A Discrete Element Method Study. *Buildings*, vol. 14, no. 9, p. 2877. https://doi.org/10.3390/buildings14092877.

Zhou, W.H., Xu, X., Garg, A., 2016. Measurement of Unsaturated Shear Strength Parameters of Silty Sand and its Correlation with Unconfined Compressive Strength. Measurement, vol. 93, pp. 351–358. https://doi.org/10.1016/j.measurement.2016.07.049.

Zhu, F., Zhang, W. Puzrin, A.M., 2024. The Slip Surface Mechanism of Delayed Failure of the Brumadinho Tailings Dam in 2019. *Communication Earth Environment*. vol. 5, no.1, p. 33. https://doi.org/10.1038/s43247-023-01086-9.

8. Appendix

		Specimen		1	
#		Stage	Shear		
#		Schedule	Shear		
#		Time	ipStrain	ipLoad	ipPwP
	0	00:00:00	0,21	38	399
	4	00:04:00	0,28	52	400
	6	00:06:00	0,32	56	400
	8	00:08:00	0,35	58	401
	10	00:10:00	0,39	60	401
	12	00:12:00	0,41	62	401
	14	00:14:00	0,44	63	401
	16	00:16:00	0,48	62	401
	18	00:18:00	0,51	62	401
	20	00:20:00	0,55	60	401
	22	00:22:00	0,58	60	402
	24	00:24:00	0,62	59	401
	26	00:26:00	0,65	59	401
	28	00:28:00	0,69	59	401
	30	00:30:00	0,72	59	401
	32	00:32:00	0,76	59	402
	34	00:34:00	0,79	58	402
	36	00:36:00	0,82	58	402
	38	00:38:00	0,86	59	402
	40	00:40:00	0,89	60	403
	42	00:42:00	0,93	64	403
	44	00:44:00	0,95	70	404
	46	00:46:00	0,99	85	407
	48	00:48:00	1,02	101	411
	50	00:50:00	1,05	115	415
	52	00:52:00	1,09	127	418
	54	00:54:00	1,11	138	421
	56	00:56:00	1,15	147	424
	58	00:58:00	1,17	157	426
	60	01:00:00	1,2	166	428
	62	01:02:00	1,24	175	430
	64	01:04:00	1,27	183	431
	66	01:06:00	1,31	191	432
	68	01:08:00	1,33	198	433
	70	01:10:00	1,37	203	434
	72	01:12:00	1,39	211	435
	74	01:14:00	1,42	217	435
	76	01:16:00	1,45	224	435
	78	01:18:00	1,48	231	435
	80	01:20:00	1,5	238	435
	82	01:22:00	1,54	246	435
	84	01:24:00	1,57	252	435
	86	01:26:00	1,61	258	435
	88	01:28:00	1,64	264	434
	90	01:30:00	1,68	269	434
	92	01:32:00	1,7	276	433
	94	01:34:00	1,73	283	433
	96	01:36:00	1,77	291	432
	98	01:38:00	1,8	296	431
	100	01:40:00	1,84	302	431
	102	01:42:00	1,87	307	430
	104	01:44:00	1,91	314	429
	106	01:46:00	1,94	320	428
	108	01:48:00	1,96	325	428
	110	01:50:00	2	331	427
	112	01:52:00	2,03	336	426
	114	01:54:00	2,08	339	425
	116	01:56:00	2,1	345	424
	118	01:58:00	2,14	349	423
	120	02:00:00	2,17	354	422
	122	02:02:00	2,21	359	421
	124	02:04:00	2,24	363	420
	126	02:06:00	2,28	368	419
	128	02:08:00	2,31	372	419
	130	02:10:00	2,35	376	418
	132	02:12:00	2,38	381	417
	134	02:14:00	2,41	386	416
	136	02:16:00	2,45	390	415
	138	02:18:00	2,47	393	414
	140	02:20:00	2,51	395	413
	142	02:22:00	2,54	398	412
	144	02:24:00	2,58	404	411
	146	02:26:00	2,62	407	410
	148	02:28:00	2,64	410	409
	150	02:30:00	2,68	412	408
	152	02:32:00	2,71	415	407
	154	02:34:00	2,75	419	406
	156	02:36:00	2,78	423	405
	158	02:38:00	2,82	426	404
	160	02:40:00	2,85	428	404
	162	02:42:00	2,89	432	402
	164	02:44:00	2,92	434	401
	166	02:46:00	2,96	437	401
	168	02:48:00	2,99	440	400
	170	02:50:00	3,02	443	399
	172	02:52:00	3,06	446	398
	174	02:54:00	3,08	448	397
	176	02:56:00	3,13	449	396
	178	02:58:00	3,16	450	395
	180	03:00:00	3,2	454	395
	182	03:02:00	3,23	457	394
	184	03:04:00	3,27	460	393
	186	03:06:00	3,3	461	392
	188	03:08:00	3,34	463	391
	190	03:10:00	3,36	465	391
	192	03:12:00	3,39	468	390
	194	03:14:00	3,44	470	389
	196	03:16:00	3,46	471	388

		Specimen		1	
#		Stage	Shear		
#		Schedule	Shear		
#		Time	ipStrain	ipLoad	ipPwP
	198	03:18:00	3,5	475	388
	200	03:20:00	3,53	474	387
	202	03:22:00	3,57	477	386
	204	03:24:00	3,6	479	385
	206	03:26:00	3,64	481	385
	208	03:28:00	3,67	484	384
	210	03:30:00	3,7	484	383
	212	03:32:00	3,74	486	382
	214	03:34:00	3,77	488	382
	216	03:36:00	3,81	490	381
	218	03:38:00	3,84	492	381
	220	03:40:00	3,88	494	380
	222	03:42:00	3,91	497	379
	224	03:44:00	3,95	497	379
	226	03:46:00	3,97	499	378
	228	03:48:00	4,02	502	377
	230	03:50:00	4,05	504	377
	232	03:52:00	4,07	505	376
	234	03:54:00	4,11	506	376
	236	03:56:00	4,14	507	375
	238	03:58:00	4,18	510	374
	240	04:00:00	4,21	513	374
	242	04:02:00	4,25	514	373
	244	04:04:00	4,28	515	372
	246	04:06:00	4,3	517	372
	248	04:08:00	4,34	519	371
	250	04:10:00	4,37	520	370
	252	04:12:00	4,41	521	370
	254	04:14:00	4,44	523	369
	256	04:16:00	4,48	525	368
	258	04:18:00	4,51	527	368
	260	04:20:00	4,55	528	368
	262	04:22:00	4,58	528	367
	264	04:24:00	4,61	531	367
	266	04:26:00	4,65	532	366
	268	04:28:00	4,68	535	366
	270	04:30:00	4,72	535	365
	272	04:32:00	4,75	538	365
	274	04:34:00	4,79	538	364
	276	04:36:00	4,82	539	364
	278	04:38:00	4,86	541	364
	280	04:40:00	4,89	542	363
	282	04:42:00	4,93	544	363
	284	04:44:00	4,95	547	363
	286	04:46:00	4,98	549	362
	288	04:48:00	5,02	550	362
	290	04:50:00	5,05	551	361
	292	04:52:00	5,09	555	361
	294	04:54:00	5,12	555	360
	296	04:56:00	5,16	556	360
	298	04:58:00	5,19	558	360
	300	05:00:00	5,22	560	359
	302	05:02:00	5,26	561	359
	304	05:04:00	5,29	563	358
	306	05:06:00	5,33	565	358
	308	05:08:00	5,36	566	358
	310	05:10:00	5,4	569	357
	312	05:12:00	5,43	570	357
	314	05:14:00	5,47	572	357
	316	05:16:00	5,5	573	356
	318	05:18:00	5,52	576	356
	320	05:20:00	5,56	577	356
	322	05:22:00	5,59	578	355
	324	05:24:00	5,63	580	355
	326	05:26:00	5,66	581	355
	328	05:28:00	5,7	583	355
	330	05:30:00	5,73	584	354
	332	05:32:00	5,77	586	354
	334	05:34:00	5,8	587	354
	336	05:36:00	5,84	589	353
	338	05:38:00	5,87	592	353
	340	05:40:00	5,9	592	352
	342	05:42:00	5,94	594	352
	344	05:44:00	5,97	594	352
	346	05:46:00	6	596	352
	348	05:48:00	6,03	597	351
	350	05:50:00	6,07	599	351
	352	05:52:00	6,11	600	351
	354	05:54:00	6,14	601	351
	356	05:56:00	6,18	603	350
	358	05:58:00	6,2	604	350
	360	06:00:00	6,24	606	350
	362	06:02:00	6,27	608	349
	364	06:04:00	6,31	607	349
	366	06:06:00	6,34	608	349
	368	06:08:00	6,38	611	349
	370	06:10:00	6,41	611	348
	372	06:12:00	6,45	611	348
	374	06:14:00	6,48	613	348
	376	06:16:00	6,52	615	347
	378	06:18:00	6,55	615	347
	380	06:20:00	6,58	615	347
	382	06:22:00	6,62	617	347
	384	06:24:00	6,64	619	346
	386	06:26:00	6,69	620	346
	388	06:28:00	6,72	621	346
	390	06:30:00	6,76	623	346
	392	06:32:00	6,78	623	345

		Specimen		1	
#		Stage	Shear		
#		Schedule	Shear		
#		Time	ipStrain	ipLoad	ipPwP
	394	06:34:00	6,81	626	345
	396	06:36:00	6,85	627	344
	398	06:38:00	6,88	627	344
	400	06:40:00	6,92	628	343
	402	06:42:00	6,95	628	343
	404	06:44:00	6,99	629	343
	406	06:46:00	7,02	631	343
	408	06:48:00	7,07	633	342
	410	06:50:00	7,09	633	342
	412	06:52:00	7,13	634	342
	414	06:54:00	7,16	636	342
	416	06:56:00	7,19	635	342
	418	06:58:00	7,23	636	342
	420	07:00:00	7,26	637	341
	422	07:02:00	7,3	638	341
	424	07:04:00	7,33	639	341
	426	07:06:00	7,37	640	341
	428	07:08:00	7,4	639	341
	430	07:10:00	7,44	639	341
	432	07:12:00	7,47	642	341
	434	07:14:00	7,51	643	340
	436	07:16:00	7,54	644	340
	438	07:18:00	7,57	643	340
	440	07:20:00	7,61	645	340
	442	07:22:00	7,64	645	340
	444	07:24:00	7,68	647	339
	446	07:26:00	7,71	648	339
	448	07:28:00	7,75	649	339
	450	07:30:00	7,78	649	339
	452	07:32:00	7,82	649	339
	454	07:34:00	7,85	650	339
	456	07:36:00	7,87	651	339
	458	07:38:00	7,92	651	338
	460	07:40:00	7,94	652	338
	462	07:42:00	7,99	652	338
	464	07:44:00	8,02	651	338
	466	07:46:00	8,05	654	338
	468	07:48:00	8,08	655	338
	470	07:50:00	8,12	657	338
	472	07:52:00	8,15	656	337
	474	07:54:00	8,19	656	337
	476	07:56:00	8,22	656	337
	478	07:58:00	8,25	657	337
	480	08:00:00	8,29	658	337
	482	08:02:00	8,32	657	337
	484	08:04:00	8,36	656	337
	486	08:06:00	8,39	657	337
	488	08:08:00	8,43	658	337
	490	08:10:00	8,46	658	337
	492	08:12:00	8,5	659	337
	494	08:14:00	8,53	660	337
	496	08:16:00	8,57	661	337
	498	08:18:00	8,6	661	337
	500	08:20:00	8,63	662	337
	502	08:22:00	8,67	663	337
	504	08:24:00	8,7	663	337
	508	08:28:00	8,77	665	336
	510	08:30:00	8,81	665	336
	512	08:32:00	8,84	665	336
	514	08:34:00	8,87	666	336
	516	08:36:00	8,9	668	336
	518	08:38:00	8,95	669	336
	520	08:40:00	8,98	671	336
	522	08:42:00	9,01	673	336
	524	08:44:00	9,05	673	336
	526	08:46:00	9,07	673	336
	528	08:48:00	9,11	675	336
	530	08:50:00	9,14	675	336
	532	08:52:00	9,18	676	336
	534	08:54:00	9,21	678	336
	536	08:56:00	9,25	678	336
	538	08:58:00	9,28	679	336
	540	09:00:00	9,31	682	335
	542	09:02:00	9,35	682	335
	544	09:04:00	9,38	684	335
	546	09:06:00	9,42	685	335
	548	09:08:00	9,45	685	335
	550	09:10:00	9,49	686	334
	552	09:12:00	9,52	687	334
	554	09:14:00	9,56	688	334
	556	09:16:00	9,59	690	334
	558	09:18:00	9,63	691	334
	560	09:20:00	9,66	692	334
	562	09:22:00	9,68	694	334
	564	09:24:00	9,72	695	334
	566	09:26:00	9,76	694	334
	568	09:28:00	9,8	698	333
	570	09:30:00	9,82	696	333
	572	09:32:00	9,86	699	333
	574	09:34:00	9,9	699	333
	576	09:36:00	9,92	700	333
	578	09:38:00	9,96	701	333
	580	09:40:00	9,99	701	333
	582	09:42:00	10,03	703	332
	584	09:44:00	10,06	705	332
	586	09:46:00	10,09	705	332
	588	09:48:00	10,13	706	332
	590	09:50:00	10,16	707	331

Table 1: Depicts shear strength1 from number 1 to 590 consolidation on specimen one

#	Specimen	1		
#	Stage	Shear		
#	Schedule	Shear		
#	Time	ipStrain	ipLoad	ipPwP
592	09:52:00	10,19	707	331
594	09:54:00	10,22	707	331
596	09:56:00	10,26	710	331
598	09:58:00	10,29	710	331
600	10:00:00	10,33	712	331
602	10:02:00	10,36	712	331
604	10:04:00	10,4	714	330
606	10:06:00	10,43	714	330
608	10:08:00	10,47	714	330
610	10:10:00	10,5	717	330
612	10:12:00	10,54	717	330
614	10:14:00	10,57	717	330
616	10:16:00	10,6	718	330
618	10:18:00	10,64	719	330
620	10:20:00	10,67	718	330
622	10:22:00	10,71	720	330
624	10:24:00	10,74	721	329
626	10:26:00	10,78	721	329
628	10:28:00	10,81	721	329
630	10:30:00	10,85	723	329
632	10:32:00	10,88	724	329
634	10:34:00	10,92	724	329
636	10:36:00	10,95	725	329
638	10:38:00	10,98	727	329
640	10:40:00	11,02	727	329
642	10:42:00	11,05	727	328
644	10:44:00	11,08	729	328
646	10:46:00	11,11	729	328
648	10:48:00	11,15	730	328
650	10:50:00	11,19	731	328
652	10:52:00	11,22	730	328
654	10:54:00	11,25	732	328
656	10:56:00	11,28	732	328
658	10:58:00	11,32	733	328
660	11:00:00	11,35	734	327
662	11:02:00	11,39	736	327
664	11:04:00	11,42	736	327
666	11:06:00	11,46	737	327
668	11:08:00	11,49	739	327
670	11:10:00	11,53	739	327
672	11:12:00	11,56	739	327
674	11:14:00	11,6	740	326
676	11:16:00	11,63	740	326
678	11:18:00	11,66	740	326
680	11:20:00	11,7	740	326
682	11:22:00	11,73	741	326
684	11:24:00	11,77	743	326
686	11:26:00	11,8	743	326
688	11:28:00	11,84	743	326
690	11:30:00	11,87	744	325
692	11:32:00	11,91	745	325
694	11:34:00	11,94	748	325
696	11:36:00	11,98	748	325
698	11:38:00	12,01	748	325
700	11:40:00	12,04	749	325
702	11:42:00	12,07	750	324
704	11:44:00	12,1	750	324
706	11:46:00	12,14	751	324
708	11:48:00	12,17	751	324
710	11:50:00	12,21	751	324
712	11:52:00	12,25	754	324
714	11:54:00	12,28	753	324
716	11:56:00	12,31	753	324
718	11:58:00	12,34	755	323
720	12:00:00	12,38	757	323
722	12:02:00	12,41	757	323
724	12:04:00	12,45	757	323
726	12:06:00	12,48	757	323
728	12:08:00	12,52	759	323
730	12:10:00	12,55	758	323
732	12:12:00	12,59	761	323
734	12:14:00	12,62	760	322
736	12:16:00	12,66	761	322
738	12:18:00	12,69	761	322
740	12:20:00	12,72	762	322
742	12:22:00	12,76	763	322
744	12:24:00	12,79	764	322
746	12:26:00	12,83	764	322
748	12:28:00	12,86	765	321
750	12:30:00	12,9	766	321
752	12:32:00	12,93	767	321
754	12:34:00	12,97	767	321
756	12:36:00	13	767	321
758	12:38:00	13,04	767	321
760	12:40:00	13,07	768	321
762	12:42:00	13,1	768	321
764	12:44:00	13,14	769	321
766	12:46:00	13,16	770	320
768	12:48:00	13,21	771	320
770	12:50:00	13,23	773	320
772	12:52:00	13,27	773	320
774	12:54:00	13,3	771	320
776	12:56:00	13,33	773	320
778	12:58:00	13,38	774	320
780	13:00:00	13,4	774	319
782	13:02:00	13,44	774	319
784	13:04:00	13,47	775	319
786	13:06:00	13,51	777	319
788	13:08:00	13,54	776	319
790	13:10:00	13,58	776	319
792	13:12:00	13,61	779	319
794	13:14:00	13,65	779	318
796	13:16:00	13,68	781	318
798	13:18:00	13,71	782	318
800	13:20:00	13,75	781	318
802	13:22:00	13,78	784	318
804	13:24:00	13,82	783	318
806	13:26:00	13,85	785	318
808	13:28:00	13,89	785	317
810	13:30:00	13,92	786	317
812	13:32:00	13,96	785	317
814	13:34:00	13,98	788	317
816	13:36:00	14,01	788	316
818	13:38:00	14,05	787	316
820	13:40:00	14,08	789	316
822	13:42:00	14,12	789	316
824	13:44:00	14,15	790	315
826	13:46:00	14,19	791	315
828	13:48:00	14,22	792	315
830	13:50:00	14,26	794	315
832	13:52:00	14,29	795	315
834	13:54:00	14,33	794	315
836	13:56:00	14,36	795	315
838	13:58:00	14,38	796	315
840	14:00:00	14,42	796	315
842	14:02:00	14,45	797	315
844	14:04:00	14,5	797	314
846	14:06:00	14,53	797	314
848	14:08:00	14,57	797	314
850	14:10:00	14,6	797	314
852	14:12:00	14,63	798	314
854	14:14:00	14,66	798	314
856	14:16:00	14,69	798	314
858	14:18:00	14,73	799	314
860	14:20:00	14,76	801	314
862	14:22:00	14,8	800	313
864	14:24:00	14,83	801	313
866	14:26:00	14,87	802	313
868	14:28:00	14,9	802	313
870	14:30:00	14,94	803	313
872	14:32:00	14,97	804	313
874	14:34:00	15,01	804	313
876	14:36:00	15,04	804	313
878	14:38:00	15,07	806	313
880	14:40:00	15,11	806	312
882	14:42:00	15,14	806	312
884	14:44:00	15,18	808	312
886	14:46:00	15,2	809	312
888	14:48:00	15,24	809	312
890	14:50:00	15,28	810	312
892	14:52:00	15,32	811	312
894	14:54:00	15,35	810	312
896	14:56:00	15,39	811	312
898	14:58:00	15,41	810	311
900	15:00:00	15,44	812	311
902	15:02:00	15,48	813	311
904	15:04:00	15,51	814	311
906	15:06:00	15,56	813	311
908	15:08:00	15,58	814	311
910	15:10:00	15,62	815	311
912	15:12:00	15,65	814	310
914	15:14:00	15,68	816	310
916	15:16:00	15,72	815	310
918	15:18:00	15,75	816	310
920	15:20:00	15,79	817	310
922	15:22:00	15,82	816	310
924	15:24:00	15,86	816	310
926	15:26:00	15,89	819	309
928	15:28:00	15,93	816	309
930	15:30:00	15,96	817	309
932	15:32:00	16	819	309
934	15:34:00	16,03	820	309
936	15:36:00	16,07	821	309
938	15:38:00	16,1	822	309
940	15:40:00	16,13	821	309
942	15:42:00	16,17	823	309
944	15:44:00	16,19	824	308
946	15:46:00	16,23	825	308
948	15:48:00	16,26	825	308
950	15:50:00	16,3	827	307
952	15:52:00	16,33	824	307
954	15:54:00	16,36	826	307
956	15:56:00	16,4	828	307
958	15:58:00	16,43	827	307
960	16:00:00	16,47	829	307
962	16:02:00	16,5	827	307
964	16:04:00	16,54	830	307
966	16:06:00	16,57	829	307
968	16:08:00	16,61	828	307
970	16:10:00	16,64	830	307
972	16:12:00	16,68	829	307
974	16:14:00	16,71	829	307
976	16:16:00	16,74	830	306
978	16:18:00	16,78	830	306
980	16:20:00	16,81	831	306
982	16:22:00	16,85	832	306
984	16:24:00	16,88	832	306
986	16:26:00	16,92	830	305
988	16:28:00	16,95	831	305
990	16:30:00	16,98	831	305
992	16:32:00	17,01	833	305
994	16:34:00	17,04	833	305
996	16:36:00	17,08	834	304
998	16:38:00	17,11	833	305
1000	16:40:00	17,15	833	305
1002	16:42:00	17,18	836	304
1004	16:44:00	17,22	837	304
1006	16:46:00	17,25	836	304
1008	16:48:00	17,29	837	304
1010	16:50:00	17,32	836	304
1012	16:52:00	17,36	836	304
1014	16:54:00	17,39	837	304
1016	16:56:00	17,42	838	304
1018	16:58:00	17,45	837	304
1020	17:00:00	17,48	840	303
1022	17:02:00	17,52	838	303
1024	17:04:00	17,55	838	303
1026	17:06:00	17,59	839	303
1028	17:08:00	17,63	839	303
1030	17:10:00	17,65	840	303
1032	17:12:00	17,7	839	303
1034	17:14:00	17,72	838	303
1036	17:16:00	17,77	839	303
1038	17:18:00	17,8	838	303
1040	17:20:00	17,84	840	302
1042	17:22:00	17,87	839	302
1044	17:24:00	17,91	840	302
1046	17:26:00	17,93	840	302
1048	17:28:00	17,97	840	302
1050	17:30:00	18	841	302
1052	17:32:00	18,03	840	302
1054	17:34:00	18,07	841	301
1056	17:36:00	18,1	840	301
1058	17:38:00	18,14	839	301
1060	17:40:00	18,17	839	301
1062	17:42:00	18,21	838	301
1064	17:44:00	18,24	838	300
1066	17:46:00	18,28	839	300
1068	17:48:00	18,31	839	300
1070	17:50:00	18,35	839	300
1072	17:52:00	18,38	839	300
1074	17:54:00	18,42	838	300
1076	17:56:00	18,45	841	300
1078	17:58:00	18,48	840	300
1080	18:00:00	18,52	836	300
1082	18:02:00	18,55	835	300
1084	18:04:00	18,59	835	300
1086	18:06:00	18,62	835	300
1088	18:08:00	18,66	835	300
1090	18:10:00	18,69	837	299
1092	18:12:00	18,73	834	299
1094	18:14:00	18,76	834	300
1096	18:16:00	18,8	833	299
1098	18:18:00	18,83	834	299
1100	18:20:00	18,86	834	299
1102	18:22:00	18,9	834	299
1104	18:24:00	18,93	833	299
1106	18:26:00	18,97	833	299
1108	18:28:00	18,99	831	299
1110	18:30:00	19,03	833	299
1112	18:32:00	19,06	832	299
1114	18:34:00	19,09	833	299
1116	18:36:00	19,13	832	298
1118	18:38:00	19,16	833	298
1120	18:40:00	19,2	833	298
1122	18:42:00	19,23	835	298
1124	18:44:00	19,27	835	297
1126	18:46:00	19,3	833	297
1128	18:48:00	19,34	832	297
1130	18:50:00	19,37	832	297
1132	18:52:00	19,41	831	297
1134	18:54:00	19,44	833	297
1136	18:56:00	19,47	831	297
1138	18:58:00	19,51	831	297
1140	19:00:00	19,54	832	297
1142	19:02:00	19,58	832	297
1144	19:04:00	19,61	833	297
1146	19:06:00	19,65	832	297
1148	19:08:00	19,68	833	297
1150	19:10:00	19,72	832	297
1152	19:12:00	19,75	831	297
1154	19:14:00	19,79	831	297
1156	19:16:00	19,82	831	297
1158	19:18:00	19,85	831	297
1160	19:20:00	19,89	830	297
1162	19:22:00	19,92	830	297
1164	19:24:00	19,96	830	297
1166	19:26:00	19,99	830	297
1168	19:28:00	20,03	830	297
1170	19:30:00	20,06	830	297
1172	19:32:00	20,1	830	296
1174	19:34:00	20,13	829	296
1176	19:36:00	20,15	829	296
1178	19:36:05	20,17	829	296

Table 2: Depicts specimen one from no 592 to 1178 consolidation on specimen no 1

The following diagram illustrates the shear strength results from specimen no two tested

	Test	-		
	Specimen	2		
	Stage	Shear		
	Schedule	Shear		
no	Time	ipStrain	ipLoad	ipPwP
0	00:00:00	0,37	56	399
2	00:02:00	0,4	60	400
4	00:04:00	0,44	62	401
6	00:06:00	0,47	63	402
8	00:08:00	0,51	64	403
10	00:10:00	0,54	64	403
12	00:12:00	0,58	64	404
14	00:14:00	0,61	64	405
16	00:16:00	0,64	64	405
18	00:18:00	0,68	64	406
20	00:20:00	0,71	64	406
22	00:22:00	0,75	64	406
24	00:24:00	0,78	64	407
26	00:26:00	0,81	65	407
28	00:28:00	0,85	65	407
30	00:30:00	0,87	65	407
32	00:32:00	0,92	65	407
34	00:34:00	0,95	65	407
36	00:36:00	0,98	65	408
38	00:38:00	1,02	65	408
40	00:40:00	1,05	65	408
42	00:42:00	1,09	65	409
44	00:44:00	1,12	66	409
46	00:46:00	1,13	71	411
48	00:48:00	1,17	76	413
50	00:50:00	1,19	83	416
52	00:52:00	1,22	94	421
54	00:54:00	1,27	102	427
56	00:56:00	1,3	109	432
58	00:58:00	1,33	123	438
60	01:00:00	1,36	136	444
62	01:02:00	1,38	148	449
64	01:04:00	1,41	159	454
66	01:06:00	1,44	170	460
68	01:08:00	1,46	179	464
70	01:10:00	1,5	187	469
72	01:12:00	1,52	196	473
74	01:14:00	1,55	203	477
76	01:16:00	1,59	212	480
78	01:18:00	1,62	218	483
80	01:20:00	1,64	225	486
82	01:22:00	1,68	231	488
84	01:24:00	1,71	238	491
86	01:26:00	1,75	243	493
88	01:28:00	1,78	250	495
90	01:30:00	1,82	256	496
92	01:32:00	1,84	260	498
94	01:34:00	1,87	266	499
96	01:36:00	1,91	271	500
98	01:38:00	1,94	276	501
100	01:40:00	1,97	282	502
102	01:42:00	2,01	287	503
104	01:44:00	2,04	292	504
106	01:46:00	2,08	298	504
108	01:48:00	2,1	302	505
110	01:50:00	2,13	308	506
112	01:52:00	2,17	313	506
114	01:54:00	2,2	319	506
116	01:56:00	2,24	324	506
118	01:58:00	2,27	329	507
120	02:00:00	2,3	334	507
122	02:02:00	2,34	339	507
124	02:04:00	2,37	342	507
126	02:06:00	2,41	347	508
128	02:08:00	2,44	352	507
130	02:10:00	2,48	356	507
132	02:12:00	2,5	360	507
134	02:14:00	2,53	366	507
136	02:16:00	2,57	370	507
138	02:18:00	2,6	374	507
140	02:20:00	2,63	380	507
142	02:22:00	2,67	384	507
144	02:24:00	2,7	388	507
146	02:26:00	2,73	393	506
148	02:28:00	2,76	397	506
150	02:30:00	2,79	400	505
152	02:32:00	2,83	404	505
154	02:34:00	2,86	408	504
156	02:36:00	2,9	411	504
158	02:38:00	2,93	414	503
160	02:40:00	2,96	418	503
162	02:42:00	3	423	502
164	02:44:00	3,02	427	502
166	02:46:00	3,06	431	501
168	02:48:00	3,09	435	500
170	02:50:00	3,12	440	500
172	02:52:00	3,16	444	499
174	02:54:00	3,19	448	499
176	02:56:00	3,23	452	498
178	02:58:00	3,25	456	497
180	03:00:00	3,28	460	496
182	03:02:00	3,32	465	496
184	03:04:00	3,35	468	495
186	03:06:00	3,39	472	494
188	03:08:00	3,42	476	493
190	03:10:00	3,45	480	492
192	03:12:00	3,48	484	491
194	03:14:00	3,51	487	490
196	03:16:00	3,55	491	490

	Test	-		
	Specimen	2		
	Stage	Shear		
	Schedule	Shear		
no	Time	ipStrain	ipLoad	ipPwP
198	03:18:00	3,58	494	489
200	03:20:00	3,61	499	488
202	03:22:00	3,65	502	487
204	03:24:00	3,67	506	486
206	03:26:00	3,7	510	485
208	03:28:00	3,74	513	484
210	03:30:00	3,77	517	483
212	03:32:00	3,81	522	482
214	03:34:00	3,84	525	481
216	03:36:00	3,88	528	480
218	03:38:00	3,9	533	479
220	03:40:00	3,93	537	478
222	03:42:00	3,97	541	477
224	03:44:00	4,01	544	476
226	03:46:00	4,03	547	475
228	03:48:00	4,07	552	474
230	03:50:00	4,1	556	473
232	03:52:00	4,14	558	472
234	03:54:00	4,17	562	471
236	03:56:00	4,21	565	470
238	03:58:00	4,24	569	469
240	04:00:00	4,26	572	468
242	04:02:00	4,3	576	467
244	04:04:00	4,33	571	463
246	04:06:00	4,35	583	465
248	04:08:00	4,39	585	464
250	04:10:00	4,42	589	462
252	04:12:00	4,46	593	461
254	04:14:00	4,49	596	460
256	04:16:00	4,52	599	459
258	04:18:00	4,55	603	458
260	04:20:00	4,58	606	457
262	04:22:00	4,61	609	456
264	04:24:00	4,65	613	455
266	04:26:00	4,68	617	454
268	04:28:00	4,72	621	453
270	04:30:00	4,75	625	452
272	04:32:00	4,77	628	451
274	04:34:00	4,81	632	450
276	04:36:00	4,84	636	449
278	04:38:00	4,88	640	448
280	04:40:00	4,9	643	448
282	04:42:00	4,93	648	447
284	04:44:00	4,97	651	446
286	04:46:00	5	655	445
288	04:48:00	5,04	659	443
290	04:50:00	5,07	663	443
292	04:52:00	5,09	668	442
294	04:54:00	5,13	672	441
296	04:56:00	5,16	676	440
298	04:58:00	5,19	681	439
300	05:00:00	5,23	684	438
302	05:02:00	5,26	688	437
304	05:04:00	5,29	693	436
306	05:06:00	5,32	697	435
308	05:08:00	5,35	700	435
310	05:10:00	5,39	704	434
312	05:12:00	5,42	708	433
314	05:14:00	5,46	712	432
316	05:16:00	5,48	717	431
318	05:18:00	5,51	721	430
320	05:20:00	5,55	725	430
322	05:22:00	5,58	729	429
324	05:24:00	5,62	734	428
326	05:26:00	5,65	738	427
328	05:28:00	5,68	742	426
330	05:30:00	5,71	747	425
332	05:32:00	5,74	751	425
334	05:34:00	5,78	754	424
336	05:36:00	5,81	759	423
338	05:38:00	5,84	763	422
340	05:40:00	5,88	768	422
342	05:42:00	5,91	772	421
344	05:44:00	5,95	777	420
346	05:46:00	5,98	781	419
348	05:48:00	6,01	785	418
350	05:50:00	6,04	790	417
352	05:52:00	6,07	794	417
354	05:54:00	6,11	798	416
356	05:56:00	6,14	802	415
358	05:58:00	6,17	807	414
360	06:00:00	6,21	811	414
362	06:02:00	6,24	814	413
364	06:04:00	6,28	818	412
366	06:06:00	6,31	822	412
368	06:08:00	6,34	826	411
370	06:10:00	6,37	830	410
372	06:12:00	6,4	833	409
374	06:14:00	6,44	838	409
376	06:16:00	6,47	842	408
378	06:18:00	6,5	845	407
380	06:20:00	6,54	851	407
382	06:22:00	6,57	855	406
384	06:24:00	6,61	859	405
386	06:26:00	6,64	864	405
388	06:28:00	6,67	868	404
390	06:30:00	6,7	872	403
392	06:32:00	6,73	877	402

	Test	-		
	Specimen	2		
	Stage	Shear		
	Schedule	Shear		
no	Time	ipStrain	ipLoad	ipPwP
394	06:34:00	6,77	881	402
396	06:36:00	6,8	885	401
398	06:38:00	6,83	889	400
400	06:40:00	6,87	894	399
402	06:42:00	6,9	898	398
404	06:44:00	6,92	902	397
406	06:46:00	6,96	905	396
408	06:48:00	6,99	909	395
410	06:50:00	7,03	913	394
412	06:52:00	7,06	916	394
414	06:54:00	7,1	919	393
416	06:56:00	7,13	925	392
418	06:58:00	7,16	928	392
420	07:00:00	7,2	933	391
422	07:02:00	7,23	937	390
424	07:04:00	7,27	941	390
426	07:06:00	7,3	945	389
428	07:08:00	7,33	949	389
430	07:10:00	7,37	954	388
432	07:12:00	7,4	956	387
434	07:14:00	7,43	960	387
436	07:16:00	7,46	963	387
438	07:18:00	7,49	965	386
440	07:20:00	7,53	969	386
442	07:22:00	7,56	973	386
444	07:24:00	7,6	976	386
446	07:26:00	7,63	979	386
448	07:28:00	7,66	981	386
450	07:30:00	7,7	984	386
452	07:32:00	7,73	985	386
454	07:34:00	7,77	988	386
456	07:36:00	7,79	992	386
458	07:38:00	7,82	994	386
460	07:40:00	7,86	998	386
462	07:42:00	7,89	1002	386
464	07:44:00	7,93	1005	386
466	07:46:00	7,96	1008	386
468	07:48:00	7,99	1011	386
470	07:50:00	8,03	1013	386
472	07:52:00	8,06	1015	385
474	07:54:00	8,1	1016	385
476	07:56:00	8,13	1020	385
478	07:58:00	8,16	1021	385
480	08:00:00	8,19	1024	385
482	08:02:00	8,22	1027	384
484	08:04:00	8,26	1027	384
486	08:06:00	8,29	1029	384
488	08:08:00	8,32	1030	384
490	08:10:00	8,36	1031	384
492	08:12:00	8,39	1034	384
494	08:14:00	8,43	1036	384
496	08:16:00	8,46	1037	384
498	08:18:00	8,49	1040	384
500	08:20:00	8,53	1041	383
502	08:22:00	8,56	1043	383
504	08:24:00	8,59	1046	383
506	08:26:00	8,62	1050	383
508	08:28:00	8,65	1053	383
510	08:30:00	8,69	1055	383
512	08:32:00	8,72	1056	383
514	08:34:00	8,76	1058	382
516	08:36:00	8,79	1060	382
518	08:38:00	8,82	1062	382
520	08:40:00	8,86	1065	382
522	08:42:00	8,89	1065	381
524	08:44:00	8,93	1069	381
526	08:46:00	8,96	1070	381
528	08:48:00	9	1073	381
530	08:50:00	9,03	1076	381
532	08:52:00	9,06	1076	381
534	08:54:00	9,1	1078	381
536	08:56:00	9,12	1081	380
538	08:58:00	9,15	1083	380
540	09:00:00	9,19	1085	380
542	09:02:00	9,22	1086	380
544	09:04:00	9,26	1090	380
546	09:06:00	9,29	1092	380
548	09:08:00	9,33	1094	380
550	09:10:00	9,36	1093	380
552	09:12:00	9,39	1095	380
554	09:14:00	9,43	1098	380
556	09:16:00	9,46	1099	379
558	09:18:00	9,5	1101	379
560	09:20:00	9,53	1104	379
562	09:22:00	9,56	1105	379
564	09:24:00	9,6	1109	379
566	09:26:00	9,63	1108	379
568	09:28:00	9,67	1111	379
570	09:30:00	9,7	1111	379
572	09:32:00	9,74	1111	379
574	09:34:00	9,77	1114	378
576	09:36:00	9,8	1114	378
578	09:38:00	9,84	1118	378
580	09:40:00	9,87	1121	378
582	09:42:00	9,91	1121	378
584	09:44:00	9,94	1123	378
586	09:46:00	9,97	1126	378
588	09:48:00	10,01	1128	378
590	09:50:00	10,03	1129	378

-

Table 3: Depicts shear strength from <u>no 1 to 590</u> consolidation on specimen 2

Test -
Specimen 2
Stage Shear
Schedule Shear

no	Time	ipStrain	ipLoad	ipPwP
592	09:52:00	10,07	1132	377
594	09:54:00	10,1	1134	377
596	09:56:00	10,13	1134	377
598	09:58:00	10,17	1138	377
600	10:00:00	10,2	1139	377
602	10:02:00	10,24	1142	377
604	10:04:00	10,27	1146	377
606	10:06:00	10,3	1145	376
608	10:08:00	10,34	1147	376
610	10:10:00	10,37	1149	376
612	10:12:00	10,41	1149	376
614	10:14:00	10,44	1151	376
616	10:16:00	10,47	1151	376
618	10:18:00	10,51	1155	376
620	10:20:00	10,54	1155	376
622	10:22:00	10,58	1156	375
624	10:24:00	10,61	1158	375
626	10:26:00	10,65	1159	375
628	10:28:00	10,68	1160	375
630	10:30:00	10,71	1161	375
632	10:32:00	10,75	1164	375
634	10:34:00	10,79	1162	374
636	10:36:00	10,83	1163	374
638	10:38:00	10,87	1166	374
640	10:40:00	10,91	1165	374
642	10:42:00	10,94	1166	374
644	10:44:00	10,99	1167	374
646	10:46:00	11,02	1166	374
648	10:48:00	11,04	1168	374
650	10:50:00	11,09	1170	373
652	10:52:00	11,11	1171	373
654	10:54:00	11,15	1171	373
656	10:56:00	11,18	1173	373
658	10:58:00	11,2	1176	373
660	11:00:00	11,24	1175	373
662	11:02:00	11,26	1175	373
664	11:04:00	11,29	1178	373
666	11:06:00	11,33	1179	372
668	11:08:00	11,36	1181	372
670	11:10:00	11,4	1182	372
672	11:12:00	11,43	1184	372
674	11:14:00	11,46	1185	372
676	11:16:00	11,5	1184	372
678	11:18:00	11,53	1187	372
680	11:20:00	11,57	1185	371
682	11:22:00	11,6	1189	371
684	11:24:00	11,64	1190	371
686	11:26:00	11,66	1192	371
688	11:28:00	11,7	1195	371
690	11:30:00	11,74	1196	371
692	11:32:00	11,76	1197	371
694	11:34:00	11,79	1197	371
696	11:36:00	11,84	1198	371
698	11:38:00	11,86	1198	370
700	11:40:00	11,9	1202	370
702	11:42:00	11,94	1203	370
704	11:44:00	11,97	1204	370
706	11:46:00	12	1201	370
708	11:48:00	12,03	1203	370
710	11:50:00	12,07	1208	370
712	11:52:00	12,1	1208	369
714	11:54:00	12,14	1207	369
716	11:56:00	12,17	1207	369
718	11:58:00	12,2	1208	369
720	12:00:00	12,24	1212	369
722	12:02:00	12,27	1211	369
724	12:04:00	12,31	1211	369
726	12:06:00	12,34	1212	368
728	12:08:00	12,37	1214	368
730	12:10:00	12,41	1212	368
732	12:12:00	12,44	1213	368
734	12:14:00	12,48	1217	368
736	12:16:00	12,51	1215	368
738	12:18:00	12,55	1217	368
740	12:20:00	12,58	1219	367
742	12:22:00	12,61	1218	367
744	12:24:00	12,65	1223	367
746	12:26:00	12,68	1223	367
748	12:28:00	12,72	1222	366
750	12:30:00	12,74	1225	366
752	12:32:00	12,77	1224	366
754	12:34:00	12,81	1228	366
756	12:36:00	12,84	1229	365
758	12:38:00	12,88	1228	365
760	12:40:00	12,91	1231	365
762	12:42:00	12,94	1230	365
764	12:44:00	12,98	1232	365
766	12:46:00	13,01	1235	365
768	12:48:00	13,05	1234	365
770	12:50:00	13,07	1232	365
772	12:52:00	13,1	1233	365
774	12:54:00	13,14	1237	365
776	12:56:00	13,17	1234	364
778	12:58:00	13,21	1236	364
780	13:00:00	13,24	1237	364
782	13:02:00	13,27	1238	364
784	13:04:00	13,31	1237	364
786	13:06:00	13,34	1235	364
788	13:08:00	13,38	1237	364
790	13:10:00	13,41	1236	364
792	13:12:00	13,44	1236	364
794	13:14:00	13,48	1237	363
796	13:16:00	13,51	1236	363
798	13:18:00	13,55	1238	363
800	13:20:00	13,58	1240	363
802	13:22:00	13,62	1240	363
804	13:24:00	13,65	1241	363
806	13:26:00	13,68	1240	363
808	13:28:00	13,72	1244	363
810	13:30:00	13,75	1244	363
812	13:32:00	13,79	1243	362
814	13:34:00	13,81	1244	362
816	13:36:00	13,84	1245	362
818	13:38:00	13,88	1246	362
820	13:40:00	13,91	1245	362
822	13:42:00	13,95	1246	362
824	13:44:00	13,98	1247	362
826	13:46:00	14,01	1250	362
828	13:48:00	14,05	1250	362
830	13:50:00	14,08	1250	361
832	13:52:00	14,12	1251	361
834	13:54:00	14,15	1252	361
836	13:56:00	14,18	1253	361
838	13:58:00	14,22	1254	361
840	14:00:00	14,25	1252	361
842	14:02:00	14,29	1254	361
844	14:04:00	14,32	1253	360
846	14:06:00	14,35	1255	360
848	14:08:00	14,38	1255	360
850	14:10:00	14,41	1253	360
852	14:12:00	14,45	1256	360
854	14:14:00	14,48	1254	360
856	14:16:00	14,51	1255	360
858	14:18:00	14,55	1255	359
860	14:20:00	14,58	1255	359
862	14:22:00	14,62	1255	359
864	14:24:00	14,65	1255	359
866	14:26:00	14,68	1255	359
868	14:28:00	14,72	1255	359
870	14:30:00	14,75	1256	359
872	14:32:00	14,79	1256	359
874	14:34:00	14,82	1255	359
876	14:36:00	14,86	1256	358
878	14:38:00	14,89	1255	358
880	14:40:00	14,92	1254	358
882	14:42:00	14,96	1253	357
884	14:44:00	14,99	1255	357
886	14:46:00	15,04	1255	357
888	14:48:00	15,07	1255	357
890	14:50:00	15,09	1255	357
892	14:52:00	15,13	1256	357
894	14:54:00	15,16	1257	357
896	14:56:00	15,2	1258	357
898	14:58:00	15,23	1259	357
900	15:00:00	15,27	1258	357
902	15:02:00	15,3	1258	357
904	15:04:00	15,33	1257	357
906	15:06:00	15,37	1258	357
908	15:08:00	15,4	1258	356
910	15:10:00	15,44	1258	356
912	15:12:00	15,47	1258	356
914	15:14:00	15,5	1259	356
916	15:16:00	15,54	1259	356
918	15:18:00	15,57	1260	355
920	15:20:00	15,61	1259	355
922	15:22:00	15,64	1260	355
924	15:24:00	15,67	1259	355
926	15:26:00	15,71	1260	355
928	15:28:00	15,74	1261	354
930	15:30:00	15,78	1259	355
932	15:32:00	15,81	1260	355
934	15:34:00	15,85	1260	354
936	15:36:00	15,88	1260	354
938	15:38:00	15,91	1260	354
940	15:40:00	15,95	1260	354
942	15:42:00	15,98	1260	354
944	15:44:00	16,02	1259	354
946	15:46:00	16,05	1260	354
948	15:48:00	16,07	1259	354
950	15:50:00	16,11	1260	354
952	15:52:00	16,14	1259	353
954	15:54:00	16,18	1259	353
956	15:56:00	16,21	1260	353
958	15:58:00	16,24	1259	353
960	16:00:00	16,28	1259	353
962	16:02:00	16,31	1259	353
964	16:04:00	16,35	1258	353
966	16:06:00	16,38	1259	353
968	16:08:00	16,41	1259	353
970	16:10:00	16,45	1259	353
972	16:12:00	16,48	1261	352
974	16:14:00	16,52	1261	352
976	16:16:00	16,55	1261	352
978	16:18:00	16,58	1260	352
980	16:20:00	16,62	1260	352
982	16:22:00	16,65	1259	352
984	16:24:00	16,68	1258	352
986	16:26:00	16,71	1258	351
988	16:28:00	16,74	1255	351
990	16:30:00	16,78	1255	351
992	16:32:00	16,81	1254	351
994	16:34:00	16,85	1254	351
996	16:36:00	16,88	1253	350
998	16:38:00	16,91	1253	350
1000	16:40:00	16,95	1251	350
1002	16:42:00	16,98	1252	350
1004	16:44:00	17,02	1250	350
1006	16:46:00	17,05	1250	350
1008	16:48:00	17,07	1251	350
1010	16:50:00	17,11	1251	350
1012	16:52:00	17,14	1251	350
1014	16:54:00	17,18	1250	350
1016	16:56:00	17,21	1249	350
1018	16:58:00	17,24	1249	350
1020	17:00:00	17,28	1248	350
1022	17:02:00	17,3	1249	349
1024	17:04:00	17,34	1248	349
1026	17:06:00	17,37	1246	350
1028	17:08:00	17,4	1247	349
1030	17:10:00	17,44	1246	349
1032	17:12:00	17,47	1245	349
1034	17:14:00	17,51	1245	349
1036	17:16:00	17,54	1245	349
1038	17:18:00	17,57	1245	349
1040	17:20:00	17,61	1244	349
1042	17:22:00	17,64	1243	349
1044	17:24:00	17,68	1242	349
1046	17:26:00	17,71	1241	349
1048	17:28:00	17,75	1240	348
1050	17:30:00	17,78	1240	348
1052	17:32:00	17,81	1240	348
1054	17:34:00	17,84	1240	348
1056	17:36:00	17,87	1240	347
1058	17:38:00	17,9	1239	347
1060	17:40:00	17,94	1241	347
1062	17:42:00	17,97	1242	347
1064	17:44:00	18	1242	347
1066	17:46:00	18,03	1243	347
1068	17:48:00	18,06	1243	347
1070	17:50:00	18,1	1242	347
1072	17:52:00	18,13	1242	347
1074	17:54:00	18,17	1241	347
1076	17:56:00	18,2	1241	347
1078	17:58:00	18,25	1239	347
1080	18:00:00	18,27	1239	347
1082	18:02:00	18,3	1237	347
1084	18:04:00	18,34	1237	347
1086	18:06:00	18,37	1238	347
1088	18:08:00	18,41	1237	347
1090	18:10:00	18,44	1237	347
1092	18:12:00	18,47	1236	347
1094	18:14:00	18,51	1234	347
1096	18:16:00	18,54	1234	347
1098	18:18:00	18,58	1232	347
1100	18:20:00	18,6	1234	347
1102	18:22:00	18,63	1233	347
1104	18:24:00	18,67	1232	346
1106	18:26:00	18,7	1232	346
1108	18:28:00	18,74	1229	346
1110	18:30:00	18,77	1228	346
1112	18:32:00	18,8	1227	341
1114	18:34:00	18,84	1226	341
1116	18:36:00	18,87	1226	341
1118	18:38:00	18,91	1227	342
1120	18:40:00	18,94	1227	341
1122	18:42:00	18,96	1227	341
1124	18:44:00	19	1228	341
1126	18:46:00	19,03	1228	341
1128	18:48:00	19,07	1229	341
1130	18:50:00	19,1	1228	341
1132	18:52:00	19,13	1228	341
1134	18:54:00	19,17	1228	342
1136	18:56:00	19,19	1230	342
1138	18:58:00	19,2	1229	342
1140	19:00:00	19,22	1228	343
1142	19:02:00	19,26	1227	343
1144	19:04:00	19,29	1226	343
1146	19:06:00	19,33	1226	343
1148	19:08:00	19,36	1226	344
1150	19:10:00	19,4	1226	344
1152	19:12:00	19,42	1226	344
1154	19:14:00	19,44	1223	345
1156	19:16:00	19,48	1221	345
1158	19:18:00	19,5	1218	345
1160	19:20:00	19,52	1217	345
1162	19:22:00	19,55	1217	345
1164	19:24:00	19,59	1215	346
1166	19:26:00	19,62	1213	346
1168	19:28:00	19,66	1212	346
1170	19:30:00	19,69	1212	347
1172	19:32:00	19,71	1212	347
1174	19:34:00	19,74	1212	347
1176	19:36:00	19,77	1212	347
1178	19:38:00	19,81	1212	347

Table 4: Depicts specimen two from no 592 to 1178 consolidation

The following tables illustrate laboratory shear strength results from specimen 3 tested

Table 5: Depicts specimen three from no 1 to 592 consolidation

Test -
Specimen 3
Stage Shear
Schedule Shear

no	Time	ipStrain	ipLoad	ipPwP
0	00:00:00	0,36	79,2	400
2	00:02:00	0,38	108	404
4	00:04:00	0,39	135,6	412
6	00:06:00	0,41	160,8	421
8	00:08:00	0,43	183,6	430
10	00:10:00	0,46	211,2	440
12	00:12:00	0,49	238,8	450
14	00:14:00	0,52	266,4	459
16	00:16:00	0,55	292,8	469
18	00:18:00	0,58	316,8	479
20	00:20:00	0,61	340,8	489
22	00:22:00	0,64	363,6	498
24	00:24:00	0,67	384	506
26	00:26:00	0,7	403,2	514
28	00:28:00	0,74	421,2	521
30	00:30:00	0,77	438	527
32	00:32:00	0,8	453,6	533
34	00:34:00	0,83	468	539
36	00:36:00	0,87	483,6	544
38	00:38:00	0,9	496,8	549
40	00:40:00	0,93	510	553
42	00:42:00	0,97	523,2	557
44	00:44:00	1	536,4	560
46	00:46:00	1,03	548,4	563
48	00:48:00	1,06	559,2	566
50	00:50:00	1,1	570	569
52	00:52:00	1,13	580,8	571
54	00:54:00	1,16	591,6	573
56	00:56:00	1,19	602,4	575
58	00:58:00	1,23	612	576
60	01:00:00	1,26	622,8	578
62	01:02:00	1,29	631,2	579
64	01:04:00	1,33	640,8	580
66	01:06:00	1,36	650,4	581
68	01:08:00	1,39	660	582
70	01:10:00	1,42	669,6	583
72	01:12:00	1,46	678	583
74	01:14:00	1,49	687,6	584
76	01:16:00	1,53	696	584
78	01:18:00	1,56	704,4	584
80	01:20:00	1,59	714	584
82	01:22:00	1,62	721,2	584
84	01:24:00	1,66	729,6	584
86	01:26:00	1,69	736,8	584
88	01:28:00	1,73	744	583
90	01:30:00	1,76	751,2	583
92	01:32:00	1,79	757,2	583
94	01:34:00	1,83	764,4	583
96	01:36:00	1,86	771,6	582
98	01:38:00	1,89	778,8	582
100	01:40:00	1,93	786	582
102	01:42:00	1,96	792	581
104	01:44:00	1,99	798	581
106	01:46:00	2,03	804	580
108	01:48:00	2,06	811,2	580
110	01:50:00	2,1	818,4	579
112	01:52:00	2,13	824,4	579
114	01:54:00	2,16	831,6	578
116	01:56:00	2,19	837,6	578
118	01:58:00	2,23	843,6	577
120	02:00:00	2,26	849,6	576
122	02:02:00	2,3	855,6	576
124	02:04:00	2,33	861,6	575
126	02:06:00	2,36	866,4	574
128	02:08:00	2,4	872,4	573
130	02:10:00	2,43	878,4	573
132	02:12:00	2,46	882	572
134	02:14:00	2,5	886,8	571
136	02:16:00	2,53	890,4	571
138	02:18:00	2,56	895,2	570
140	02:20:00	2,6	901,2	569
142	02:22:00	2,63	906	568
144	02:24:00	2,67	910,8	568
146	02:26:00	2,7	916,8	567
148	02:28:00	2,73	921,6	566
150	02:30:00	2,76	925,2	565
152	02:32:00	2,8	930	564
154	02:34:00	2,83	934,8	564
156	02:36:00	2,86	938,4	563
158	02:38:00	2,9	942	562
160	02:40:00	2,93	945,6	562
162	02:42:00	2,96	949,2	561
164	02:44:00	3	954	560
166	02:46:00	3,03	957,6	559
168	02:48:00	3,06	961,2	558
170	02:50:00	3,09	966	558
172	02:52:00	3,13	970,8	557
174	02:54:00	3,16	975,6	556
176	02:56:00	3,19	979,2	556
178	02:58:00	3,22	982,8	555
180	03:00:00	3,26	988,8	554
182	03:02:00	3,29	992,4	553
184	03:04:00	3,32	994,8	552
186	03:06:00	3,35	999,6	552
188	03:08:00	3,38	1002	551
190	03:10:00	3,42	1007	550
192	03:12:00	3,45	1011	549
194	03:14:00	3,48	1014	549
196	03:16:00	3,51	1018	548
198	03:18:00	3,55	1022	547
200	03:20:00	3,58	1026	547
202	03:22:00	3,61	1030	546
204	03:24:00	3,65	1033	545
206	03:26:00	3,68	1038	544
208	03:28:00	3,71	1042	544
210	03:30:00	3,74	1045	543
212	03:32:00	3,78	1051	542
214	03:34:00	3,81	1055	542
216	03:36:00	3,84	1059	541
218	03:38:00	3,87	1064	540
220	03:40:00	3,9	1068	539
222	03:42:00	3,93	1072	539
224	03:44:00	3,97	1077	538
226	03:46:00	4	1081	537
228	03:48:00	4,02	1085	537
230	03:50:00	4,06	1089	536
232	03:52:00	4,09	1094	535
234	03:54:00	4,12	1098	535
236	03:56:00	4,16	1102	534
238	03:58:00	4,19	1105	533
240	04:00:00	4,22	1109	533
242	04:02:00	4,25	1113	532
244	04:04:00	4,28	1116	531
246	04:06:00	4,31	1119	530
248	04:08:00	4,34	1125	529
250	04:10:00	4,37	1128	528
252	04:12:00	4,41	1133	527
254	04:14:00	4,44	1137	526
256	04:16:00	4,47	1141	525
258	04:18:00	4,51	1145	525
260	04:20:00	4,54	1149	524
262	04:22:00	4,57	1154	523
264	04:24:00	4,6	1156	523
266	04:26:00	4,63	1160	522
268	04:28:00	4,67	1163	522
270	04:30:00	4,7	1165	521
272	04:32:00	4,73	1169	521
274	04:34:00	4,76	1173	520
276	04:36:00	4,79	1176	520
278	04:38:00	4,82	1179	519
280	04:40:00	4,86	1181	519
282	04:42:00	4,89	1184	518
284	04:44:00	4,92	1185	517
286	04:46:00	4,95	1188	517
288	04:48:00	4,99	1192	516
290	04:50:00	5,02	1194	516
292	04:52:00	5,05	1198	515
294	04:54:00	5,08	1202	515
296	04:56:00	5,11	1205	514
298	04:58:00	5,15	1208	514
300	05:00:00	5,18	1211	513
302	05:02:00	5,21	1213	513
304	05:04:00	5,25	1215	512
306	05:06:00	5,27	1216	512
308	05:08:00	5,3	1220	511
310	05:10:00	5,32	1221	511
312	05:12:00	5,35	1224	510
314	05:14:00	5,39	1227	510
316	05:16:00	5,42	1227	509
318	05:18:00	5,46	1229	509
320	05:20:00	5,49	1230	508
322	05:22:00	5,52	1231	508
324	05:24:00	5,55	1234	507
326	05:26:00	5,59	1236	507
328	05:28:00	5,62	1237	506
330	05:30:00	5,65	1240	506
332	05:32:00	5,68	1241	506
334	05:34:00	5,72	1243	505
336	05:36:00	5,75	1246	504
338	05:38:00	5,79	1250	504
340	05:40:00	5,82	1253	503
342	05:42:00	5,85	1255	503
344	05:44:00	5,89	1256	502
346	05:46:00	5,92	1258	502
348	05:48:00	5,95	1260	501
350	05:50:00	5,99	1262	501
352	05:52:00	6,02	1265	501
354	05:54:00	6,05	1265	500
356	05:56:00	6,09	1269	500
358	05:58:00	6,12	1270	499
360	06:00:00	6,16	1273	499
362	06:02:00	6,19	1276	498
364	06:04:00	6,23	1276	498
366	06:06:00	6,26	1278	497
368	06:08:00	6,29	1281	497
370	06:10:00	6,33	1283	497
372	06:12:00	6,36	1285	496
374	06:14:00	6,39	1286	496
376	06:16:00	6,43	1290	495
378	06:18:00	6,46	1292	495
380	06:20:00	6,5	1294	495
382	06:22:00	6,53	1293	494
384	06:24:00	6,57	1295	494
386	06:26:00	6,6	1298	493
388	06:28:00	6,63	1299	493
390	06:30:00	6,67	1301	493
392	06:32:00	6,7	1304	493
394	06:34:00	6,73	1305	493
396	06:36:00	6,77	1309	492
398	06:38:00	6,8	1308	491
400	06:40:00	6,83	1311	491
402	06:42:00	6,86	1311	490
404	06:44:00	6,9	1311	489
406	06:46:00	6,93	1314	488
408	06:48:00	6,97	1314	488
410	06:50:00	7	1318	488
412	06:52:00	7,04	1321	488
414	06:54:00	7,07	1321	488
416	06:56:00	7,1	1323	488
418	06:58:00	7,14	1326	488
420	07:00:00	7,17	1328	487
422	07:02:00	7,21	1329	487
424	07:04:00	7,24	1332	487
426	07:06:00	7,27	1334	487
428	07:08:00	7,31	1334	487
430	07:10:00	7,34	1338	487
432	07:12:00	7,38	1339	487
434	07:14:00	7,41	1342	487
436	07:16:00	7,44	1346	487
438	07:18:00	7,48	1345	487
440	07:20:00	7,51	1347	487
442	07:22:00	7,54	1349	487
444	07:24:00	7,58	1349	487
446	07:26:00	7,61	1351	487
448	07:28:00	7,64	1351	487
450	07:30:00	7,68	1355	487
452	07:32:00	7,71	1355	487
454	07:34:00	7,75	1356	487
456	07:36:00	7,78	1358	487
458	07:38:00	7,81	1359	487
460	07:40:00	7,85	1360	487
462	07:42:00	7,88	1361	487
464	07:44:00	7,91	1364	487
466	07:46:00	7,95	1362	487
468	07:48:00	7,98	1363	487
470	07:50:00	8	1366	487
472	07:52:00	8,04	1365	487
474	07:54:00	8,07	1366	487
476	07:56:00	8,11	1367	488
478	07:58:00	8,14	1366	488
480	08:00:00	8,17	1368	488
482	08:02:00	8,2	1370	488
484	08:04:00	8,24	1371	488
486	08:06:00	8,27	1371	488
488	08:08:00	8,3	1373	488
490	08:10:00	8,34	1376	488
492	08:12:00	8,37	1375	489
494	08:14:00	8,4	1375	489
496	08:16:00	8,44	1378	489
498	08:18:00	8,47	1379	489
500	08:20:00	8,51	1381	489
502	08:22:00	8,54	1382	489
504	08:24:00	8,57	1384	489
506	08:26:00	8,61	1385	489
508	08:28:00	8,64	1384	490
510	08:30:00	8,67	1387	490
512	08:32:00	8,71	1385	490
514	08:34:00	8,74	1389	490
516	08:36:00	8,78	1390	490
518	08:38:00	8,81	1392	490
520	08:40:00	8,84	1395	490
522	08:42:00	8,88	1396	490
524	08:44:00	8,91	1397	490
526	08:46:00	8,94	1397	490
528	08:48:00	8,97	1398	490
530	08:50:00	9,01	1398	491
532	08:52:00	9,04	1402	491
534	08:54:00	9,08	1403	491
536	08:56:00	9,11	1404	491
538	08:58:00	9,14	1401	490
540	09:00:00	9,18	1403	490
542	09:02:00	9,21	1408	490
544	09:04:00	9,25	1408	490
546	09:06:00	9,28	1407	490
548	09:08:00	9,31	1407	491
550	09:10:00	9,35	1408	490
552	09:12:00	9,38	1412	491
554	09:14:00	9,41	1411	491
556	09:16:00	9,45	1411	491
558	09:18:00	9,48	1412	491
560	09:20:00	9,51	1414	491
562	09:22:00	9,55	1412	491
564	09:24:00	9,58	1413	491
566	09:26:00	9,61	1417	491
568	09:28:00	9,65	1415	491
570	09:30:00	9,68	1417	491
572	09:32:00	9,72	1419	491
574	09:34:00	9,75	1418	491
576	09:36:00	9,78	1423	491
578	09:38:00	9,82	1423	491
580	09:40:00	9,85	1422	491
582	09:42:00	9,89	1425	491
584	09:44:00	9,92	1424	491
586	09:46:00	9,95	1428	492
588	09:48:00	9,98	1429	492
590	09:50:00	10,02	1428	491

Table 6: Depicts specimen three from <u>no 592 to 1178</u> consolidation

	Test	-		
	Specimen	3		
	Stage	Shear		
	Schedule	Shear		
no	Time	ipStrain	ipLoad	ipPwP
592	09:52:00	10,05	1431	491
594	09:54:00	10,08	1430	490
596	09:56:00	10,12	1432	490
598	09:58:00	10,15	1435	490
600	10:00:00	10,18	1434	489
602	10:02:00	10,22	1432	489
604	10:04:00	10,25	1433	490
606	10:06:00	10,29	1437	490
608	10:08:00	10,32	1434	490
610	10:10:00	10,35	1436	490
612	10:12:00	10,39	1437	490
614	10:14:00	10,42	1438	490
616	10:16:00	10,46	1437	490
618	10:18:00	10,49	1435	490
620	10:20:00	10,52	1437	490
622	10:22:00	10,56	1436	490
624	10:24:00	10,59	1436	491
626	10:26:00	10,63	1437	491
628	10:28:00	10,66	1436	491
630	10:30:00	10,69	1438	491
632	10:32:00	10,73	1440	491
634	10:34:00	10,76	1440	491
636	10:36:00	10,8	1440	491
638	10:38:00	10,83	1440	491
640	10:40:00	10,86	1440	492
642	10:42:00	10,9	1441	492
644	10:44:00	10,93	1443	492
646	10:46:00	10,97	1443	492
648	10:48:00	11	1443	492
650	10:50:00	11,03	1444	492
652	10:52:00	11,07	1445	492
654	10:54:00	11,1	1448	492
656	10:56:00	11,14	1448	492
658	10:58:00	11,17	1448	492
660	11:00:00	11,21	1449	492
662	11:02:00	11,24	1450	492
664	11:04:00	11,27	1450	492
666	11:06:00	11,31	1451	492
668	11:08:00	11,34	1451	492
670	11:10:00	11,37	1451	492
672	11:12:00	11,41	1454	492
674	11:14:00	11,44	1453	492
676	11:16:00	11,48	1453	493
678	11:18:00	11,51	1455	492
680	11:20:00	11,54	1457	493
682	11:22:00	11,58	1457	493
684	11:24:00	11,61	1457	493
686	11:26:00	11,65	1457	493
688	11:28:00	11,68	1459	493
690	11:30:00	11,71	1458	493
692	11:32:00	11,75	1461	493
694	11:34:00	11,78	1460	493
696	11:36:00	11,82	1461	493
698	11:38:00	11,85	1461	494
700	11:40:00	11,87	1462	494
702	11:42:00	11,91	1463	494
704	11:44:00	11,94	1464	494
706	11:46:00	11,98	1464	494
708	11:48:00	12	1465	494
710	11:50:00	12,03	1466	495
712	11:52:00	12,07	1467	495
714	11:54:00	12,1	1467	495
716	11:56:00	12,14	1467	495
718	11:58:00	12,18	1467	496
720	12:00:00	12,2	1468	496
722	12:02:00	12,24	1468	496
724	12:04:00	12,26	1469	496
726	12:06:00	12,29	1470	496
728	12:08:00	12,29	1471	496
730	12:10:00	12,32	1473	496
732	12:12:00	12,36	1473	497
734	12:14:00	12,4	1471	497
736	12:16:00	12,43	1473	497
738	12:18:00	12,47	1474	497
740	12:20:00	12,5	1474	497
742	12:22:00	12,53	1474	497
744	12:24:00	12,55	1475	497
746	12:26:00	12,56	1477	497
748	12:28:00	12,56	1476	497
750	12:30:00	12,58	1476	497
752	12:32:00	12,61	1479	497
754	12:34:00	12,65	1479	497
756	12:36:00	12,68	1481	498
758	12:38:00	12,72	1482	498
760	12:40:00	12,75	1481	498
762	12:42:00	12,78	1484	498
764	12:44:00	12,81	1483	498
766	12:46:00	12,84	1485	498
768	12:48:00	12,86	1485	498
770	12:50:00	12,89	1486	498
772	12:52:00	12,93	1485	498
774	12:54:00	12,96	1488	498
776	12:56:00	13	1488	498
778	12:58:00	13,03	1487	498
780	13:00:00	13,06	1489	498
782	13:02:00	13,09	1489	498
784	13:04:00	13,11	1490	498
786	13:06:00	13,15	1491	498

	Test	-		
	Specimen	3		
	Stage	Shear		
	Schedule	Shear		
no	Time	ipStrain	ipLoad	ipPwP
788	13:08:00	13,17	1492	498
790	13:10:00	13,2	1494	499
792	13:12:00	13,21	1495	498
794	13:14:00	13,24	1494	498
796	13:16:00	13,27	1495	498
798	13:18:00	13,29	1496	498
800	13:20:00	13,32	1496	498
802	13:22:00	13,35	1497	498
804	13:24:00	13,38	1497	498
806	13:26:00	13,41	1497	498
808	13:28:00	13,44	1497	498
810	13:30:00	13,47	1497	498
812	13:32:00	13,51	1498	498
814	13:34:00	13,54	1498	498
816	13:36:00	13,57	1498	498
818	13:38:00	13,6	1499	498
820	13:40:00	13,62	1501	497
822	13:42:00	13,64	1500	497
824	13:44:00	13,67	1501	496
826	13:46:00	13,69	1502	495
828	13:48:00	13,72	1502	495
830	13:50:00	13,74	1503	495
832	13:52:00	13,76	1504	495
834	13:54:00	13,8	1504	495
836	13:56:00	13,83	1504	495
838	13:58:00	13,87	1506	495
840	14:00:00	13,9	1506	495
842	14:02:00	13,94	1506	495
844	14:04:00	13,97	1508	495
846	14:06:00	14	1509	495
848	14:08:00	14,03	1509	495
850	14:10:00	14,07	1510	495
852	14:12:00	14,1	1511	495
854	14:14:00	14,13	1510	495
856	14:16:00	14,16	1511	495
858	14:18:00	14,2	1510	495
860	14:20:00	14,23	1512	495
862	14:22:00	14,26	1513	495
864	14:24:00	14,29	1514	495
866	14:26:00	14,32	1513	495
868	14:28:00	14,36	1514	495
870	14:30:00	14,39	1515	494
872	14:32:00	14,42	1514	495
874	14:34:00	14,45	1516	495
876	14:36:00	14,49	1515	495
878	14:38:00	14,52	1516	495
880	14:40:00	14,55	1517	494
882	14:42:00	14,58	1516	494
884	14:44:00	14,61	1516	494
886	14:46:00	14,63	1519	494
888	14:48:00	14,67	1516	494
890	14:50:00	14,7	1517	494
892	14:52:00	14,73	1519	494
894	14:54:00	14,76	1520	494
896	14:56:00	14,79	1521	494
898	14:58:00	14,82	1522	494
900	15:00:00	14,84	1521	494
902	15:02:00	14,88	1523	494
904	15:04:00	14,91	1524	494
906	15:06:00	14,93	1525	494
908	15:08:00	14,97	1525	494
910	15:10:00	15	1527	494
912	15:12:00	15,04	1524	494
914	15:14:00	15,07	1526	494
916	15:16:00	15,1	1528	494
918	15:18:00	15,14	1527	494
920	15:20:00	15,17	1529	494
922	15:22:00	15,2	1527	494
924	15:24:00	15,23	1530	494
926	15:26:00	15,27	1529	494
928	15:28:00	15,3	1528	494
930	15:30:00	15,33	1530	494
932	15:32:00	15,36	1529	494
934	15:34:00	15,39	1529	494
936	15:36:00	15,43	1530	494
938	15:38:00	15,46	1530	494
940	15:40:00	15,49	1531	494
942	15:42:00	15,53	1532	494
944	15:44:00	15,56	1532	494
946	15:46:00	15,59	1530	494
948	15:48:00	15,62	1531	493
950	15:50:00	15,65	1531	493
952	15:52:00	15,69	1533	493
954	15:54:00	15,72	1533	492
956	15:56:00	15,75	1534	492
958	15:58:00	15,79	1533	492
960	16:00:00	15,82	1533	492
962	16:02:00	15,85	1536	492
964	16:04:00	15,89	1537	491
966	16:06:00	15,92	1536	492
968	16:08:00	15,96	1537	492
970	16:10:00	15,99	1536	492
972	16:12:00	16,02	1536	492
974	16:14:00	16,06	1537	492
976	16:16:00	16,09	1538	492
978	16:18:00	16,13	1537	492
980	16:20:00	16,16	1540	492
982	16:22:00	16,19	1538	493

	Test	-		
	Specimen	3		
	Stage	Shear		
	Schedule	Shear		
no	Time	ipStrain	ipLoad	ipPwP
984	16:24:00	16,23	1538	493
986	16:26:00	16,26	1539	493
988	16:28:00	16,29	1539	493
990	16:30:00	16,32	1540	492
992	16:32:00	16,36	1539	492
994	16:34:00	16,39	1538	492
996	16:36:00	16,42	1539	492
998	16:38:00	16,46	1538	492
1000	16:40:00	16,49	1540	491
1002	16:42:00	16,52	1539	492
1004	16:44:00	16,56	1540	492
1006	16:46:00	16,59	1540	492
1008	16:48:00	16,62	1540	492
1010	16:50:00	16,65	1541	492
1012	16:52:00	16,69	1540	492
1014	16:54:00	16,72	1541	493
1016	16:56:00	16,76	1540	493
1018	16:58:00	16,79	1539	493
1020	17:00:00	16,82	1539	492
1022	17:02:00	16,85	1538	492
1024	17:04:00	16,89	1538	492
1026	17:06:00	16,92	1539	491
1028	17:08:00	16,95	1539	491
1030	17:10:00	16,99	1539	491
1032	17:12:00	17,02	1539	491
1034	17:14:00	17,05	1538	491
1036	17:16:00	17,09	1541	491
1038	17:18:00	17,12	1540	492
1040	17:20:00	17,15	1536	491
1042	17:22:00	17,19	1535	492
1044	17:24:00	17,22	1535	492
1046	17:26:00	17,25	1535	492
1048	17:28:00	17,29	1535	492
1050	17:30:00	17,32	1537	492
1052	17:32:00	17,35	1534	492
1054	17:34:00	17,38	1534	492
1056	17:36:00	17,41	1533	492
1058	17:38:00	17,45	1534	491
1060	17:40:00	17,48	1534	491
1062	17:42:00	17,51	1534	491
1064	17:44:00	17,54	1533	491
1066	17:46:00	17,58	1533	491
1068	17:48:00	17,61	1531	491
1070	17:50:00	17,64	1533	491
1072	17:52:00	17,68	1532	491
1074	17:54:00	17,71	1533	491
1076	17:56:00	17,74	1532	491
1078	17:58:00	17,78	1533	491
1080	18:00:00	17,81	1533	491
1082	18:02:00	17,84	1535	491
1084	18:04:00	17,88	1535	491
1086	18:06:00	17,91	1533	491
1088	18:08:00	17,94	1532	492
1090	18:10:00	17,98	1532	492
1092	18:12:00	18,01	1531	492
1094	18:14:00	18,04	1533	492
1096	18:16:00	18,08	1531	492
1098	18:18:00	18,11	1531	492
1100	18:20:00	18,14	1532	492
1102	18:22:00	18,18	1532	492
1104	18:24:00	18,21	1533	492
1106	18:26:00	18,24	1532	492
1108	18:28:00	18,27	1533	492
1110	18:30:00	18,3	1532	492
1112	18:32:00	18,34	1531	492
1114	18:34:00	18,37	1531	492
1116	18:36:00	18,4	1531	492
1118	18:38:00	18,44	1531	493
1120	18:40:00	18,46	1530	493
1122	18:42:00	18,49	1530	492
1124	18:44:00	18,52	1530	492
1126	18:46:00	18,55	1530	492
1128	18:48:00	18,58	1530	491
1130	18:50:00	18,62	1530	491
1132	18:52:00	18,65	1530	491
1134	18:54:00	18,68	1529	491
1136	18:56:00	18,72	1529	491
1138	18:58:00	18,75	1529	491
1140	19:00:00	18,78	1530	491
1142	19:02:00	18,81	1533,2	491
1144	19:04:00	18,85	1533,2	492
1146	19:06:00	18,88	1534,4	491
1148	19:08:00	18,91	1535,6	491
1150	19:10:00	18,95	1535,6	492
1152	19:12:00	18,98	1538	492
1154	19:14:00	19,01	1539,2	492
1156	19:16:00	19,04	1540,4	492
1158	19:18:00	19,07	1541,6	492
1160	19:20:00	19,11	1542,8	492
1162	19:22:00	19,14	1541,6	492
1164	19:24:00	19,17	1541,6	492
1166	19:26:00	19,2	1542,8	493
1168	19:28:00	19,23	1542,8	493
1170	19:30:00	19,27	1542,8	493
1172	19:32:00	19,29	1544	493
1174	19:34:00	19,31	1545,2	493
1176	19:36:00	19,34	1547,6	493
1178	19:38:00	19,37	1548,8	493

Table 7: Depicts a consolidation stage of triaxial test for shear parameter analysis

Specimer 1
Stage Consolidation
Schedule Consolidation

Time	ipPwP	ipVol	Dissipatic	ipCPVol	dVol
00:00:00	478	102,96	0	55,384	0
00:02:00	400	104,341	100	54,147	1,381
00:04:00	399	104,403	101,28	54,079	1,443
00:06:00	399	104,431	101,28	54,045	1,471
00:08:00	399	104,452	101,28	54,024	1,492
00:10:00	399	104,466	101,28	54,01	1,506
00:12:00	399	104,477	101,28	54,003	1,517
00:14:00	399	104,483	101,28	53,992	1,523
00:16:00	399	104,487	101,28	53,988	1,527
00:18:00	399	104,494	101,28	53,978	1,534
00:20:00	399	104,497	101,28	53,973	1,537
00:22:00	399	104,505	101,28	53,973	1,545
00:24:00	399	104,518	101,28	53,983	1,558
00:26:00	399	104,531	101,28	54,011	1,571
00:28:00	399	104,541	101,28	54,024	1,581
00:30:00	399	104,546	101,28	54,031	1,586
00:32:00	399	104,554	101,28	54,042	1,594
00:34:00	399	104,558	101,28	54,05	1,598
00:36:00	399	104,564	101,28	54,064	1,604
00:38:00	399	104,567	101,28	54,064	1,607
00:40:00	398	104,57	102,56	54,064	1,61
00:42:00	399	104,565	101,28	54,057	1,605
00:43:42	399	104,562	101,28	54,045	1,602

Specimer 2
Stage Consolidation
Schedule Consolidation

Time	ipPwP	ipVol	Dissipatic	ipCPVol	dVol
00:00:00	585	199,845	0	81,674	0
00:02:00	400	203,141	100	78,564	3,296
00:04:00	400	203,23	100	78,455	3,385
00:06:00	399	203,278	100,54	78,394	3,433
00:08:00	399	203,306	100,54	78,35	3,461
00:10:00	399	203,327	100,54	78,318	3,482
00:12:00	400	203,344	100	78,286	3,499
00:14:00	399	203,36	100,54	78,264	3,515
00:16:00	399	203,374	100,54	78,234	3,529
00:18:00	399	203,385	100,54	78,215	3,54
00:20:00	399	203,398	100,54	78,187	3,553
00:22:00	400	203,404	100	78,172	3,559
00:24:00	399	203,421	100,54	78,182	3,576
00:26:00	399	203,436	100,54	78,207	3,591
00:28:00	399	203,448	100,54	78,212	3,603
00:30:00	399	203,458	100,54	78,218	3,613
00:32:00	399	203,468	100,54	78,222	3,623
00:34:00	399	203,475	100,54	78,226	3,63
00:36:00	399	203,484	100,54	78,229	3,639
00:38:00	399	203,489	100,54	78,221	3,644
00:40:00	399	203,487	100,54	78,218	3,642
00:42:00	399	203,484	100,54	78,196	3,639
00:43:36	399	203,48	100,54	78,176	3,635

Specimer 3
Stage Consolidation
Schedule Consolidation

Time	ipPwP	ipVol	Dissipatic	ipCPVol	dVol
00:00:00	769	78,546	0	42,244	0
00:02:00	400	83,469	100	37,591	4,923
00:04:00	400	83,607	100	37,433	5,061
00:06:00	400	83,656	100	37,347	5,11
00:08:00	400	83,694	100	37,284	5,148
00:10:00	400	83,714	100	37,233	5,168
00:12:00	400	83,735	100	37,184	5,189
00:14:00	400	83,751	100	37,143	5,205
00:16:00	400	83,758	100	37,105	5,212
00:18:00	400	83,774	100	37,073	5,228
00:20:00	400	83,784	100	37,039	5,238
00:22:00	400	83,792	100	37,009	5,246
00:24:00	400	83,807	100	37,003	5,261
00:26:00	400	83,813	100	37,015	5,267
00:28:00	400	83,827	100	37,01	5,281
00:30:00	400	83,828	100	36,992	5,282
00:32:00	400	83,833	100	36,98	5,287
00:34:00	400	83,846	100	36,962	5,3
00:36:00	400	83,851	100	36,95	5,305
00:38:00	400	83,856	100	36,932	5,31
00:40:00	400	83,855	100	36,909	5,309
00:42:00	400	83,849	100	36,879	5,303
00:43:32	400	83,85	100	36,855	5,304

Consolidation stage

Table 8: depicts the initial stage of consolidation

Initial conditions	1	2	3	SI units
Cell Pressure	499	599	798	kPa
Back pressure	399	399	398	kPa
Void ratio	0.535	0.535	0.535	
Side drain used	yes	yes	yes	

Table 9: depicts the final stage of consolidation

Final conditions	1	2	3	
Volume change	-1.6	-3,6	-5.3	ml
Volumetric strain	-0.82	-1,85	-2.70	%
Corrected length	99.73	99,38	99.10	mm
Corrected diameter	49.69	49.69	49.54	mm
Void ratio	0.523	0.506	0.494	

Table 10: depicts the final results based on consolidation stage

Final sample details	**1**	**2**	**3**	
Dry density	2026	2048	2065	kg/m^3
density	2427	2410	2445	kg/m^3
Void ratio	0.523	0.506	0.494	
Moisture content	19.79	17.69	18.39	%

Shear stage

Table 11: depicts the shear stage of triaxial test for shear strength parameters test

shear	**1**	**2**	**3**	**si units**
σ'_1 at failure	257.3	753.1	937.8	kPa
σ'_3 at failure	83.0	229.0	299.0	kPa
Failure criteria	MSR	MSR	MSR	
Deviator stress at failure	174.3	524.1	638.8	kPa
Stress Ratio at failure	3.1	3.3	3.1	
Strain at failure	2.2	11.8	13.0	
Calculated shear speed	0.0167	0.0167	0.0167	mm/min
Actual shear speed	0.0170	0.0166	0.0163	mm/min

SUMMARY FOR ALL STAGES (INITIAL STAGE, SHEAR, CONSOLIDATION, AND FLUSH)

Sample details before analysis		
sample condition	Disturbed	
remould effort	95.00	%
remould MDD	2116	kgm^3
remould OMC	3.5	%
ϕ'	31.5	°
c'	0.0	kPa

Initial sample	1	2	3	
Sample length	100	100	100	mm
Sample diameter	50	50	50	mm
Sample mass	408.4	408.5	408.4	g
Dry density	2010	2010	2010	kg/m^3
Bulk density	2080	2080	2080	kg/m^3
Void ratio		0.535	0.535	
Moisture content		3.5	3.5	%
Specific gravity		3.085		mg/m^3

Flush stage	1	2	3	

Volume change	N/A	N/A	N/A	ml
% Volume change	N/A	N/A	N/A	%

Saturation stage	1	2	3	
Final B pressure	0.95	0.96	0.98	kPa
Final back pressure	400	400	400	kPa

Consolidation stage	**1**	**2**	**3**	SI unit
Effective stress	100	200	400	kPa
Volume change	-1.602	-3.635	-5.304	ml
height after consolidation	99.73	99.38	99.10	mm
Diameter after consolidation	49.86	49.69	49.54	mm
Void ratio before consolidation	0.535	0.535	0.535	
Void ratio After consolidation	0.523	0.506	0.494	
Coef of volume (mvi)	0.125	0.142	0.104	m^2MN

Shear stage	**1**	**2**	**3**	SI unit
Rate of shear	0.01702	0.01655	0.01627	mm/min
Failure criteria	MSR	MSR	MSR	
Deviator stess at failure	174.3	524.1	638.8	kPa
stress ratio at failure	3.1	3.3	3.1	
Strain at failure	2.2	11.8	13.0	

Calculations and Parameters	1	2	3	SI unit
Calculated Shear Speed:	0.0167	0.0167	0.0167	mm/min
Coeff of Volume Comp (m_{vi}):	0.125	0.142	0.104	m^2MN

Table 12: A table depicting tailings poissan's ratio parameters

Calcul parameters		SI unit
Parameters	Values	
σ' ava	77.76	kPa
c	0	kPa
ϕ	31.5	°
τ	47.66	kPa
ε_{axial} av	0.61	
E	311.04	kPa
$\varepsilon v_{lateral}$ av	0,25	
P_v	0.41	

Table 13: Shear strength parameters

Parameters	Values	Si unit
σ' ava	77.76	kPa
c	0	kPa
ϕ	31.5	°

Table 14: Depicts results of the percentage material passing from sieve analysis

Screen analysis (%passing)- SANS 3001-GR1	
sieve size	%passings
75.00mm	100
63.00mm	100
50.00mm	100
37.50mm	100
28.00mm	100
20.00mm	100
14.00mm	100
5.00mm	100
2.00mm	99
0.425mm	81
0.075mm	17

Table 15: Depicts tailings sand particles size distribution

Soil mortar percentage- SANS 300-PR5		
Grain fraction	grain range	%
Coarse sand	2.000-0.425mm	19
coarse fine sand	0.425-0.250mm	20
Medium fine sand	0.250-0.150mm	25
Fine fine sand	0.150-0.075mm	20

Table 16: Tailings particle size

Particles size distribution	
%clay	3
%silt	7
%sand	89
%gravel	1

Table17: depicting the hydrometer analysis results and tailings classification based on USCS (Unified Soil Classification System)

Hydrometer analysis (%) passings SANS 3001:GR3	
67μm	10%
39μm	6%
16μm	5%
7μm	3%
2μm	1%
Grains classification	
%clay	3%
%silt	7%
%sand	89%
%gravel	1%

Table 18: Atterberg limits properties

Atterberg limits SANS 3001-GR10	
LL	0
PL	NP
LS	0
Grading modulus	1.04
Classification	A-2-4 (0)
USCS	SM

Table 19: Unit weight parameters

Unit weight(y) variables		
MDD	2116	kg/m3
g	9.8	m/s2
γ	20736.8	Nm3

Table 20: Tailings Atterberg limits results

Atterberg limits SANS 3001-GR10	
LL	0
PL	NP
LS	0
Grading modulus	1.04
Classification	A-2-4 (0)
USCS	SM

Table 21: PWP parameters

pore water pressure parameters		
unit weight	values	SI unit
γ_w	9.81	kN/m3
γ	20.76	kN/m3
Height/depth	60	m
waterhead	5	kPa
PWP	588.6	kPa

specimen 1		specimen 2		specimen 3	
mineral	%	mineral	%	mineral	%
U	0.01	U	0.02	U	0.09
Th	0.018	Th	0.023	Th	0.014
Pb	0.03	Pb	0.004	Pb	
Rb	0.003	Ba	0.076	Ba	0.058
Sn	0.045	Sn	0.047	Sn	0.055
Y	0.005	Y	0.008	Y	0.004
Sr	0.265	Sr	0.375	Sr	0.230
Fe_2O_3	21.032	Fe_2O_3	12.832	Fe_2O_3	16.414
MnO	0.100	MnO	0.053	MnO	0.080
Zr	0.031	Cu	0.119	Zr	0.029
Ni	0.007	Ni	0.003	Ni	0.006
TiO_2	0.334	TiO_2	0.23	TiO_2	0.258
CaO	25.494	CaO	24.677	CaO	25.004
K_2O	0.088	K_2O	0.033	K_2O	0.051
Cu	0.417	Cu	0.417	Cu	0.126
S	0.043	S	0.022	S	0.073
P_2O_5	1.807	P_2O_5	1.077	P_2O_5	1.724
SiO_2	4.013	SiO_2	2.987	SiO_2	3.332
Al_2O_3	0.690	Al_2O_3	0.590	$Al2O_3$	0.426
MgO	5.539	MgO	5.101	MgO	5.165

Table 22: Mineral composition of tailings from XRF analysis